



Politecnico di Torino

Master of Science in Automotive Engineering

A.Y. 2023/2024

Graduation Session December 2024

Analysis of Metamaterials in the Automotive Sector

Supervisors

Prof. Luigi Garibaldi

Prof. Alessandro Paolo Daga

Candidate

Fernando Messina s292793

Abstract

The scope of this work is to evaluate and highlight metamaterials properties and their possible applications in automotive field. Starting from a general overview of metamaterials characteristics the work will follow a practical approach with the attempt to reproduce the study presented in the paper “Metamaterials for simultaneous acoustic and elastic bandgaps” by Waiel Elmadih, Dimitrios Chronopoulos & Jian Zhu.

The simulation software chosen to perform the analysis is COMSOL Multiphysics® since it allows to design the material, shape it and perform very accurate studies in vibroacoustic scenario.

The work commenced with the digital design of a single metamaterial unit cell, for an investigation into its structural properties. Following this initial design phase, various boundary conditions were applied to ensure that the simulations replicate the desired physical environment. The primary objective of this phase was to obtain similar results presented in published article, which serve as key references for this study.

In the second part, simplified versions of the metamaterial design, inspired by the structure used in the physical tests referenced in the literature, were created. These simplified configurations are intended to serve as benchmarks for additional virtual analyses aimed at exploring the metamaterial's behavior. This section of the study is particularly focused on understanding if these simpler shapes can perform in acceptable way as the original shape. By examining these modified designs, the study seeks to determine if the essential properties of the metamaterial can be preserved even with a simplified structure, potentially encouraging its applicability in real-world scenarios where manufacturing constraints and costs are crucial considerations.

Index

1 NVH automotive sector and metamaterial characteristics	4
1.1 NVH automotive sector description	4
1.2 Metamaterial characteristics.....	6
1.3 Metamaterials in Vibrational and Acoustic Applications.....	7
1.4 Acoustic Metamaterials for Sound Control,.....	7
1.5 Automotive Applications of Metamaterials.....	8
2 Metamaterial analysis	10
2.1 Model description	10
2.2 Model geometric validation.....	16
2.3 Paper presented results.....	24
3 Carried out simulations	25
3.1 Simulation with Floquet periodicity along X axis and k_x wave vector	25
3.2 Simulation with Floquet periodicity along X axis and k_x, k_y, k_z wave vector	26
3.3 Simulation with Floquet periodicity along X,Y,Z axis and k_x, k_y, k_z wave vector	27
3.4 Simulation with Floquet periodicity along X,Y,Z axis and k_x, k_y, k_z wave vector with scaling factor	29
3.5 Simulation with Floquet periodicity along X,Y,Z axis and k_x, k_y, k_z wave vector with scaling factor 0	31
4 Carried out simulations on finite elements	32
4.1 Simulation with Floquet periodicity along X axis and k_x wave vector for plate with reduced thickness.....	32
4.2 Simulation with Floquet periodicity along X axis and k_x wave vector for 7 cube cells beam	33
4.3 Simulation with Floquet periodicity along X axis and k_x wave vector for single reduced thickness plate	36
4.4 Simulation with Floquet periodicity along X,Y,Z axis and k_x, k_y, k_z wave vector with scaling factor	36
5 Experimental analyses	38
5.1 Chladni experiment setup.....	38
5.2 Chladni results.....	41
5.2 Laser probe experiment setup	49
5.3 Laser probe results	49
6 Conclusions	54
References	56

Chapter 1

NVH automotive sector and metamaterial characteristics

1.1 NVH automotive sector description

NVH is the acronym for Noise, Vibration, and Harshness and is the study and measurement of aural and tactile feedback in an object¹. This area of study helps the understanding and the identification where a sound is coming from and why. In modern world where automotive customers are more demanding and pay attention to the product they are buying, NVH plays a relevant role among most of design and development project phases.

The three parts mentioned above can be defined in simple way as follow

- **noise** is the sound propagation caused by a specific object¹and is transmitted by air
- **vibration** is the oscillations that occur at a certain frequency¹ and is transmitted by structures
- **harshness** is the subjective quality associated with noise and vibration¹.

Is important to remind that harshness is a subjective feeling so in not measurable in measurable terms. Harshness can induce fatigue, annoyance, lower concentration and attention, missed alarms, vision and acoustic stress: it is a potential source of danger².

Main sources for NVH phenomena in a car can be divided into three main categories: **wind** excitation, **road** excitation and **powertrain** excitation. In addition, can be also mentioned the noise coming from electrical signals like driver alerts used by ADAS.

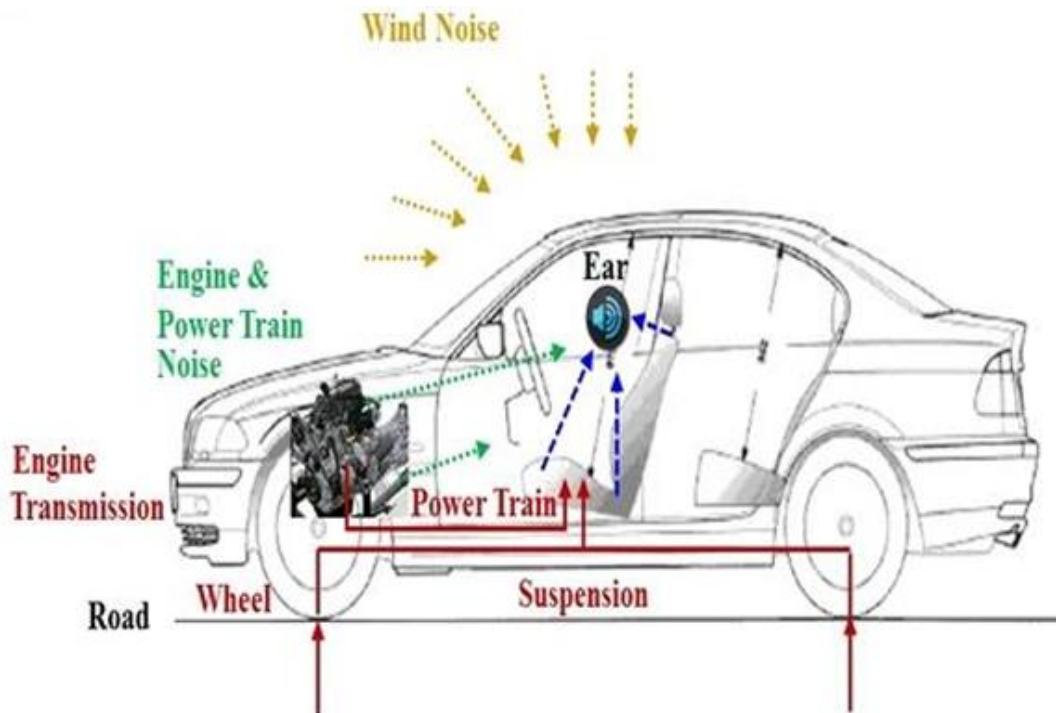


Figure 1 Main noise sources in a vehicle

Wind excitations are the one related to the air acting on the body. Wind noise is transmitted to the interior through the body. At the same time, the wind excites the body panels, and the excited panels radiate noise to the interior. Generally, for speed above 120 km/h, the wind noise overwhelms the powertrain noise and the road noise, making it the largest noise source². Under this category we can also mention HVAC fans.

Road excitations collect all Interaction between the tires and the road generates noise that is directly transferred into the interior. Vibration generated by the action between the road and the tires is transmitted to the body through the suspension system. Of course, these effects are more present when driving on rough or with disconnected surfaces roads.

Powertrain excitations include all noises related to the powertrain system and. considering this definition, is not only considered as source the engine but also transmission and gearbox, intake and exhaust systems, and driveshaft.

With the advent of new technologies in the automotive field like electric and hybrid propulsion, new NVH phenomena need to be take in account. This is due to different vehicle architecture, due to different working condition of the components and due to the different nature of the propulsion system itself (think to combustion engine vs EDM).

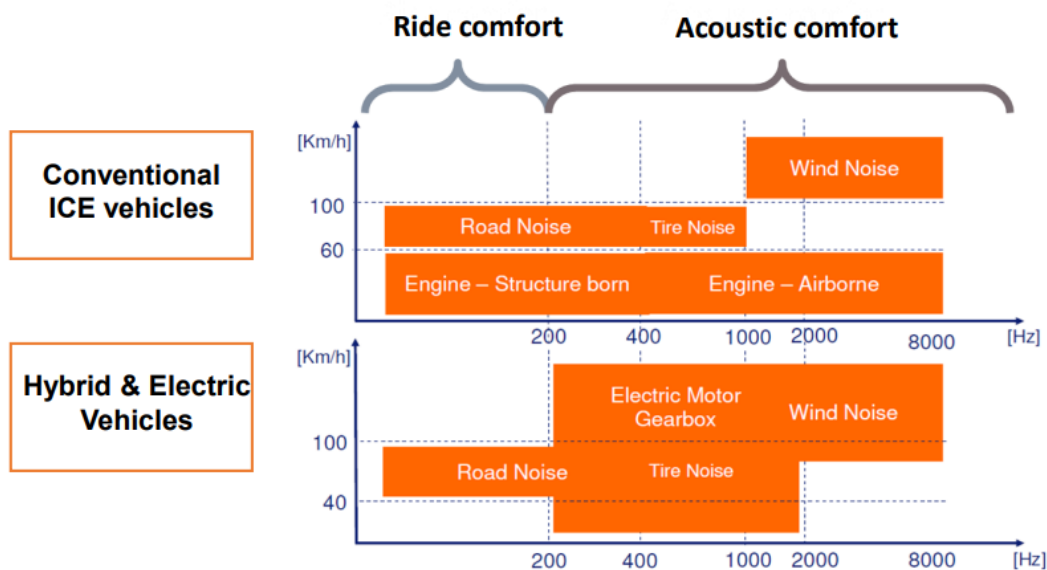


Figure 2 frequency spectrum of noises in ICE vs HEV and EV

With the help of fig.2 we can easily get an overview of how different type of noises affect different vehicle typology. Depending on the speed each source has different contribution to the overall noise level and can be more perceptible than other sources. What is important to highlight is that each source has a sort of characteristic frequency range in which it propagates.

The loss of noise coming from internal combustion engine and transmission in electric vehicles could be seen as a big advantage in terms of noise reduction. Undoubtedly it helps to decrease

exterior noise level, but for what concern the in-cabin noise the loss of masking effect generated by the engine in ICE vehicles leads to increased perceived noise level of various ancillaries like pumps, compressor and the EDM noise itself that is more perceived by the passengers. This is a strong challenge for NVH engineers to give the best possible behavior for customers.

1.2 Metamaterial characteristics

Metamaterials are artificial materials designed to obtain electromagnetic, acoustic, or mechanical properties not found in natural materials. Their structure is made up of repeated substructural units that interact with waves in unique ways. These materials find applications in various fields, including optics, acoustics, telecommunications, and even the biomedical sector.

- **Electromagnetic and Optical Properties:** Metamaterials are known for their ability to influence the behavior of electromagnetic waves, including negative refraction and the creation of "invisibility cloaks." Some metamaterials can also manipulate light to deflect waves around an object.
- **Acoustic Properties:** There are metamaterials capable of influencing the propagation of sound, such as "acoustic metamaterials," which can block or manipulate sound waves, making them useful for noise control or creating sound-absorbing surfaces³.
- **Mechanical Properties:** Mechanical metamaterials can be designed to have unconventional mechanical responses, such as negative elasticity moduli or auxetic behavior (expanding when stretched, contrary to conventional materials)⁴.

Mechanical metamaterials represent one of the most promising innovations in structural engineering and in vibrational and acoustic applications. Unlike conventional materials, whose properties derive from chemical composition and molecular structure, mechanical metamaterials exploit the design of their microstructure to achieve unique behaviors not found in nature. This capability makes them ideal for addressing complex challenges in areas such as vibration control, acoustic insulation, and mechanical protection.

Characteristics of Mechanical Metamaterials

- **Auxetic behavior**
Mechanical metamaterials can be designed to exhibit auxetic behavior, meaning they expand laterally when subjected to tension, instead of contracting as typical materials do. This behavior is possible thanks to the geometric arrangement of structural units that form a network expanding in all directions under load⁵. Auxetic metamaterials are used in fields such as protective clothing and impact-absorbing coatings, where high energy absorption is required⁶.

- Negative elastic moduli

Another unique behavior of mechanical metamaterials is the ability to exhibit negative elastic moduli within certain frequency ranges, acting as "meta-springs" that store energy in unconventional ways. This property has been leveraged to design structures capable of attenuating or completely blocking specific vibrational frequencies, which is highly useful in fields like earthquake-resistant building design and protecting devices sensitive to vibrations⁷.

1.3 Metamaterials in Vibrational and Acoustic Applications

One of the most promising and extensively researched fields for mechanical metamaterials is their use in vibration control and acoustic insulation. These areas leverage the unique capabilities of metamaterials to manipulate waves—both mechanical (vibrations) and sound (acoustic waves)—in ways not possible with conventional materials.

- Vibrational Metamaterials for Isolation and Damping

Vibrational metamaterials are designed to manage mechanical vibrations in various systems, from industrial machinery to transportation systems. These materials can be engineered to block specific vibrational frequencies through mechanical bandgaps, where wave propagation is entirely suppressed. Bandgaps are achieved by designing periodic structures within the metamaterial, which interact with incoming vibrational waves, scattering or reflecting them in such a way that they are effectively canceled out⁸.

The application of these materials is particularly relevant in sectors where precision and stability are critical, such as in aerospace, civil engineering, and automotive industries. For instance, in civil engineering, buildings and bridges can be fitted with metamaterials that suppress harmful vibrational modes, such as those caused by earthquakes or wind. These materials can prevent resonance, reducing structural fatigue and extending the lifespan of the infrastructure.

Another key application is in machinery and equipment, where mechanical vibrations can reduce operational efficiency or damage sensitive components. Vibrational metamaterials embedded in machine foundations can isolate the source of vibrations, ensuring smoother operation and lower maintenance costs.

1.4 Acoustic Metamaterials for Sound Control

In the acoustic domain, metamaterials are engineered to manipulate sound waves, creating materials with exceptional sound insulation properties. Traditional materials like foam or fiberglass are often thick and heavy to provide soundproofing, especially for low-frequency sound, which is notoriously difficult to block due to its long wavelength. However, acoustic metamaterials have been shown to achieve better sound attenuation with a fraction of the thickness, particularly in the low-frequency range⁹.

This is possible because acoustic metamaterials leverage local resonances or periodic structures that interact with sound waves in unique ways. For example, when sound waves enter a metamaterial with a periodic structure, they are scattered, reflected, or even absorbed, depending on the frequency¹⁰. This results in the creation of acoustic bandgaps, which prevent the propagation of sound at specific frequencies, offering exceptional control over noise pollution.

In practical terms, acoustic metamaterials are revolutionizing industries such as construction, automotive, and aerospace, where noise reduction is a critical factor. In construction, acoustic metamaterials are used to design walls and barriers that offer superior noise insulation with thinner layers, optimizing space without sacrificing performance. Similarly, in the automotive industry, these materials contribute to reducing the noise inside vehicles, enhancing passenger comfort while minimizing added weight, which is crucial for maintaining fuel efficiency.

Advanced Acoustic Applications

Researchers are also investigating meta-lenses and meta-cloaks—advanced applications of acoustic metamaterials that can focus, guide, or shield sound waves. These technologies hold promise for fields such as medical imaging, where ultrasound meta-lenses can focus sound waves more precisely for higher-resolution imaging. Meta-cloaks, on the other hand, can render objects acoustically invisible by bending sound waves around them, making these objects undetectable by sonar systems. These innovations demonstrate the transformative potential of metamaterials in acoustic manipulation¹¹.

Moreover, metamaterials are now being developed for use in active noise control, where they can be combined with adaptive systems to dynamically respond to changing noise conditions. These smart acoustic metamaterials can adjust their structure or resonance properties in real time, effectively adapting to new acoustic environments. This has significant implications for urban planning, where adaptable noise barriers could be deployed to mitigate environmental noise in highly variable settings such as near airports or highways.

1.5 Automotive Applications of Metamaterials

Metamaterials have proven to be revolutionary in the automotive industry, particularly in the areas of vibration damping, noise reduction, and lightweight structural components. As automotive manufacturers strive to produce more energy-efficient and comfortable vehicles, metamaterials are being explored to provide solutions that enhance performance without compromising on weight or cost.

- Noise, Vibration, and Harshness (NVH) Control:

A significant focus of automotive metamaterials research is on controlling Noise, Vibration, and Harshness (NVH). These factors are critical to ensuring passenger

comfort and the structural integrity of vehicles. Traditional NVH control solutions rely on heavy insulating materials and complex damping systems, which increase the vehicle's weight and reduce fuel efficiency. Acoustic metamaterials offer an alternative by blocking unwanted noise frequencies through acoustic bandgaps, thereby reducing the need for bulky insulation¹². This leads to lighter, quieter vehicles with improved fuel efficiency. Metamaterial-based panels or inserts can be integrated into the vehicle's body, interior, and engine compartments to significantly cut down noise, particularly low-frequency engine and road noise .

- **Lightweight Structures:**

As the automotive industry shifts towards electric vehicles (EVs) and more fuel-efficient models, reducing weight without sacrificing performance is critical. Mechanical metamaterials, especially those with auxetic properties, can provide lightweight structural components that maintain or even improve mechanical strength. These materials allow for optimized crash safety, weight reduction, and flexibility in vehicle design, offering a perfect balance between strength and weight. Metamaterials with negative Poisson's ratios can absorb impacts more efficiently, providing enhanced safety while reducing mass¹³ .

- **Thermal and Acoustic Management in Electric Vehicles:**

In electric vehicles, noise sources differ from traditional internal combustion engines, with vibrations and noise often emanating from electric motors and power electronics. Acoustic metamaterials are used to address these new NVH challenges by absorbing or redirecting sound waves from these components, ensuring a quieter cabin experience. Additionally, metamaterials that control thermal and acoustic properties simultaneously are being developed to improve the overall energy management of EVs, enhancing battery life and reducing the need for active cooling systems .

- **Future Innovations:**

Looking ahead, metamaterials may play a role in active control of sound and vibrations, where the materials adapt in real-time to changing driving conditions. Smart metamaterials that adjust their structure to dynamically control the vibration and noise levels within a vehicle cabin could offer new possibilities for personalized acoustic environments, as well as improving the overall driving experience. Additionally, acoustic cloaking technology, which makes an object invisible to sound waves, could be explored in future automotive applications, reducing external noise interference¹⁴.

Chapter 2

Metamaterial analysis

2.1 Model description

In this chapter, we will illustrate the process of creating the model and detail the initial analyses performed on the metamaterial considered for this study. As mentioned in the first pages of this work, the geometry taken as reference is that presented in the article "Metamaterials for simultaneous acoustic and elastic bandgaps"¹⁵ by Waiel Elmadih, Dimitrios Chronopoulos and Jian Zhu. In detail, the unit cell is a cube with walls of predefined thickness and holes centered on each face, passing through to the opposite face. In the following table main model dimensions

C[mm]	d[mm]	L[mm]
30	15	6

Table 1 unitary cell dimensions

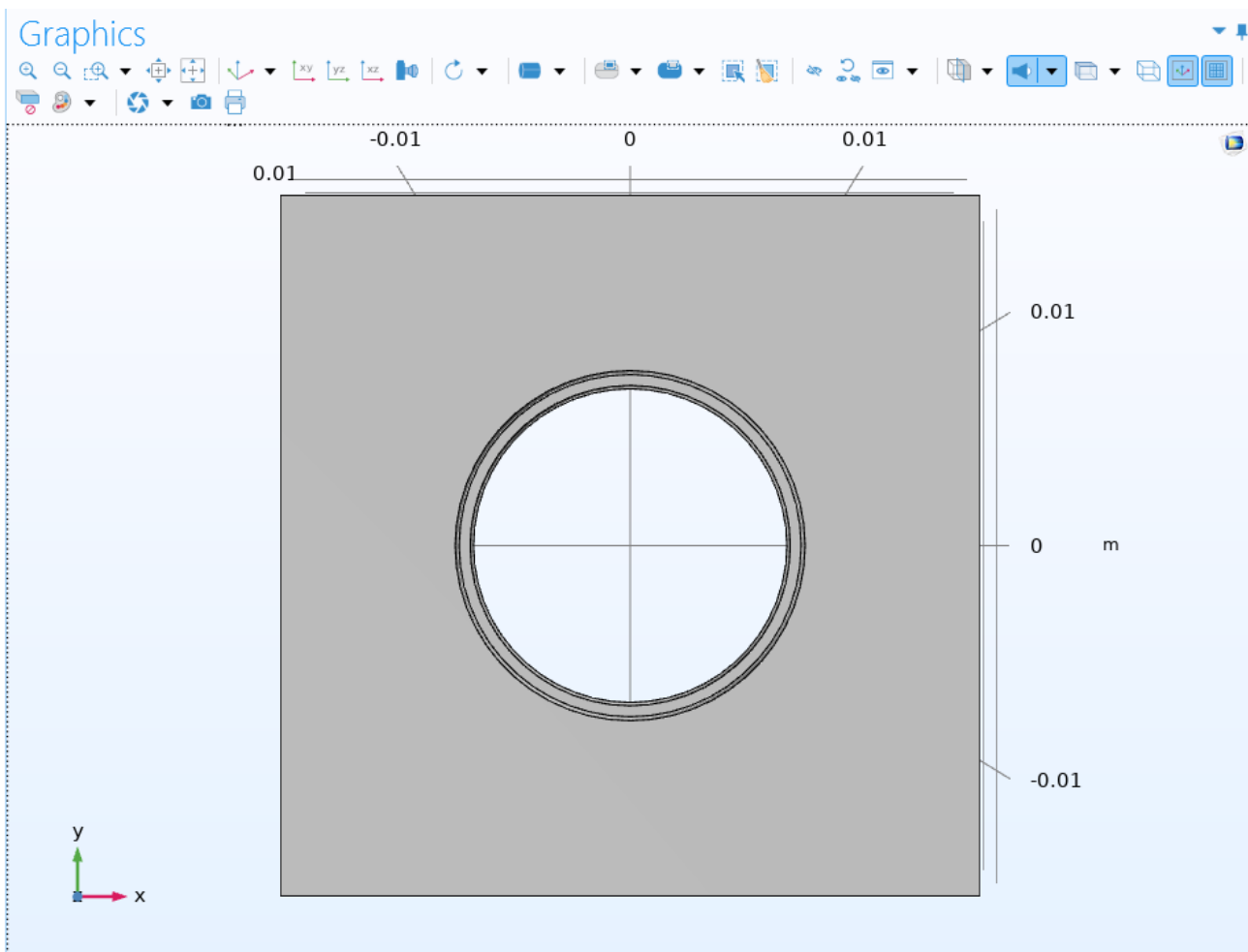


Figure 3 : metamaterial cube face

As reported in the article the parameters used for the modelling are $d/C = 0.5$, $L/C = 0.2$ where d is the diameter of the holes, C is the cube face edge length and L is the internal wall thickness.

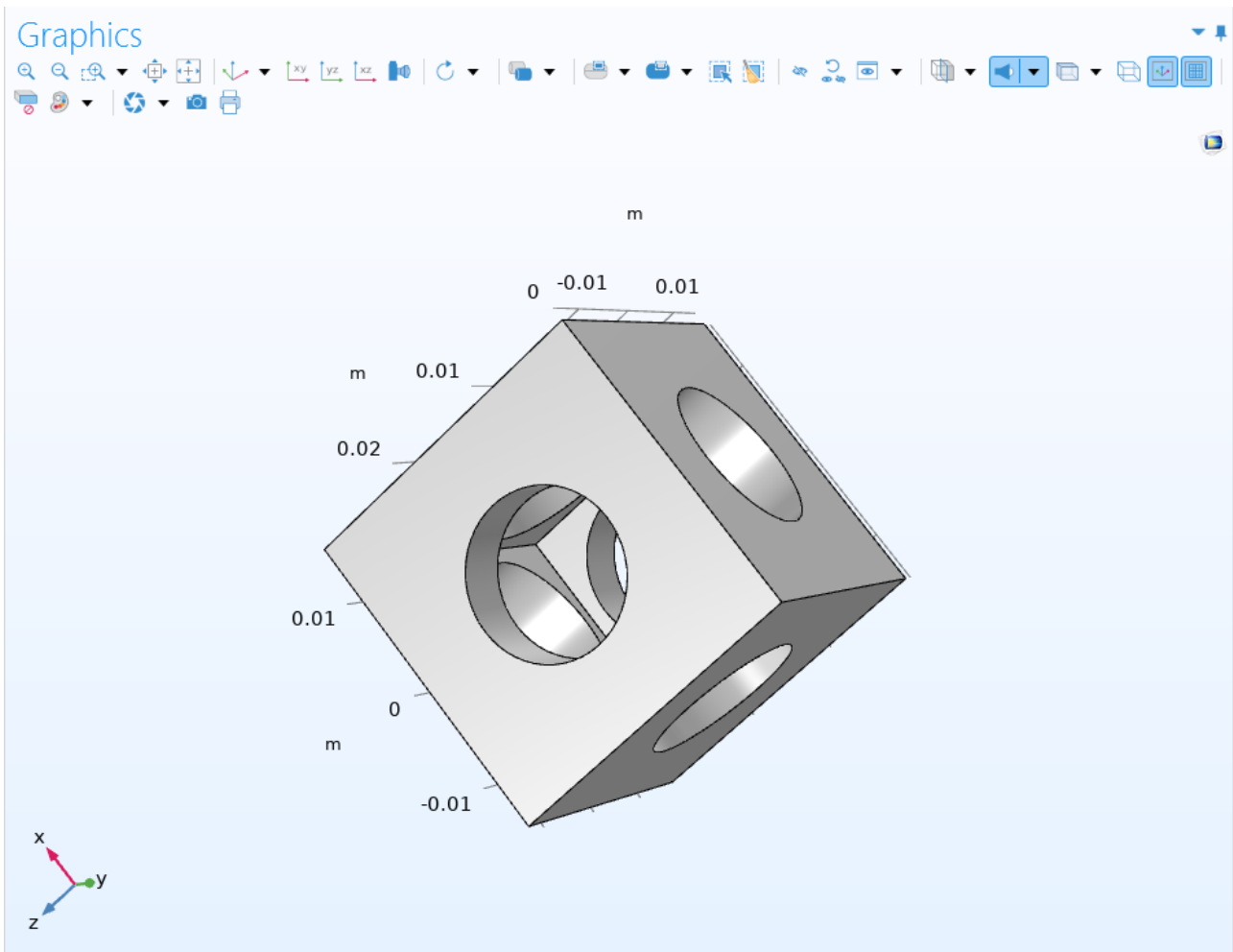


Figure 4 unitary cell

To create the object in COMSOL is important to set the tight scenario to design our model. In this case we choose to operate in *Solid Mechanics* behaviour that also allows to perform eigenfrequency analysis. Once we are in the *Solid Mechanics* is possible to proceed to the cell creation. COMSOL allows you to create objects according to the logic of full minus empty. in this way it is possible to create hollow geometries like the one in our case. To achieve this, we began by creating the objects that would be subtracted from the basic geometric shape. Specifically, three cylinders were created, one along each axis, and intersected. Next, a cube was added with dimensions equal to the side length of the unit cell minus the thickness of the internal walls. This process allowed us to generate the hollow sections of the geometry within the final unit cell. Next step is to create a cube with side size C , superimpose it on the previously created geometry and finally perform the subtraction operation between the two geometries.

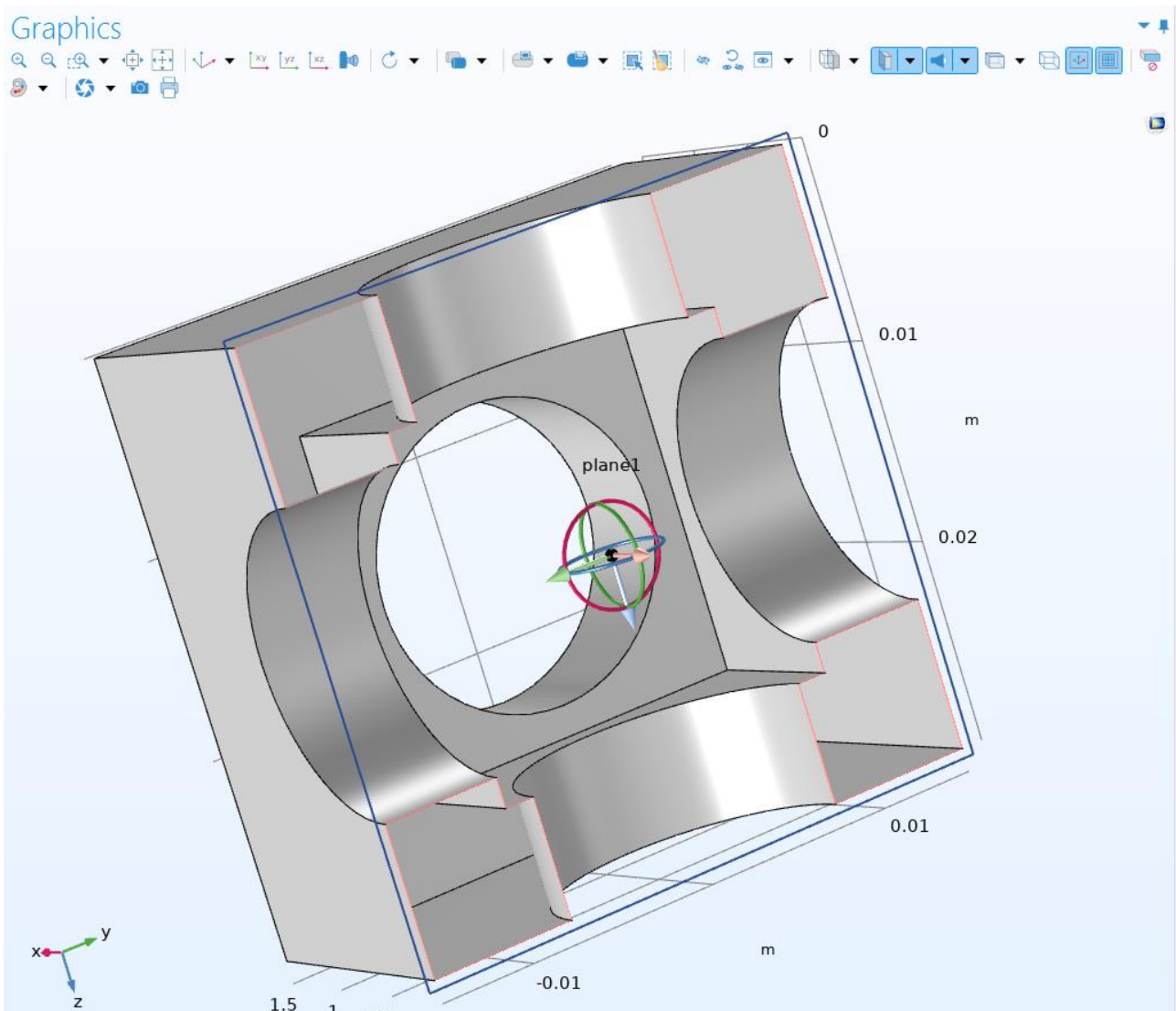


Figure 5 unitary cell section

Then is important to assign the proper material to the unitary cell. In this study the material is NYLON 12 wich has the following characteristics:

Density [kg/m ³]	1000
Young's modulus [Pa]	1.75 e ⁹
Poisson's ratio	0.33

Table 2 Metamaterial characteristics

These are the passages required to create the single cubic metamaterial unit cell. Now the process for defining the simulation is reported. First of all we list some parameters used to setup the simulation

K	0
Sr [mm]	30
kx	if((0<=k)*(k<=1), k*pi/sr,0)

Table 3 simulation main parameters

These parameters will be used to set some operation in the simulation. K is an index used to perform parametric sweep among two values so is settled to its starting value 0, Sr is the value

of the cube edge length and k_x is the wave vector: it is described with an if logic so in this way we can assure some specific in a certain coordinate window. In this case we assure that in a range between zero and $\pi \text{graco}/\text{sr}$ k_x will be computed as the index value k times $\pi \text{graco}/\text{sr}$. In this way we can cover all the values among the selected range to analyze. For all other K value k_x is setted to 0. Another important parameter to set is the mesh to apply to the model and as reported in the paper “the converged mesh lattice is the lattice model that has sufficient number of mesh elements that produce accurate results”¹⁹ and in this case a suggested mesh from COMSOL is used. In the next image is reported the unitary cell with the applied mesh, that is a *physics controlled mesh* with *fine* element size.

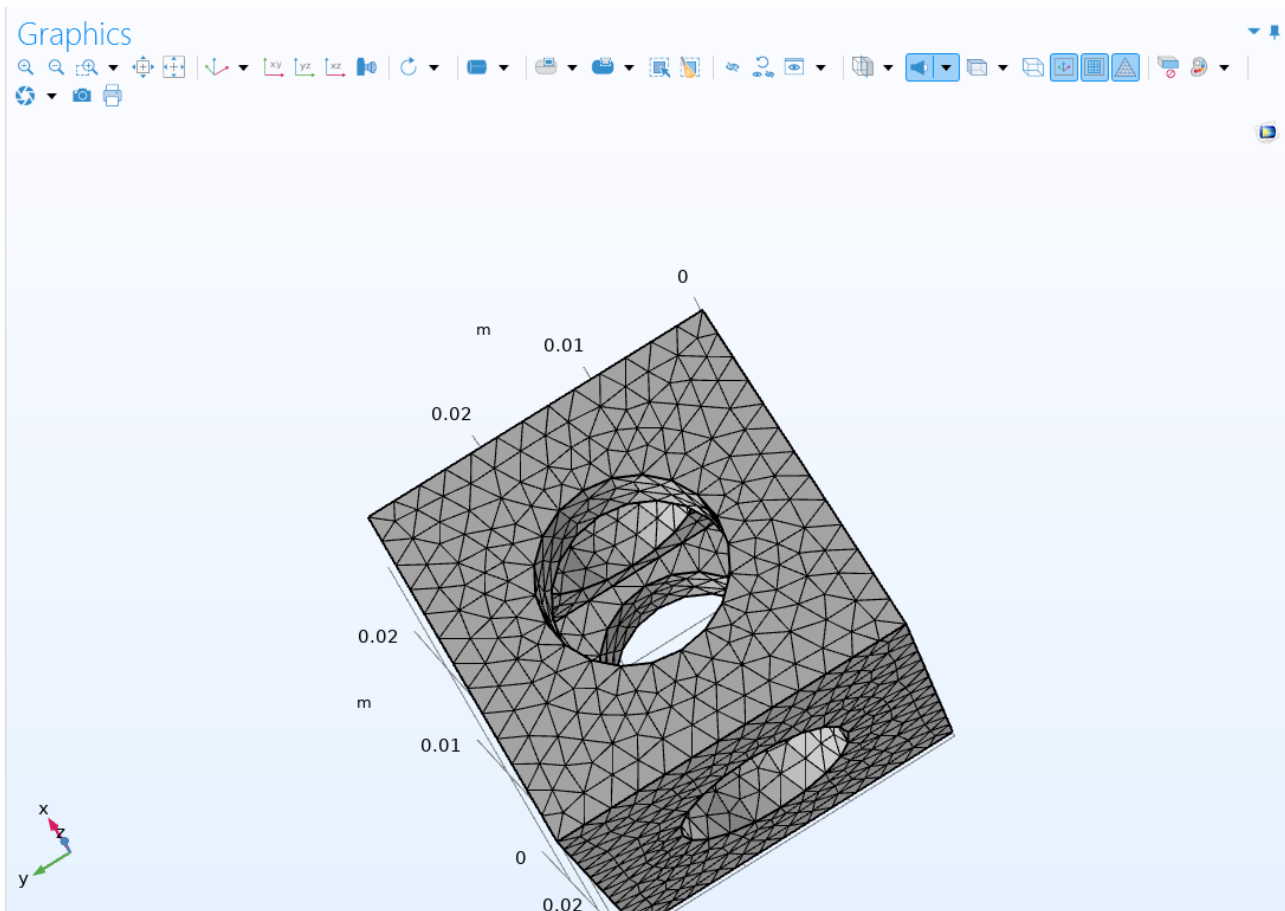


Figure 6 unitary cell mesh

Since in this study the objective is find bandgaps along only one axis, in this case the X axis, Floquet’s periodicity boundary conditions is applied only to the two faces along the X axis. To properly set this condition in COMSOL is important to specify the k-vector along the X axis that is the K_x wave vector previously described. One of the last parameter to set is the *parametric sweep* that is an option that allow us to split a predefined value range. In this case the parameter that goes under the parametric sweep is K and the range 0-1 and we can also decide how many points take in account in this range. To do this the specific function *range* is used. At this point is possible to start the simulation. When the simulation is over, last step is to set the graph representation. In the *Result* section is possible to choose the appropriate graph. In this

case the under 1D Plot Group the *Global* one is chosen. In this way we can select the dataset to display and the parameters to show on each axis. In our case we plot the k vector vector on Y axis while on X axis the frequency is plotted. In order to align the visual representation the frequency is also normalized following this rule: normalised elastic frequency¹⁹ = $f_e \cdot C \cdot v^{-1}$ where f_e is the frequency, C is the edge length, and V is the speed of wave propagation in the elastic medium that is 1322.8 m /s.

The same approach is used to set the simulation for the other two structures taken in account in this work, a beam made of seven cubic cells and a beam made of seven unit cells but with a reduced thickness of 5 mm. For simplicity now the dimensions of the two structures are reported and not the entire process of creating the model as it is identical to that explained above for the cubic cells.

The seven cells beam has a length of 210 mm while other dimensions are 30 mm like the cube cell and is made of the union of seven unitary cell along X axis. The material assigned to this structure is Nylon 12.

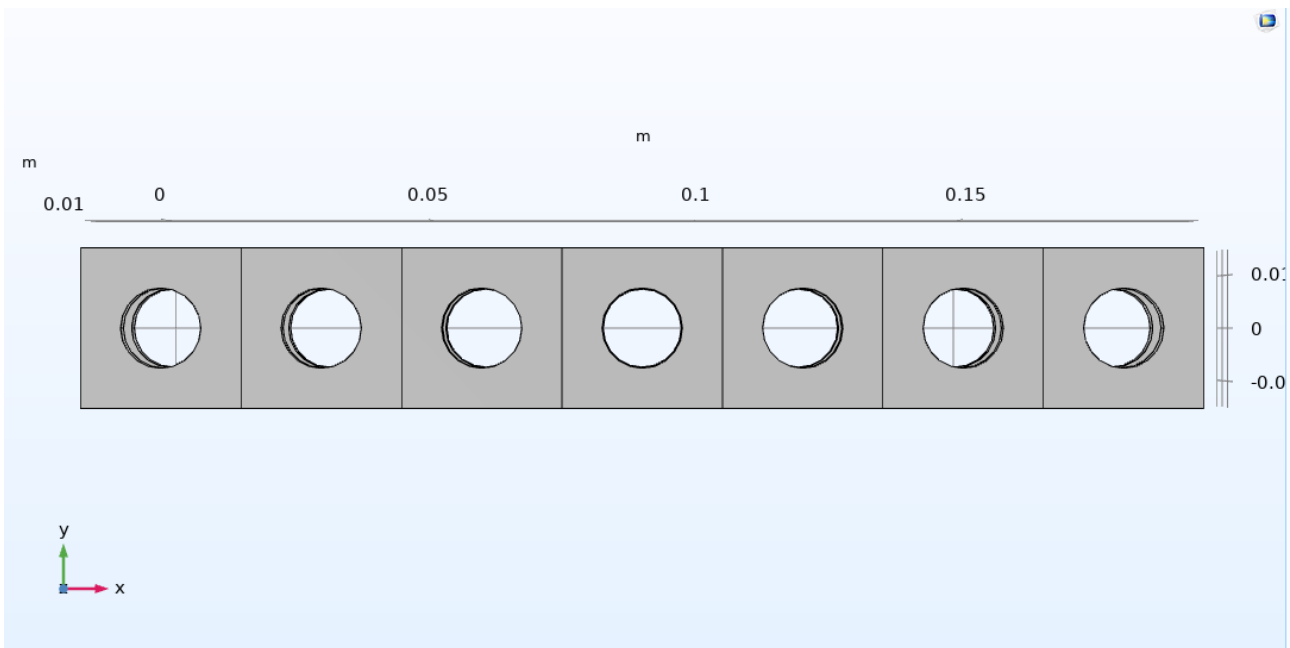


Figure 7 7 cells beam

A similar approach is applied to the thicker beam, where a series of seven unit cells, each with a reduced wall thickness of 5 mm, are connected in sequence. Unlike the thinner configuration, the thicker beam features solid faces without any perforations, meaning the holes are present only in one direction rather than passing through the entire structure. The material assigned for this configuration is also Nylon 12.

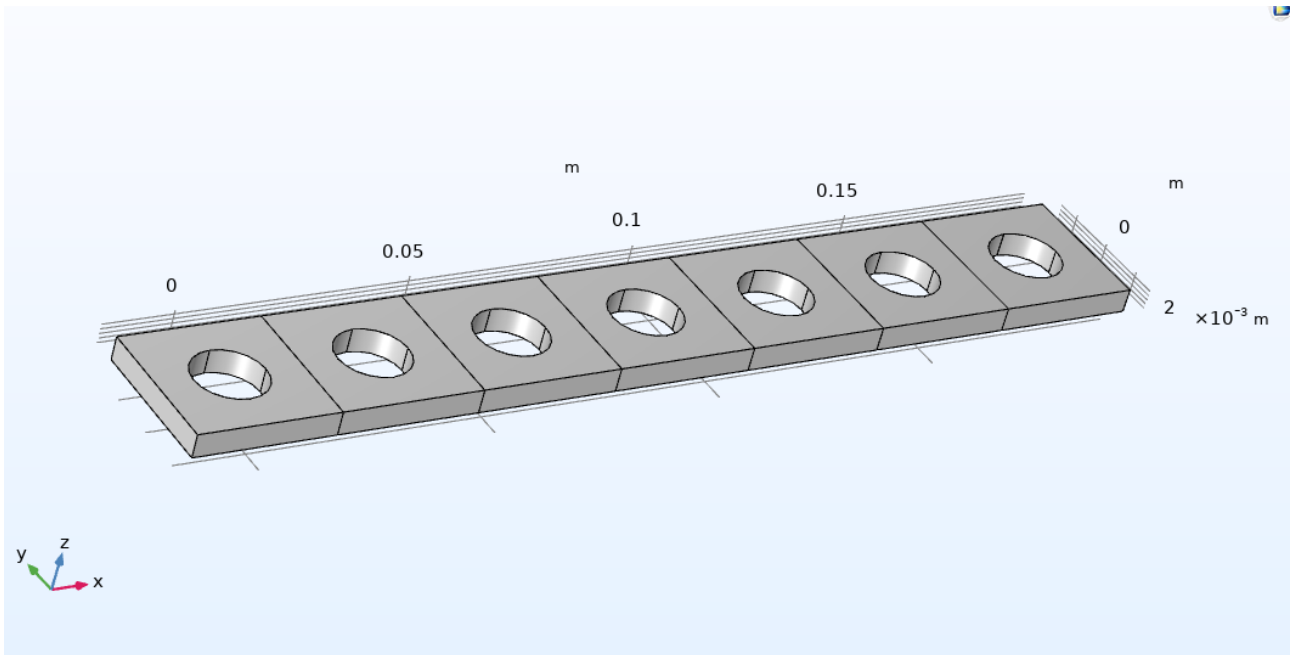


Figure 8 reduced thickness beam

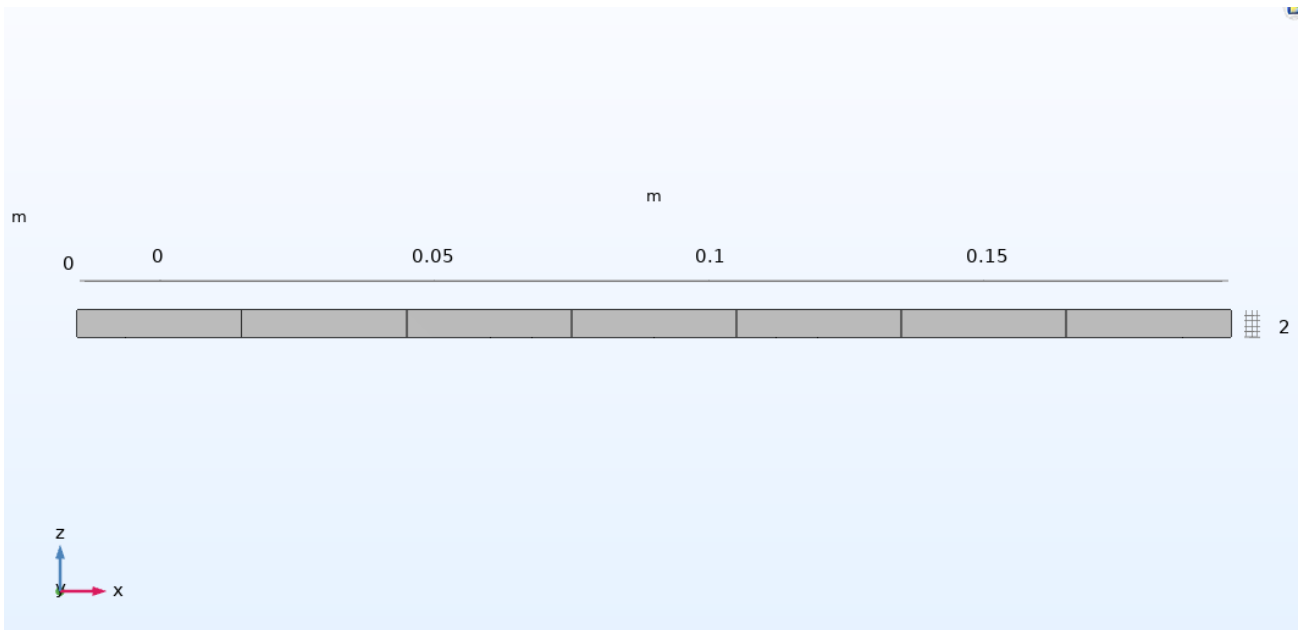


Figure 9 detail of thicker

2.2 Models geometric validation

In this part of the report will be highlighted the relative differences between the eigenfrequency presented in the paper and in another thesis work developed on metamaterials properties versus results obtained in COMSOL for the model used in this thesis. This is done in order to verify if the geometry developed in COMSOL are the same or very similar to the one presented in the paper used as reference. To do that was necessary to extrapolate some data from graphs presented both on the reference paper and from thesis work defended by one of Politecnico colleague Miceli¹⁶. Eigenfrequency values are extracted from transmissibility graphs.

First of all, a model of the structures under investigation are replicated in the COMSOL model scenario. Two different structure are replicated: a beam composed by 7 single metamaterial cell block and a plate composed by 7 single metamaterial cell block but with a reduced thickness of 5 mm. Then boundary conditions are applied. In this specific case only the first edge in X direction to simulate a structure with only one constrained extreme. All other faces are left free to move in all directions X,Y,Z. Is important to remind that also in this case the material assigned to the structure is NYLON 12. The same setup is imposed to both structures. Last passage is to assign a mesh to the structure, the select one is a *finer* mesh in order to have better confidence to obtained results.

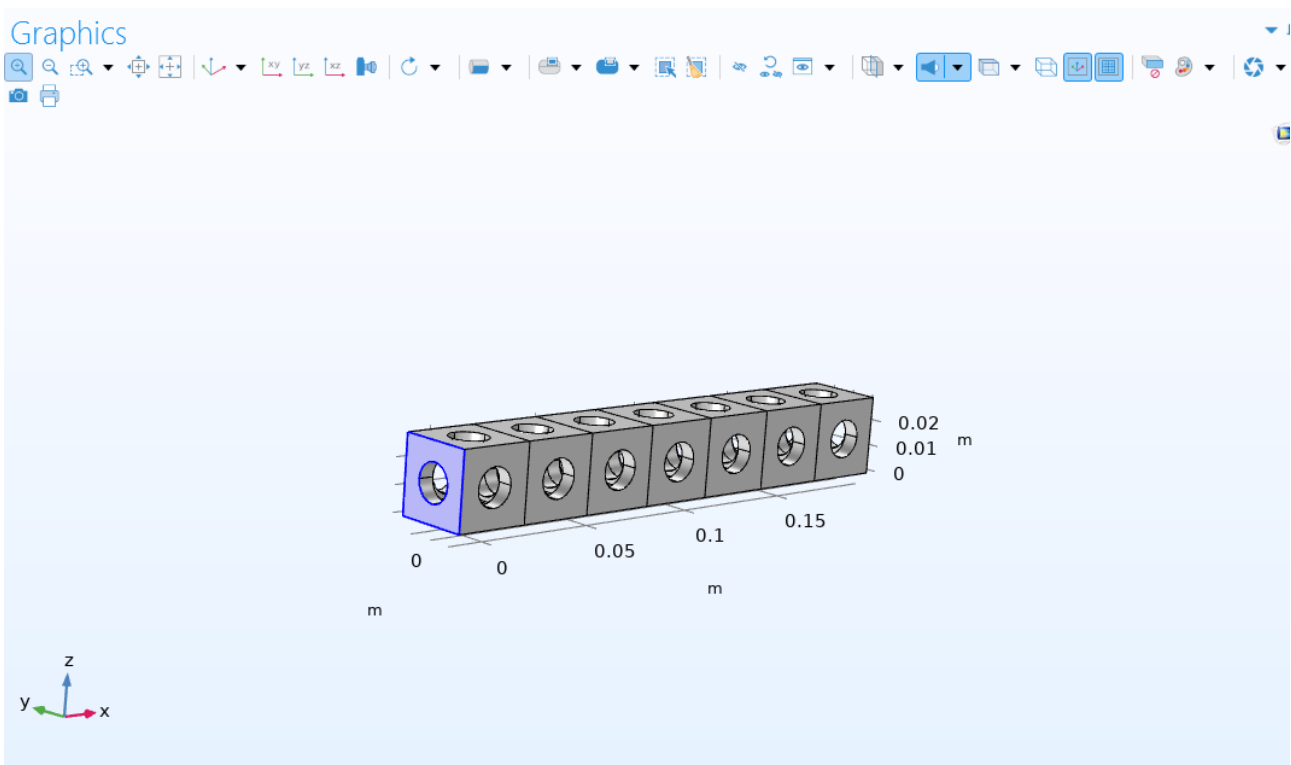


Figure 10 7 cells beam with bounded edge

The light blue faces is the one constrained. COMSOL allow to perform eigenfrequency analysis in the *Solid mechanics* scenario that was the one in which models are created. After that this brief set up is completed the other parameters to choice is number of eigenfrequency that the program will find. To cover the same frequency spectrum considered in previous work, that was

15000 Hz, is needed to find 80 eigenfrequency for the beam made of 7 cubes and 70 eigenfrequency for the plate with reduced thickness.

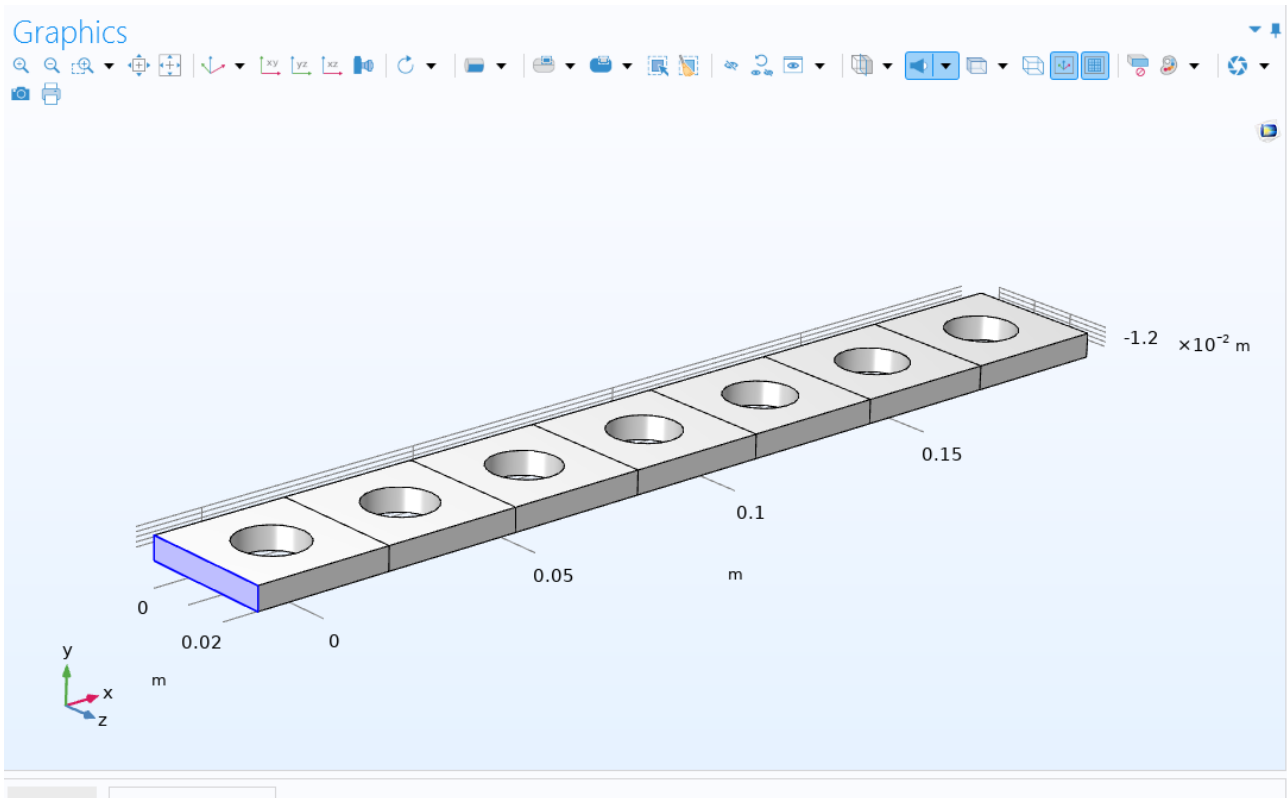


Figure 11 beam with reduced thickness with bounded edge

As example is reported a representation of the mesh applied to the structures.

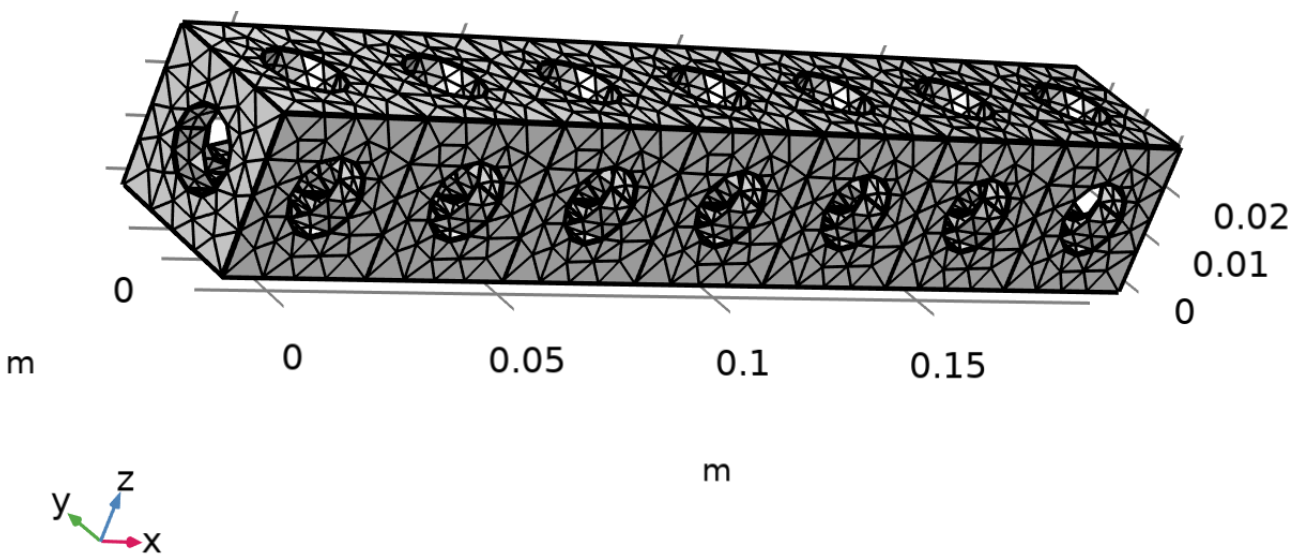


Figure 12 mesh applied to the structure

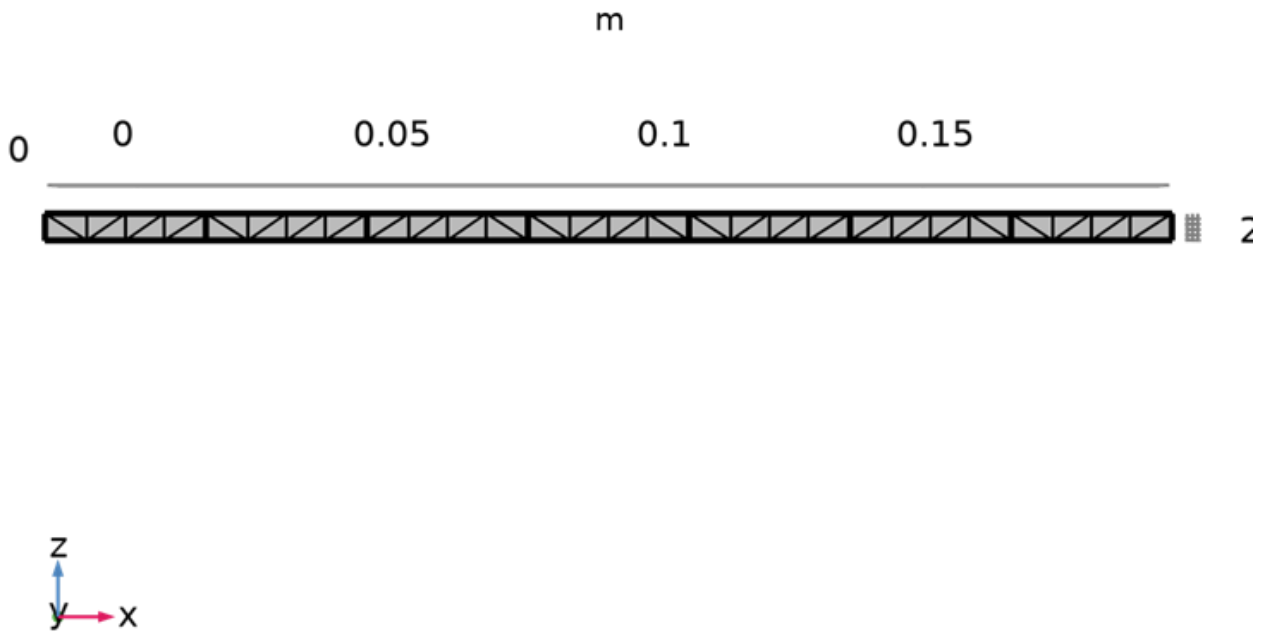


Figure 13 mesh applied to the structure

The paper graph used as reference for the comparison is the following one:

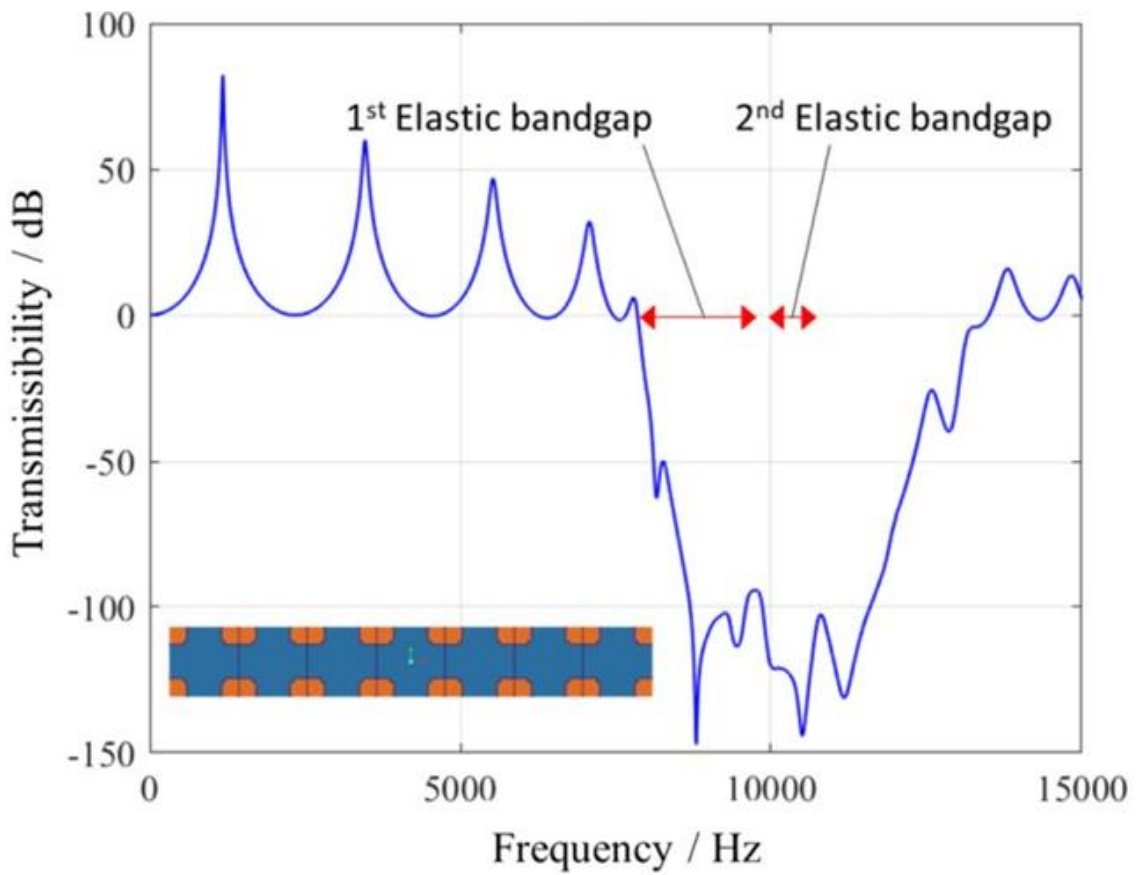


Figure 14 transmissibility of paper metamaterial

While graphs extrapolated from Miceli's thesis are:

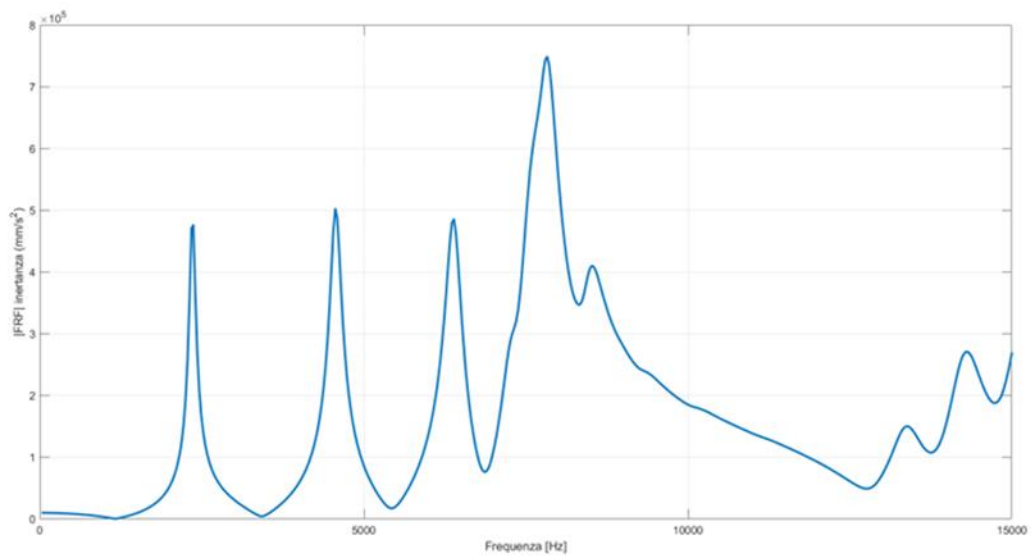
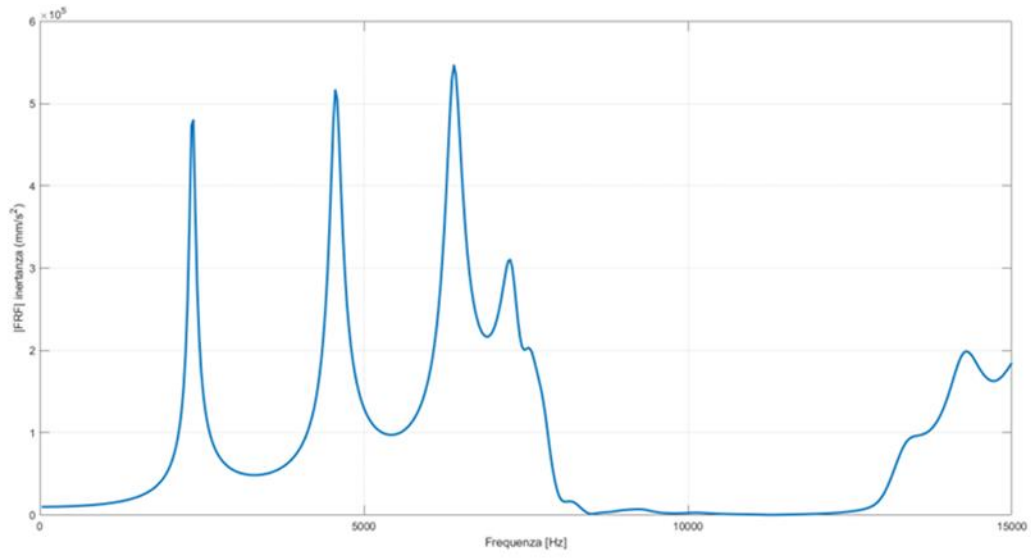


Figure 14 inertances of metamaterial from Miceli's thesis

Comparison of metamaterial(blue line) vs. Miceli thesis test sample

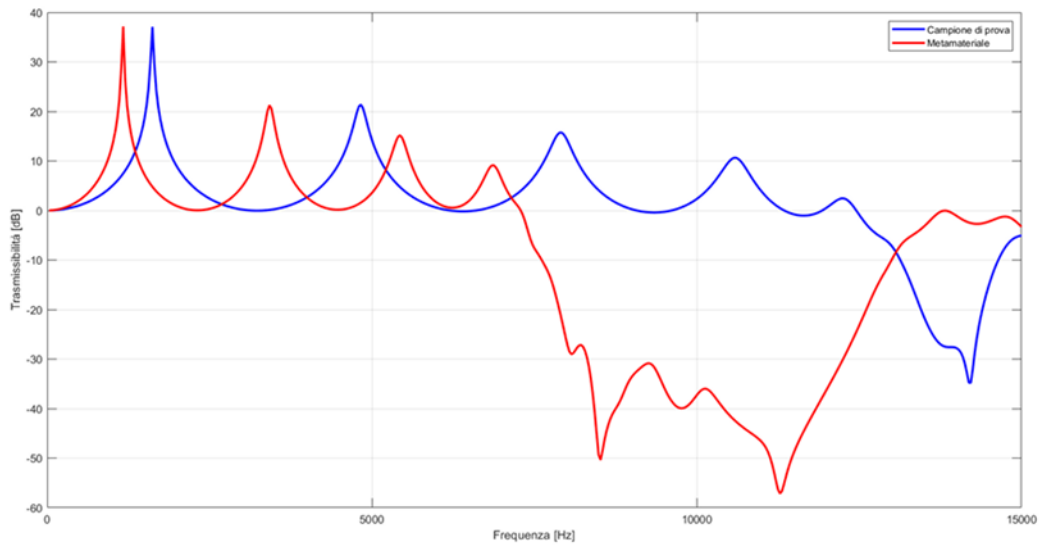


Figure 15 transmissibility comparison from Miceli's Thesis metamaterial 7 cells beam

Thesis comparison perforated flat plate vs non-perforated plate (blue line).

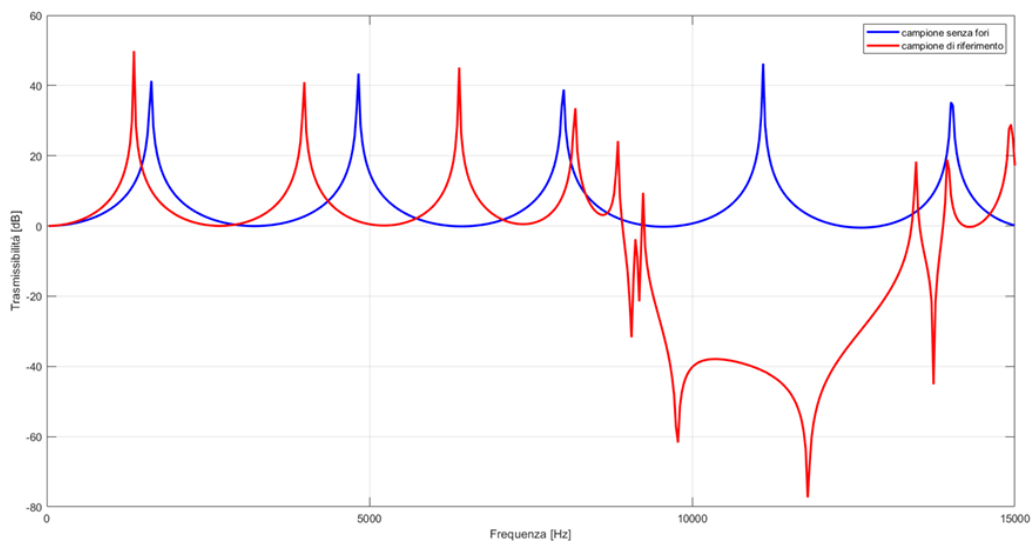


Figure 16 transmissibility comparison from Miceli's thesis of reduced thickness beam

Here are reported the results obtained carrying on this compare. Reminding that eigenfrequency taken as reference are those corresponding to the peaks in the graphs above, this comparison do not involve all eigenfrequency that came from the modal analysis. Following step is choice for each eigenfrequency used as reference the corresponding

eigenfrequency among those obtained from the analysis carried out in COMSOL. the criterion in this case was to choose an eigenfrequency that was in the same frequency range as those taken as reference. Then is just a matter to compute the percentage difference between that two values. The following tables show the eigenfrequencies considered and the relative differences. In this way it is possible to estimate the error that is created between the results taken as reference and those obtained from the COMSOL simulations used in this work.

Eigenfrequencies for 7 cells beam from paper	COMSOL values	Difference in %
1135,3	1210,1	6,18
3422,1	3558,7	3,84
5485	5268,2	-4,12
7052,2	7061,2	0,13
7803,8	7831,8	0,36
12569,2	12478	-0,73
13816,6	13839	0,16
14856	14824	-0,22

Table 4 eigenfrequency 7 cells beam from paper

Inhertances for for 7 cells beam from Miceli's Thesis	COMSOL values	Difference in %
2368,4	2610,8	9,28
4549,8	4362,8	-4,29
6398,8	6264,8	-2,14
7271,4	7259,5	-0,16
14303,7	14253	-0,36

Table 5 eigenfrequency 7 cells beam from paper

Eigenfrequencies for 7 cells beam from Miceli's thesis	COMSOL values	Difference in %
1145,1	1210,1	5,37
3435,4	3558,7	3,46
5451,6	5268,2	-3,48
6854,8	6799,3	-0,82
13838,7	13839	0,00

Table 6 eigenfrequency 7 cells beam from Miceli's thesis

Eigenfrequencies for reduced thickness 7 cells beam	COMSOL values	Difference in %
1316,3	1354	2,78
3949	4012,8	1,59
6403	6474,7	1,11
8190,6	8148,5	-0,52
8856,9	8787,2	-0,79
9263,2	9260,1	-0,03
13488,6	13675	1,36
14008,6	13675	-2,44
14983,7	14872	-0,75

Table 7 eigenfrequency 7 cells reduced thickness beam from Miceli's thesis

Looking at the results obtained it can be seen that the highest errors are found at low frequencies while going to higher frequencies the errors become much smaller, almost negligible being in the order of 0%. This trend is observed in all comparisons carried out. Taking into account the results obtained, it can be stated that, as regards the creation of the object in COMSOL and the assigned material, the model can be considered reliable for the continuation of the study being undertaken as it provides results similar to those obtained in the paper and in Miceli's thesis.

2.3 Paper presented results

Here are briefly reported results presented in the paper and used as reference for this work. The following graph report bandgaps found for the metamaterial with same characteristics and ratio between the dimensions $d/C = 0.5$, $L/C = 0.2$ and a Poisson's ratio = 0.33 where d is the diameter of the hole, C is the edge of the cube and L is the neck length.

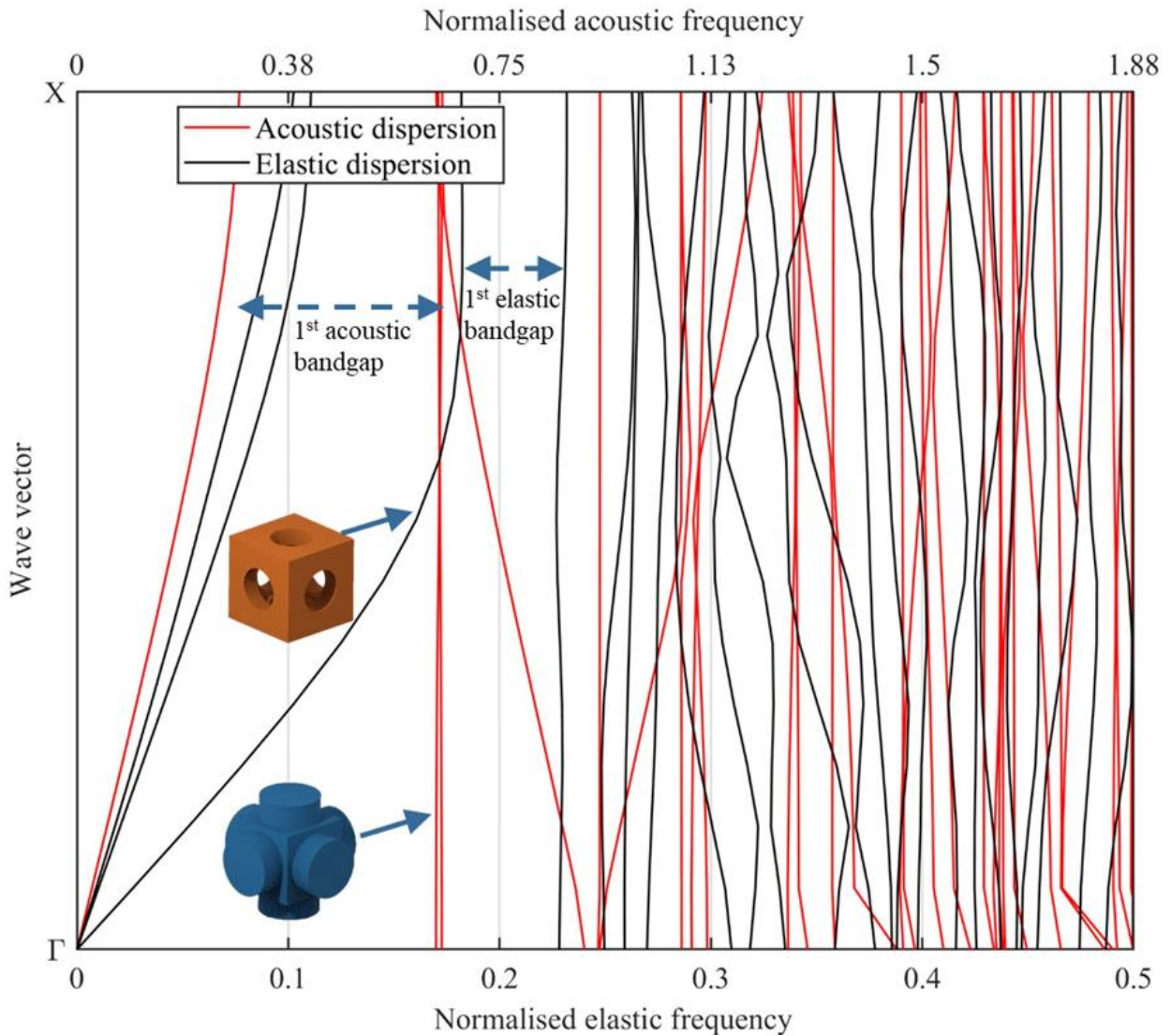


Figure 17 paper simulation result¹⁵

The part of the graph to take in account is the one related to the elastic part and so the black lines. As it possible to notice there is a very noticeable bandgap in the first half of the graph and then there are multiple smaller bandgap going up in frequency domain.

Chapter 3

Carried out simulations

3.1 Simulation with Floquet periodicity along X axis and k_x wave vector

Since the main scope of this thesis was to try to find elastic bandgaps only in one direction, many different simulation attempts were performed to try to find the best results. First of all the focus is to obtain the desired result on the cubic cell and then apply the same on the other two structures presented. The parameters on which we focused, and which therefore were subject to modifications during the various simulations, are the following: the Floquet conditions, boundary conditions or any constraints, wave vector. Wave vectors is quite the most critical parameter since it allow to describe in an effective way the irreducible Brillouin zone. The irreducible Brillouin zone is defined as “in the reciprocal-lattice space the interval $-\pi < k < \pi$ would be known as the 1st Brillouin zone, and every $2\pi /s$ interval outwards from the 1st zone would be the 2nd, 3rd, 4th, and so on. The 1st zone is usually the focal point because the dispersion curves are the same in other zones when the periodicity is simple”¹⁷. In the first simulation Floquet conditions are imposed only to the two faces along X axis. Just one wave vector is discretized along the X axis k_x and is supposed to propagate along X axis. The expression used in COMSOL is the following one $if((0 \leq k) * (k \leq \pi / sr), k * \pi / sr, 0)$. With this expression is possible to investigate all the points along the X axis.

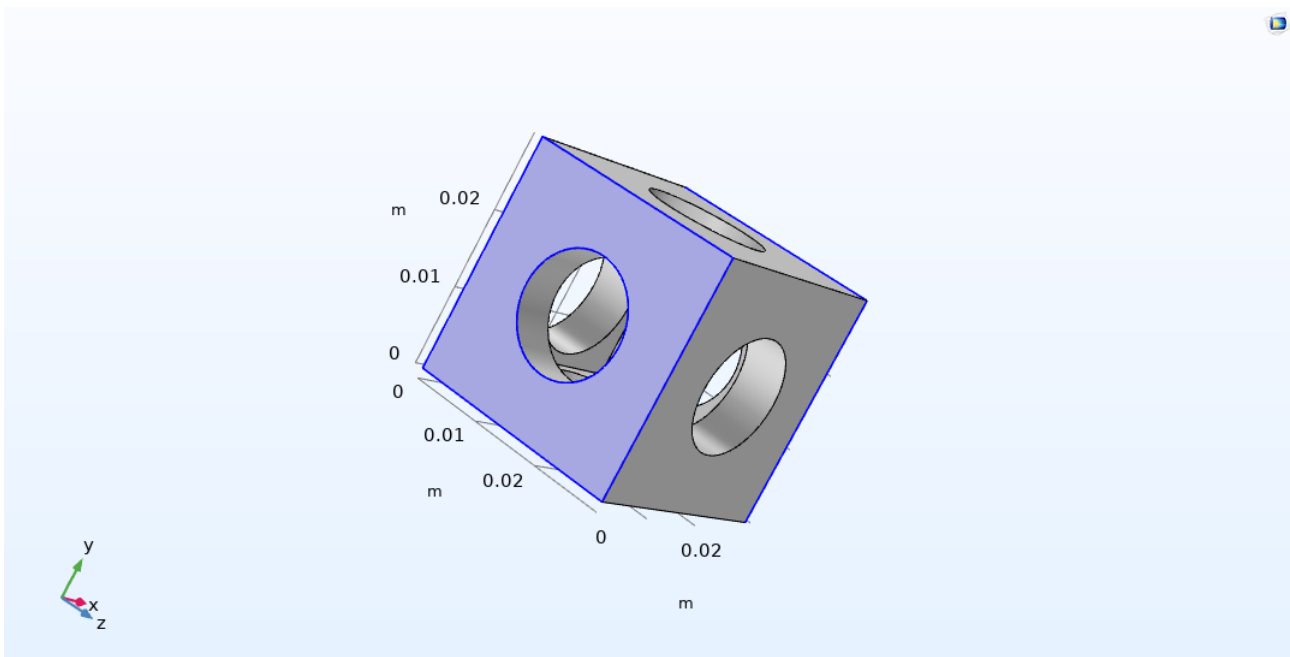


Figure 18 face with Floquet condition applied-source

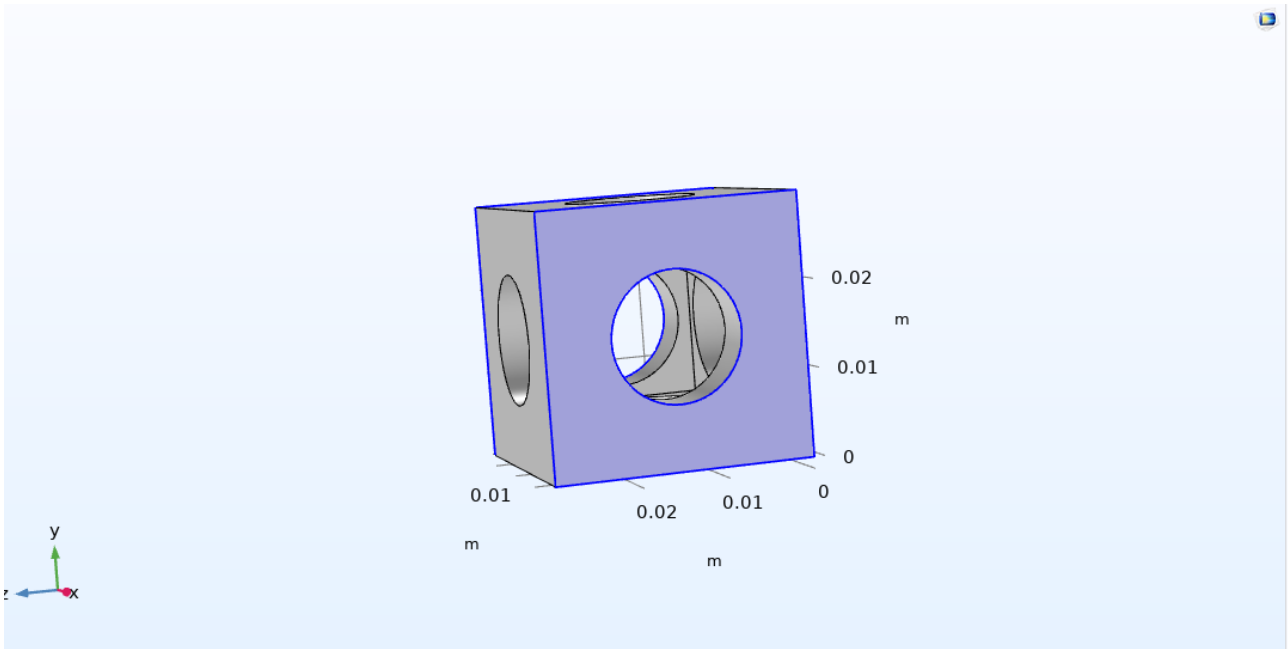


Figure 19 face with Floquet condition applied-destination

The results for this simulation are reported in the following graph

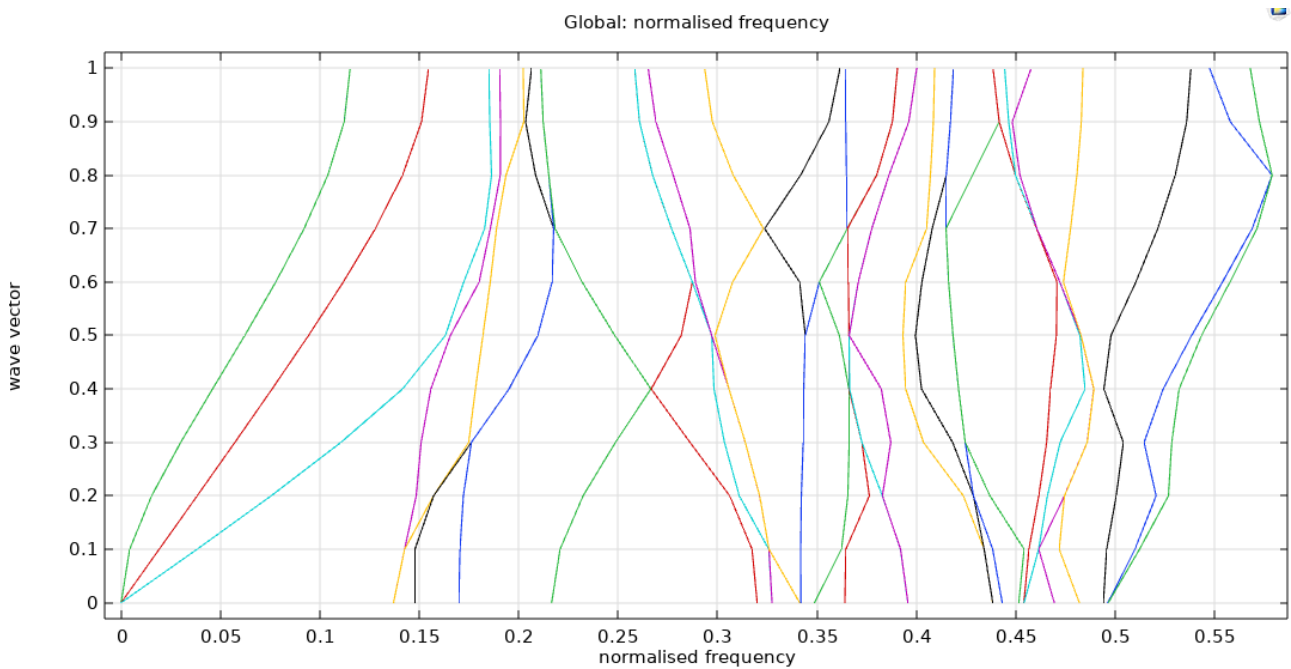


Figure 20 simulation result for Floquet periodicity along X axis and k_x wave vector

Looking at the graph is possible to notice the same frequency domain as the one presented in the paper, and also the same trend of the modes along the selected domain of propagation along the structure. What's missing is the evidence of the main bandgap in the first part of the graph. For this simulation the origin of the Cartesian axes was located at the edge of the cube. Other tests were also carried out by placing the origin of the axes both at the center of the cube and at the center of the face on which the Floquet condition had been assigned. In all cases the

results are the average, confirming the fact that the origin of the axes does not influence the behavior of the structure and the software calculation methodology.

3.2 Simulation with Floquet periodicity along X axis and k_x, k_y, k_z wave vector

In this simulation have been added other two wave vector k_y and k_z discretized in the same way as did in the previous simulation for the k_x wave vector. Doing that we can allow the wave to move in three direction but only on faces along X axis since Floquet periodicity is imposed only on the two faces along X axis.

Unfortunately result obtained is the same as the previous simulations putting in evidence that the wave vector that most influence the behavior is the vector along the same direction on which the Floquet conditions were imposed.

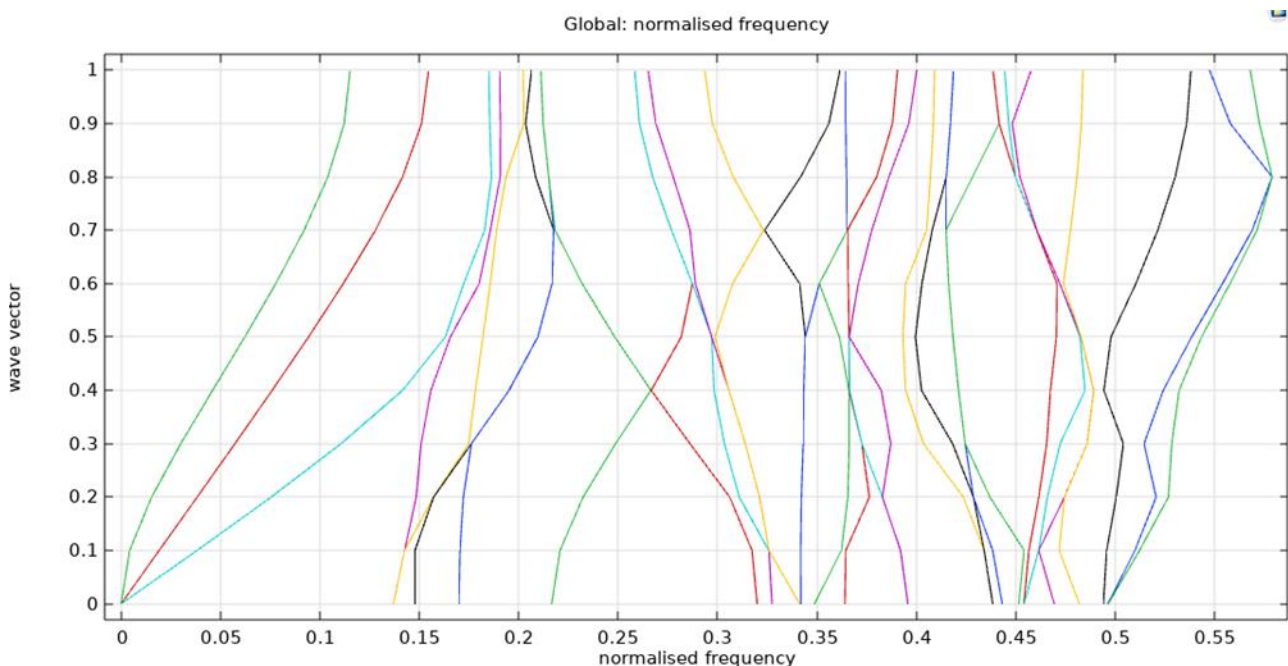


Figure 21 simulation result Floquet periodicity along X axis and k_x, k_y, k_z wave vector

Since results obtained are not good enough to put in evidence the bandgap the variables that can modify the behavior of the metamaterial are the Floquet periodicity condition and the definition of the irreducible Brillouin zone. To do that other simulation are carried out but with different parametrization of the Brillouin zone. As referred by the author “to mathematically model the elastic wave propagation, the contours of the irreducible Brillouin zone (IBZ) of the unit cells of the metamaterials were scanned”¹⁸. Following this approach is possible to define a 3D IBC putting Floquet periodicity on faces along all X,Y,Z axis and parameterizing three wave vector k_x, k_y, k_z .

3.3 Simulation with Floquet periodicity along X,Y,Z axis and k_x, k_y, k_z wave vector

As explained in the previous paragraph this simulation is settled following the approach explained to define a 3D IBC. The parametrization used for the three wave vector is the same as the previous simulation so using an *if* logic in this way we can control, thanks to a sweep, the parameter of the wave vector along the propagation axis. In the section *solid mechanics* three different Floquet periodic condition are defined one for each propagation axis, choosing a face of the cube as source and the opposite face as destination.

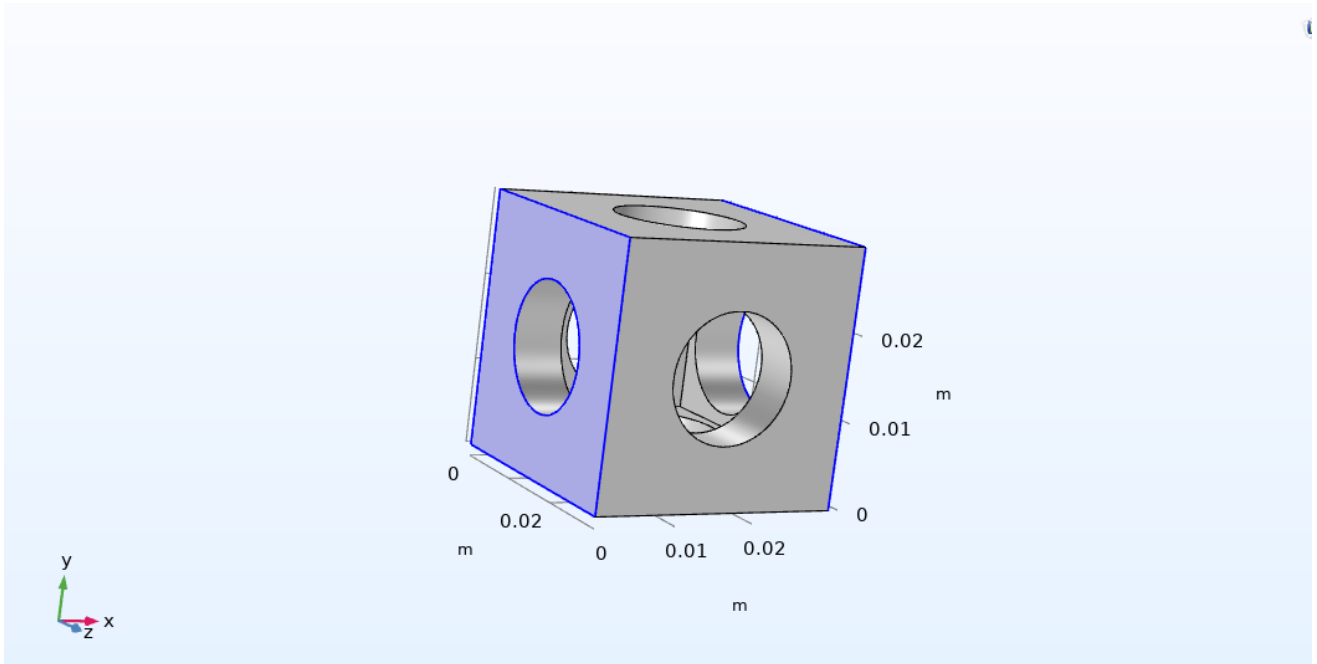


Figure 22 Floquet periodicity imposed along X axis

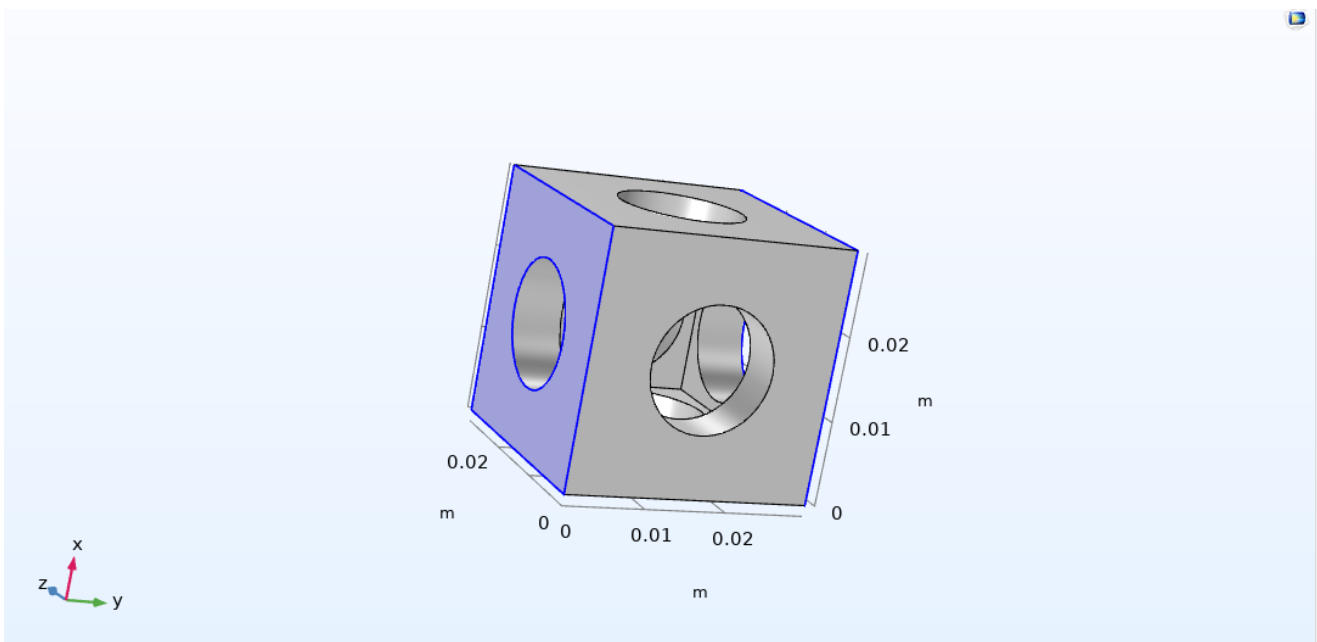


Figure 23 Floquet periodicity imposed along Y axis

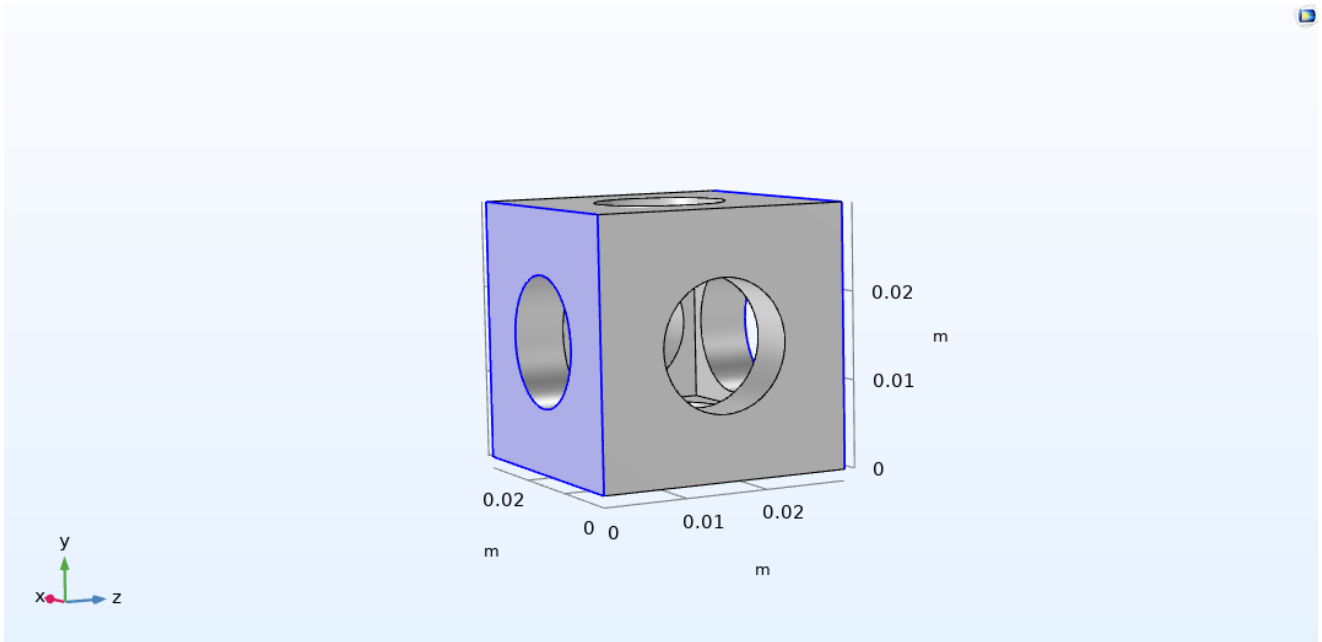


Figure 24 Floquet periodicity imposed along Z axis

Then the Floquet periodicity propagation vector is defined along three axis using the three k_x , k_y , k_z wave vectors.

Type of periodicity:

Floquet periodicity

k-vector for Floquet periodicity:

k_x	X	rad/m
k_y	Y	
k_z	Z	

Figure 25 k_f definition

Result obtained with this simulation is reported in the following image. Imposing this type of Floquet periodicity and allowing the wave to move along three axis the frequency range, for the same number of eigenfrequency found, is quite doubled. Also in this case a big evident bandgap is not found. Bandgaps are formed by the destructive interference of their waves¹⁹²⁰²¹. When a wave travels from one medium to another of less local impedance, for example, an acoustic wave changing its speed when moving from a thin neck to a larger cavity, some of the waves get reflected. When a reflected wave is in phase with the travelling wave, both waves interfere destructively with each other. This destructive interference of the reflected wave and the travelling wave results in the creation of bandgaps¹⁵. This is the physics behind bandgap formation explained by the author in the paper so it depends mostly on the shape of material and how the wave propagation is defined internally, i.e. by the boundary of the IBC.

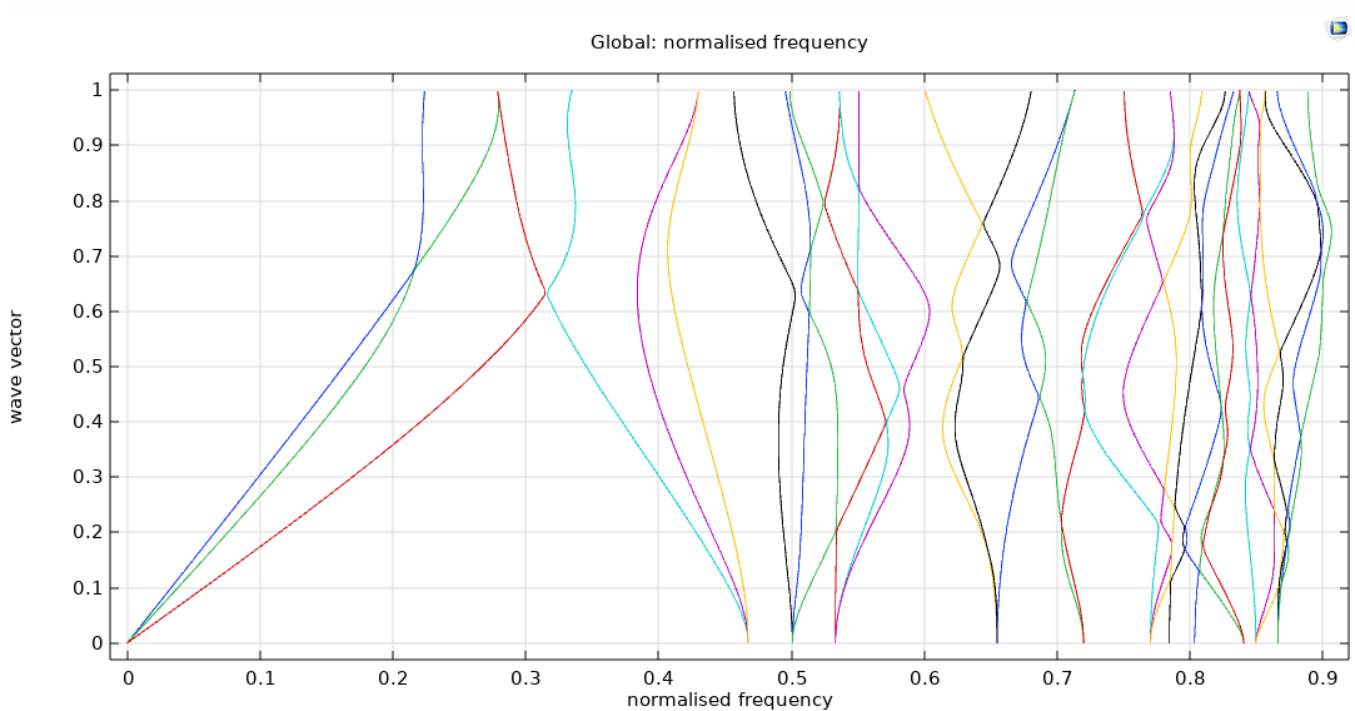


Figure 26 simulation result Floquet periodicity on X,Y,Z axis and k_x, k_y, k_z wave vectors

3.4 Simulation with Floquet periodicity along X,Y,Z axis and k_x, k_y, k_z wave vector with scaling factor

Since the approximation and simulation done till before were not good enough another approximation is tested. In this case is added a scaling factor in order to reduce the influence of the k_y and k_z wave vector in order to try to put in evidence what happens only along X axis. To do that the scaling factor is added in the wave vector parametrization and as example the expression is here reported: $\mathbf{k}((0 \leq k) * (k \leq 1), k * \pi * 0.1 / \text{sr}, 0)$. As is possible to note in this expression the highlighted number 0.1 is the scaling factor added while the k_x wave vector expression is the same as previous simulations. Different scaling factor are tested in the range of values between 0 and 1 but here for simplicity are reported just the two that gave better results that in the specific are the scaling factor 0.1 and 0.25. As is possible to note in the graphs reported in these two cases bandgaps starts to create. The frequency range is quite higher compared to the one in the paper but at least a similar behavior it was obtained. Going little bit in deep on this graph analysis, for what concern the 0.1 scaling factor case, is possible to put in evidence a bandgap in conjunction with the 0.3 value of the normalized frequencies that translated in frequency is a wide bandgap of 962 Hz between 13233 Hz and 14195 Hz. Narrower bandgap can be noted in conjunction with the 0.6 value of the normalized frequencies. On the other hand in the case where 0.25 scaling factor is imposed can be appreciated a little difference in the bandgaps position. The first big bandgap is little bit shifted at lower frequencies in fact the bandgap is between 12359 Hz and 13557 Hz.

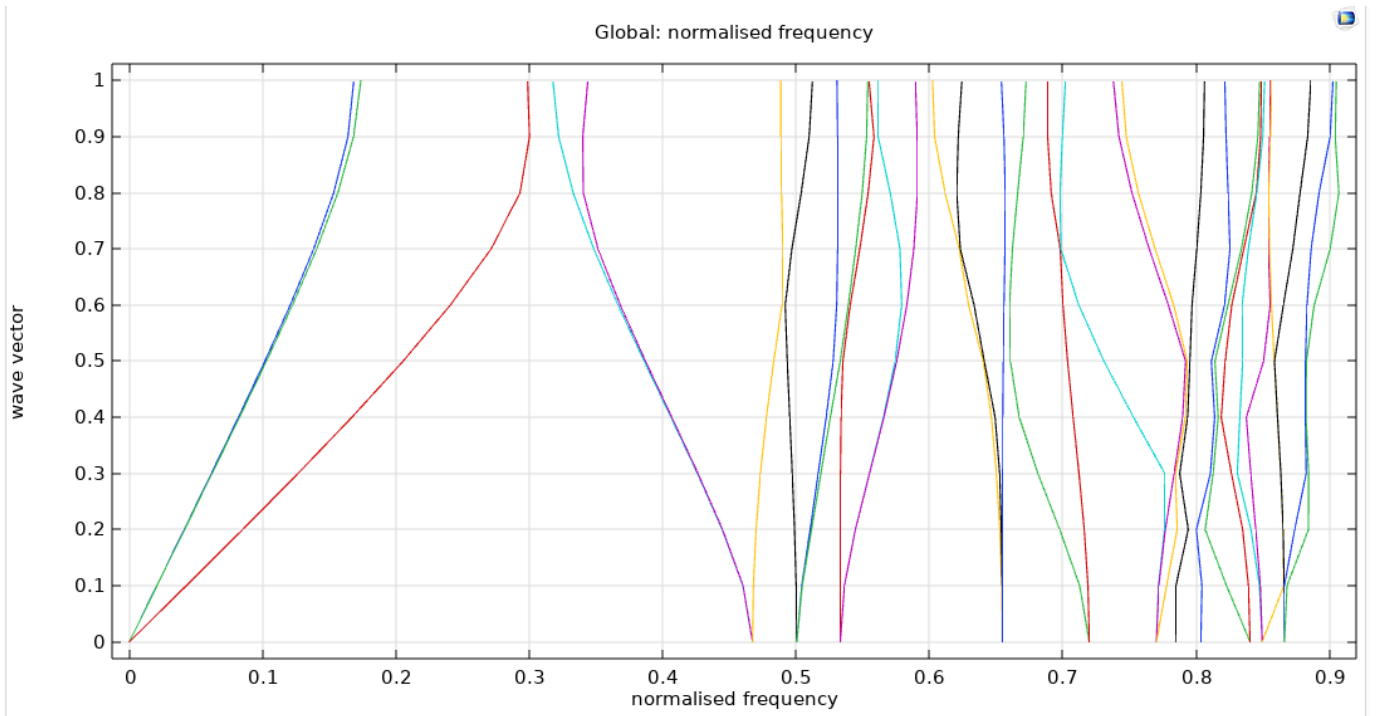


Figure 27 simulation result for k_y and k_z wave factor scaled by 0.1

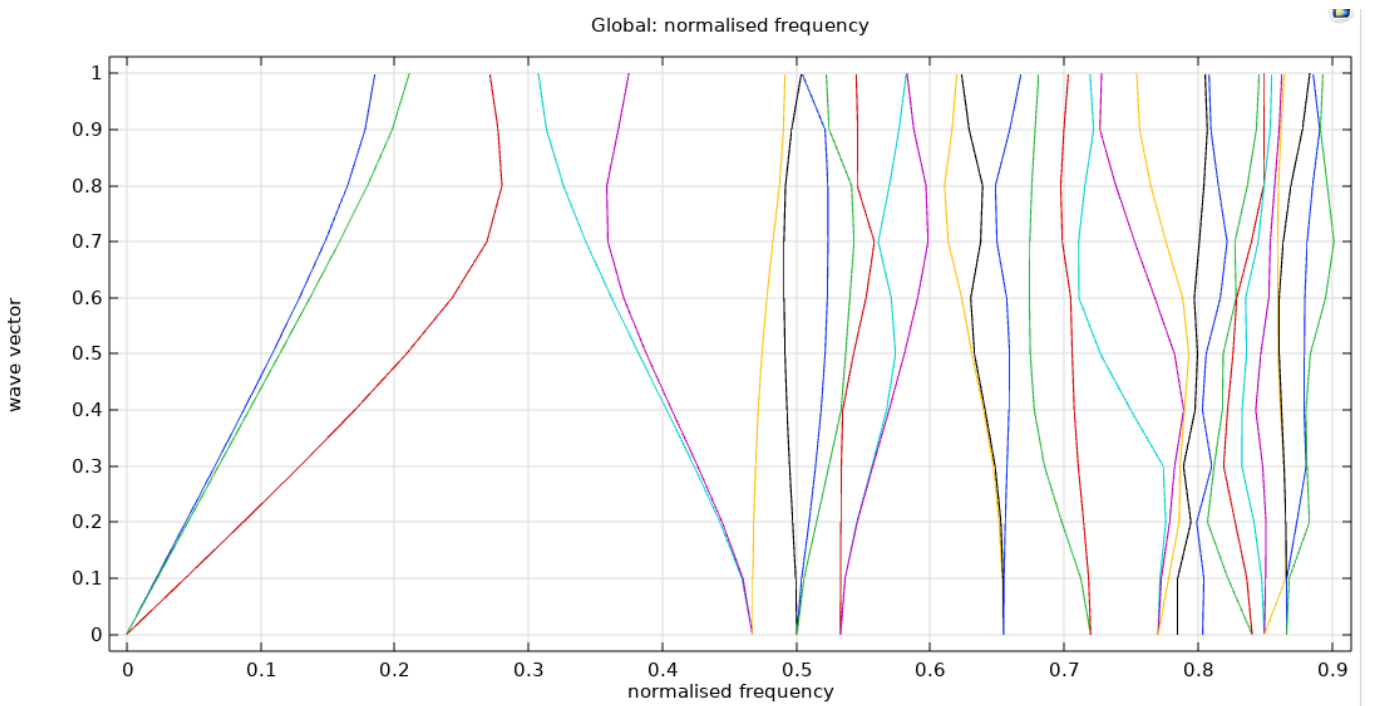


Figure 28 simulation result for k_y and k_z wave factor scaled by 0.25

Also in this case the bandgap is around 1000 Hz wide and going un in frequency domain can be found other narrower bandgaps 0.6 and 0.7 values of normalized frequency.

3.5 Simulation with Floquet periodicity along X,Y,Z axis and k_x , k_y , k_z wave vector with scaling factor 0

Following the approach described in the previous paragraph another attempt to find if despite the presence of wave vectors k_y and k_z but multiplied by a factor of 0 in such a way as to eliminate their influence in the model can lead to obtaining a more satisfactory result.

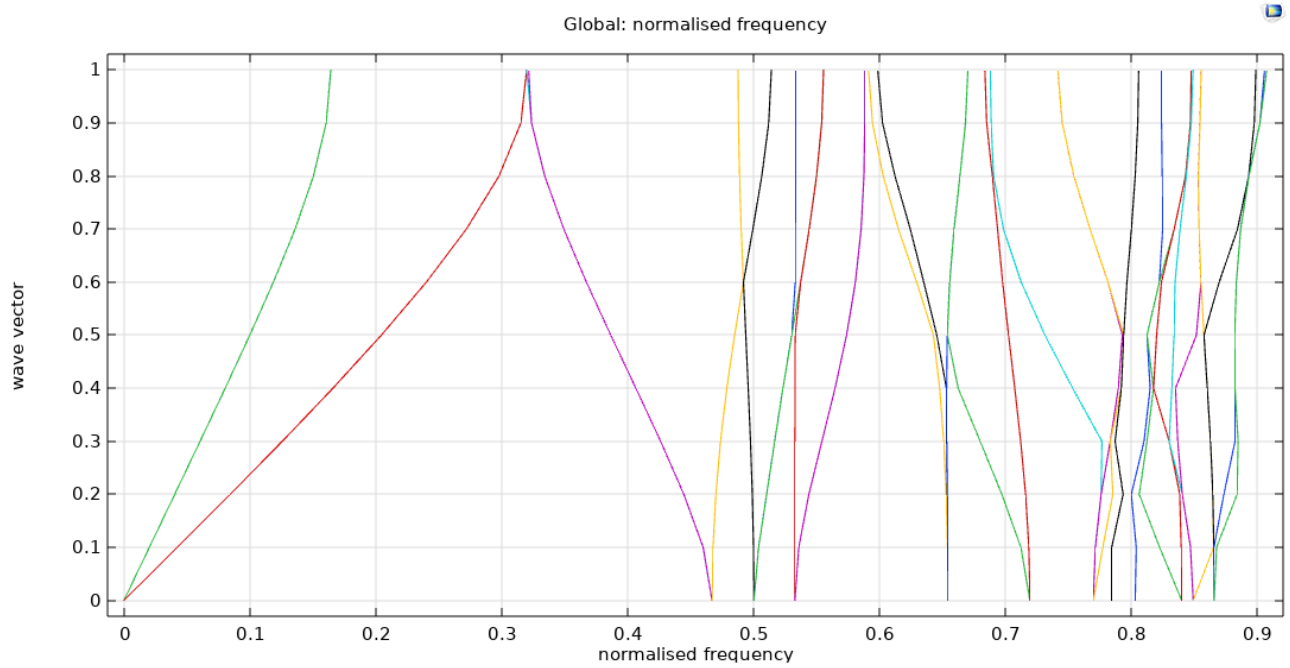


Figure 28 simulation result for k_y and k_z wave factor scaled by 0

Unfortunately this setup does not guarantee an acceptable scenario as it erases the bandgaps that were created in the previous simulations.

Chapter 4

Carried out simulations on finite elements

In this part will be reported the simulations and the analysis done on the finite elements, so the 2 beams presented in chapter 2. Moving forward in this study the second part is focused on replicate in COMSOL the results presented on paper for what concern the beam made by 7 cubic cells and on Miceli's Thesis for what concern the plate with reduced thickness. Here are not available graphs with bandgaps for both structures, but transmissibility graphs are used to carry on this comparison. The logic behind this comparison is that in concomitance of reduction of transmissibility should be find the presence of a bandgap. Graphs used as reference are the same presented in paragraph 2.2.

4.1 Simulation with Floquet periodicity along X axis and k_x wave vector for plate with reduced thickness

The simulation has the same configuration of the one carried out for the cubic cell in chapter 3. Of course the only parameter changed is the length along the X axis passing from 30 mm to 210 mm. Floquet periodicity is always imposed on the two faces along X axis, but in this case these faces are not characterized with a hole but are simple plate.

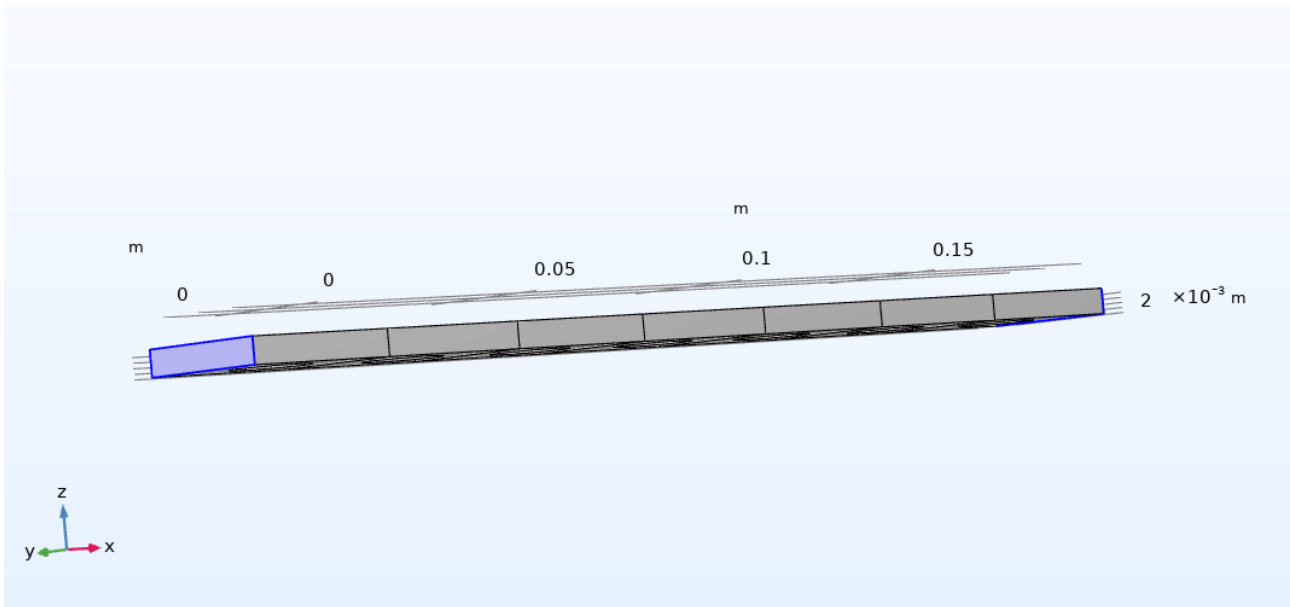


Figure 29 imposed Floquet condition representation

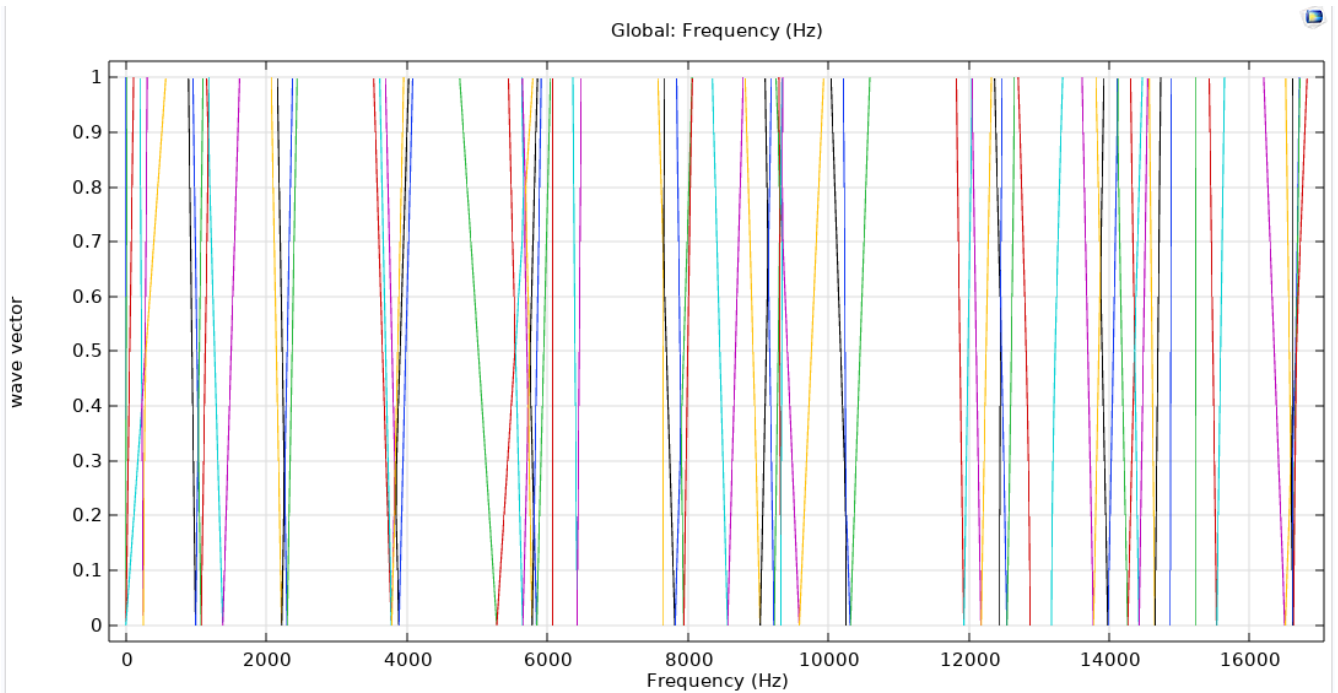


Figure 30 simulation result for plate with reduced thickness

In the transmissibility graph presented before (paragraph 2.2) the transmissibility decrease is between 9000 Hz and 1200 Hz. In this simulation is possible to appreciate a bandgap that starts around 10500 Hz and ends around 11800 Hz. The other bandgaps that can be seen in this graph are in the same frequency range of the transmissibility depression between two peaks as reported in the transmissibility graph presented in paragraph 2.2.

4.2 Simulation with Floquet periodicity along X axis and k_x wave vector for 7 cube cells beam

The simulation is settled as previously described in paragraph 4.1 and as before the comparison is done taking in account results presented in the paper and in Miceli's thesis regarding 7 cube cells beam. In both references is highlighted a bandgap, made by merging the first and second bandgap, that starts around 8500 Hz and ends around 11500 Hz. As before these graphs that are used as reference are transmissibility graph so can give an idea of where bandgaps can be found in the structure. Also in this case Floquet periodicity is on faces along X axis and the wave vector in k_x the wave propagation is studied only along X axis. As is possible to see in the following graph reporting simulation results, can't be find a big bandgap in the frequency range mentioned before. In this case is possible to notice a bandgap between 9600 Hz and 10300 Hz while in the zone before 10000 Hz can be noted different smaller bandgaps. Is important to notice that in the transmissibility graphs there are some peaks reducing the transmissibility reduction effectiveness and this is why smaller bandgaps are find putting in evidence some modes in the frequency range take in account and where the wave move on.

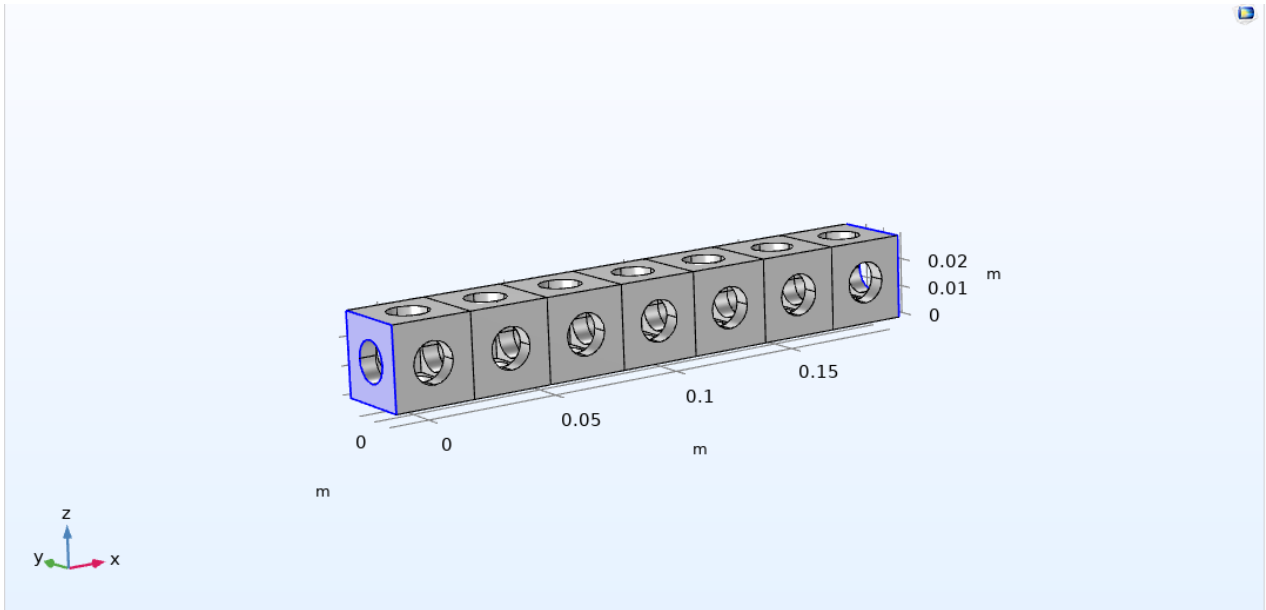


Figure 31 representation of floquet condition application

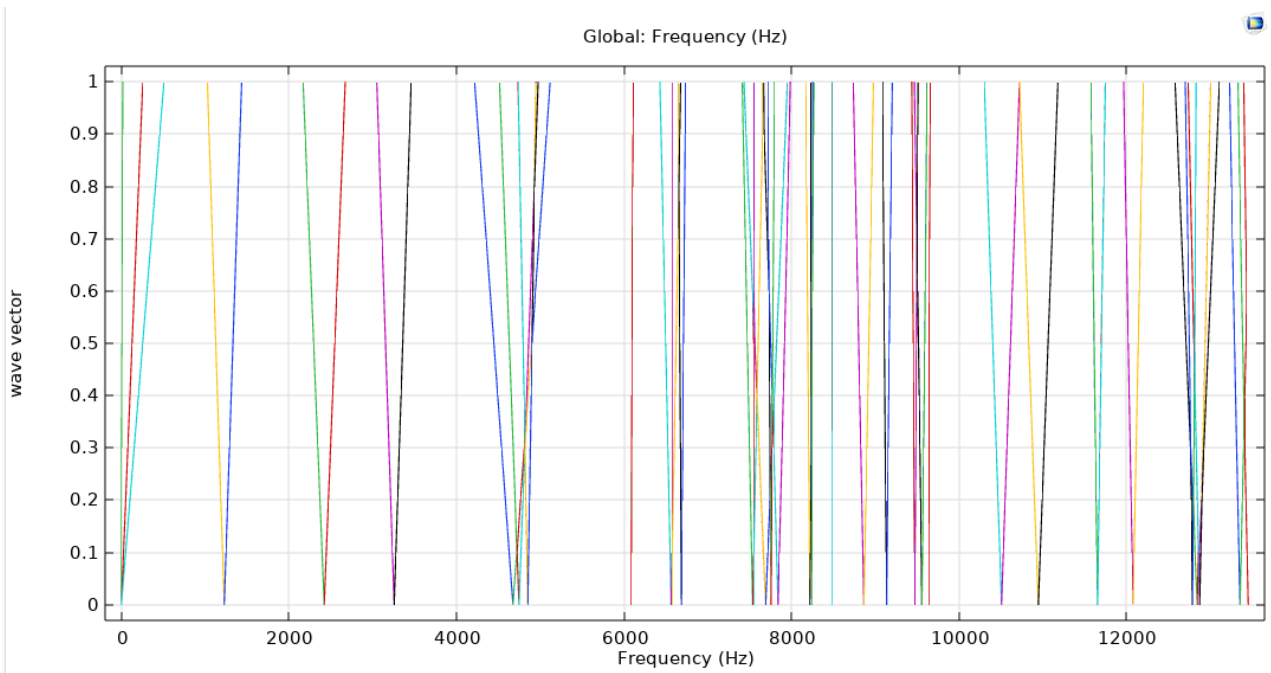


Figure 31 simulation results for 7 ccube cells beam

4.3 Simulation with Floquet periodicity along X axis and k_x wave vector for single reduced thickness plate

Now are also reported some analysis carried out for the single cell which is at the base of the plate with reduced thickness. The single cell, as previous described as a reduced thickness of 5 mm for edges along Z axis. This analysis is done with with the aim of observing the behavior of the single cell which is the basis of the structure of the plate with reduced thickness, in the

same conditions as the single cubic cell. To do this, the same analyzes to which the cubic cell was subjected were carried out.

4.3 Simulation with Floquet periodicity along X axis and k_x wave vector for single reduced thickness cell

The simulation the same as the one explained in paragraph 3.1 the only difference in the object under analysis here reported in the following image.

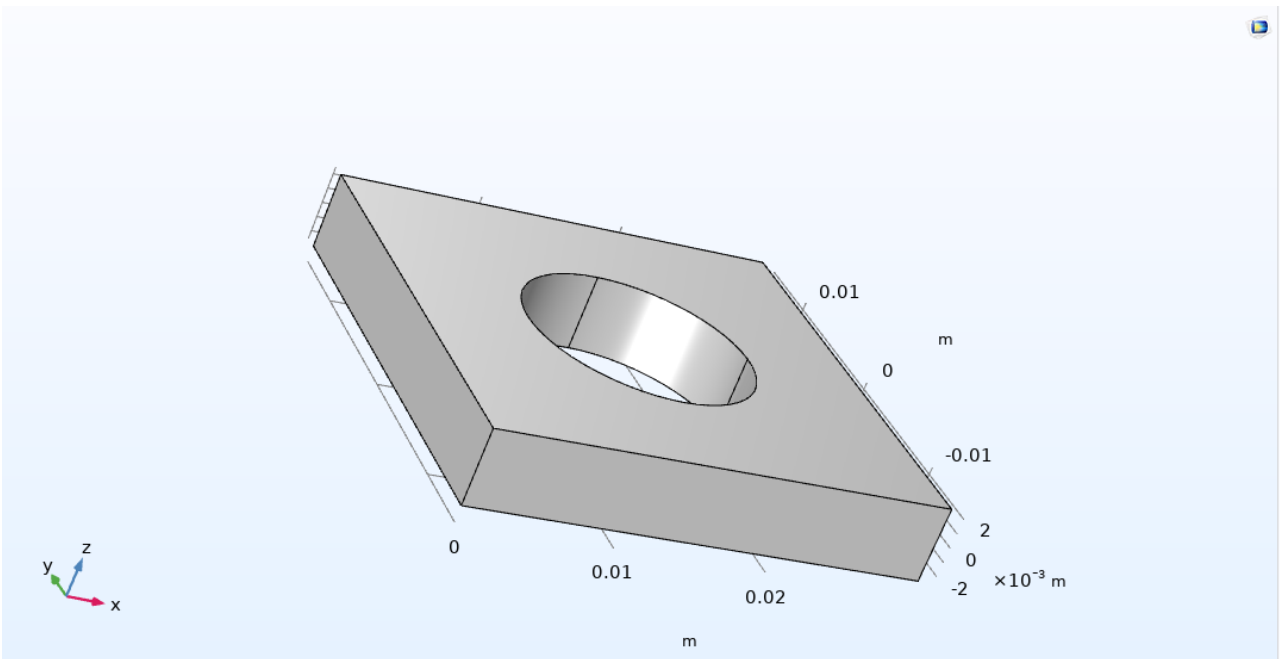


Figure 32 single reduced thickness cell

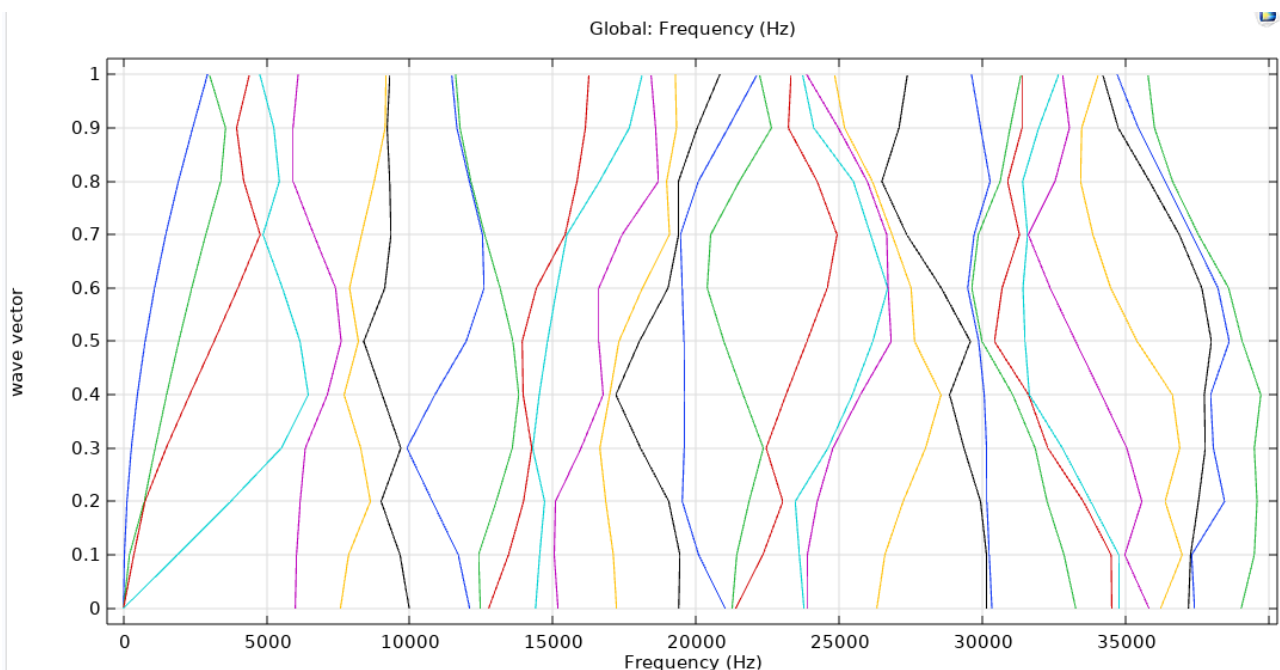


Figure 33 simulation results for single thin plate cell with Floquet periodicity along X axis and k_x wave vector

As in the case of the cubic cell, it is not possible to appreciate the presence of bandgap in the configuration of the aforementioned simulation. The fact that can be noted, however, is that the modification of the dimensions of the element leads to an increase in the frequencies of the eigenmodes.

4.3 Simulation with Floquet periodicity along X,Y,Z axis and k_x, k_y, k_z wave vector

The setup simulation is the same explained in paragraph 3.3

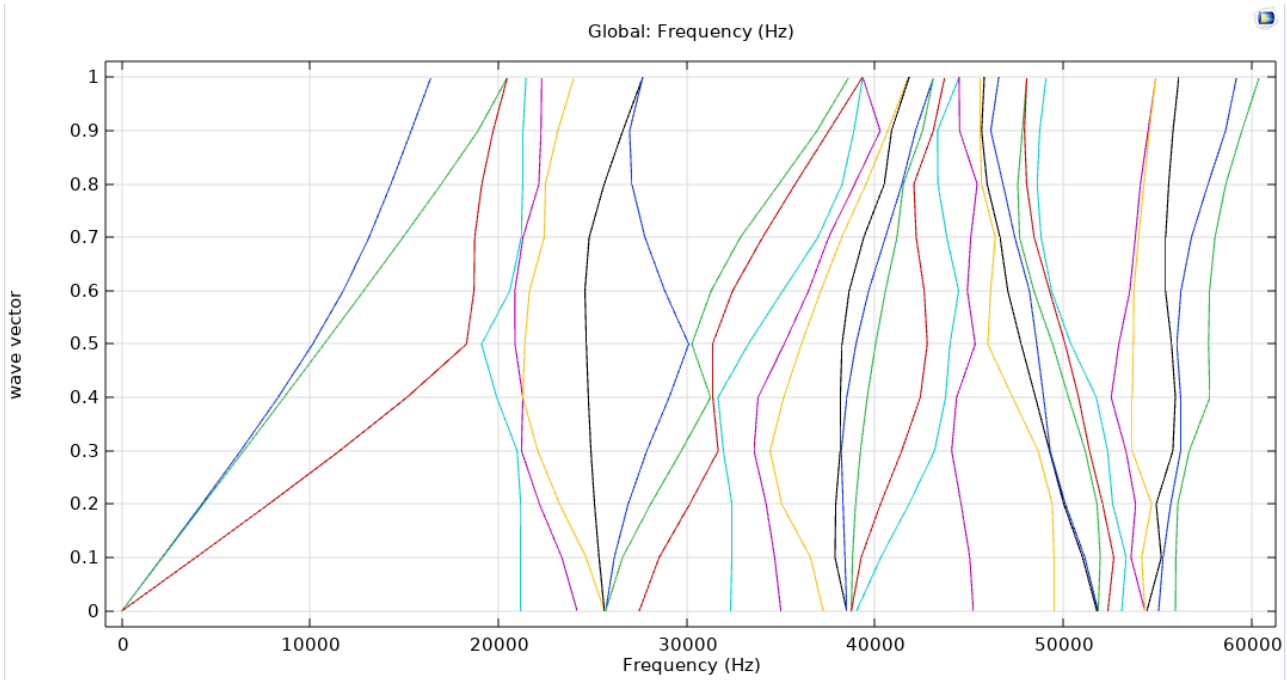
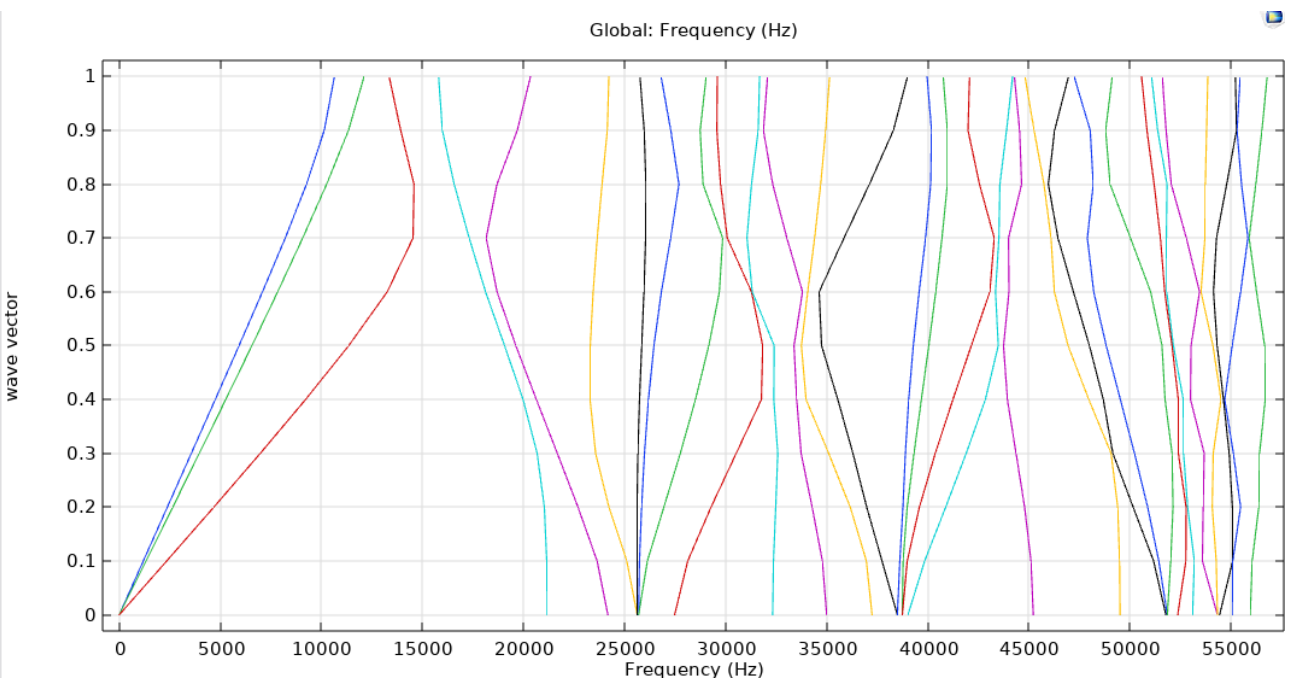
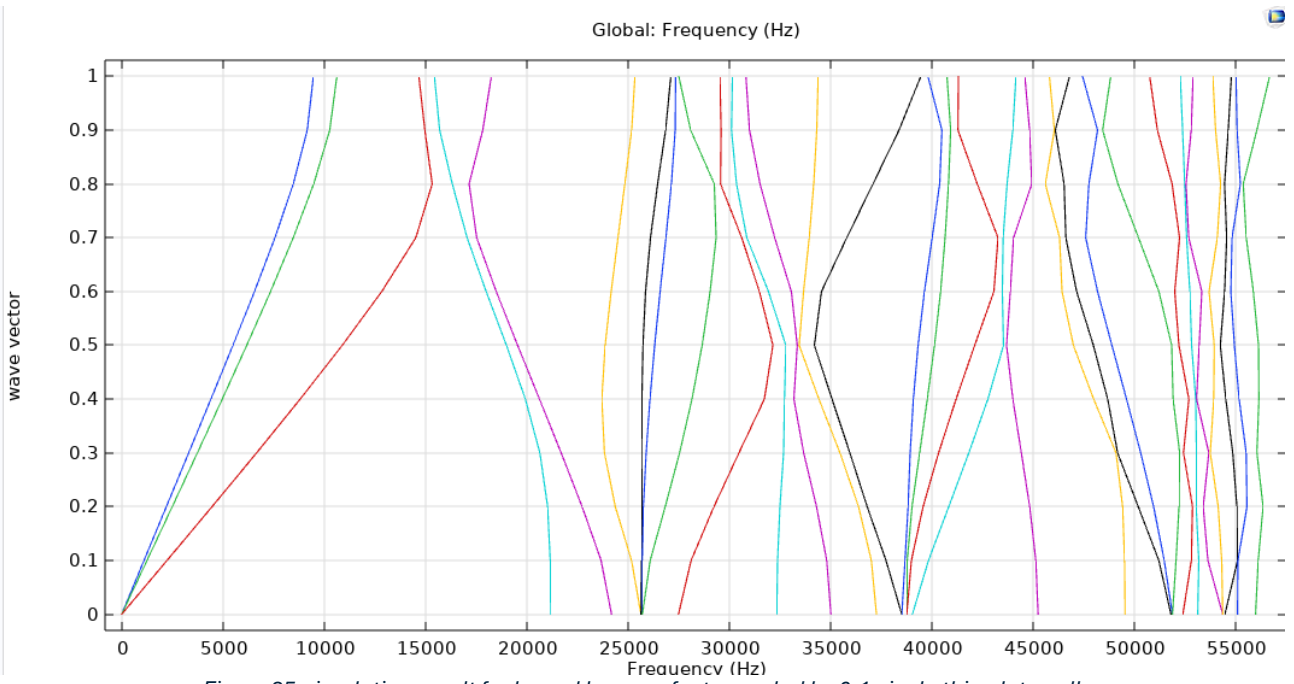


Figure 34 simulation results for Floquet periodicity on X,Y,Z axis and k_x, k_y, k_z wave vectors

Neither in this simulation is possible to find bandgaps, but in these case very high frequencies are reached.

4.4 Simulation with Floquet periodicity along X,Y,Z axis and k_x, k_y, k_z wave vector with scaling factor

Simulation setup is the same presented in paragraph 3.4. First graph is for 0.1 scaling factor, while second graph is for 0.25 scaling factor. Looking at the graphs a trend similar to that obtained for the cubic cell can be observed in the same simulation conditions. As happened in the two previous simulations, also in these two cases the frequency range reached is decidedly higher, approximately 20,000 Hz more. Furthermore, what can be noted is that in the case of the simulation with factor 0.1 the bandgap almost does not appear, in fact we have a small bandgap of around 100 Hz between 15325 and 15345 Hz. In the case of the factor 0.25 the bandgap is more evident in fact first bandgap is around 1300 Hz from 14500 Hz to 15800 Hz and then other small bandgaps are also visible at higher frequencies above 4500 Hz.



Chapter 5

Experimental analyses

5.1 Chladni experiment setup

To perform this experimental analysis and to acquire signal it was decided to take the Chladni experiment setup as a reference. In this experiment a plate fixed to its center is excited by an electromagnetic shaker which transmits the harmonic motion. Furthermore, thanks to the sand spread on the surface of the plate it is possible to highlight the modal shapes that are created when the plate is excited with frequencies identical to the natural frequencies of the system. In these acquisitions three different type of plates are compared. The first one is a metal plate with 40x40 cm face and a thickness of 1 mm. The second one is a plate with same dimension but T-shaped carvings, performed with a laser cut, are present on it with periodic repetition. This repetition, 10 unit cells per side and therefore 100 total cells on the plate, is the characteristic that defines the metamaterial. The third plate is similar to the second one but has masses added at the top of the carved Ts.

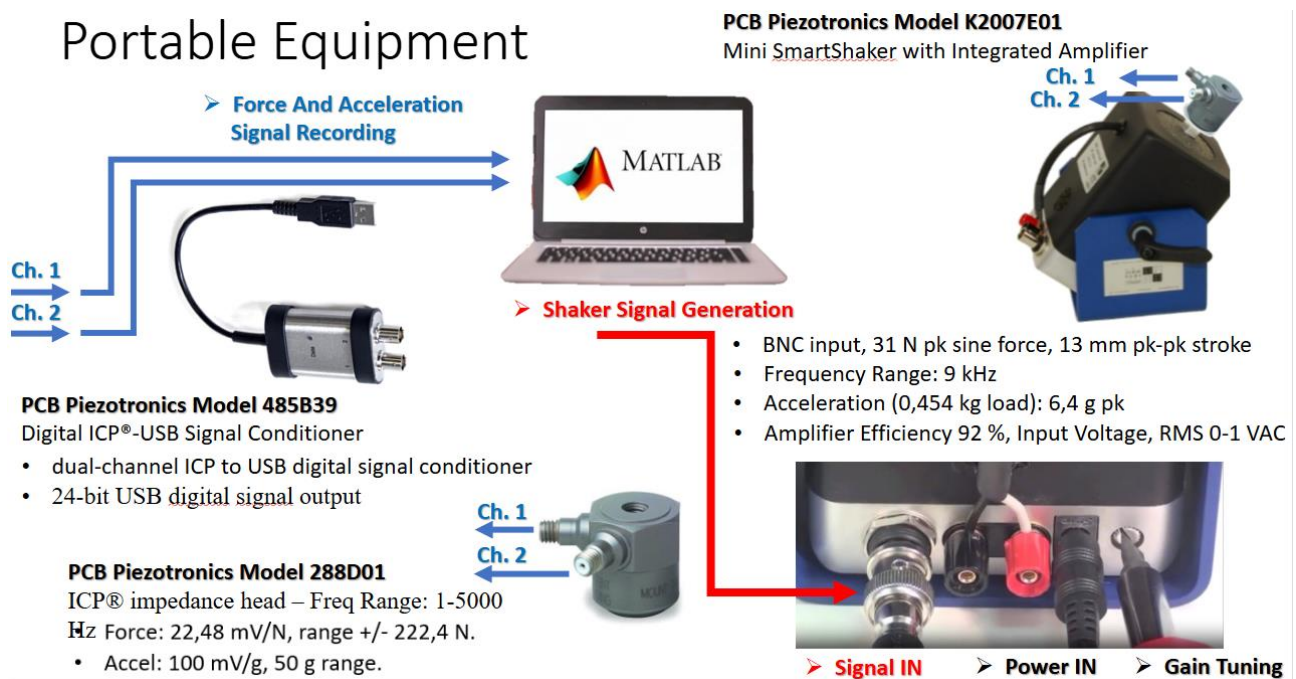


Figure 37 connection scheme Chladni experiment

A brief summary of all the equipment necessary to carry out the test and acquire the data:

- Plates mentioned before
- PCB Piezotronics Model 485B39 ICP®-USB Signal Conditioner dual channel ICP to USB 24 bit USB digital signal output
- PCB Piezotronics Model 288D01 ICP® impedance head with a 1-5000 Hz frequency range for both force and acceleration measurements

- PCB Piezotronics Model K2007E01 Mini Smart Shaker featuring a 9 kHz frequency range and maximum acceleration of 6.4 g pk with a 0.5 kg payload
- PC with MATLAB to record force and acceleration signal and to shake signal generation

The mass added to the center of the Ts is a magnet sn 05 01. In this specific case two magnets are added in the center of the T shaped resonator adding a total mass of 0.3 grams. Reminding that there are 100 Ts in the plate a total of 30 grams is added to the plate. Here magnets technical data description



Scheda tecnica articolo S-05-01-N

Dati tecnici e sicurezza nell'utilizzo

Webcraft GmbH
Industriepark 206
78244 Gottmadingen, Germania

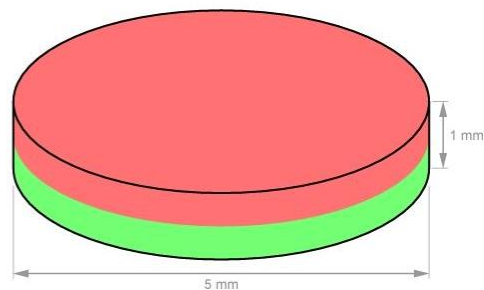
Telefono: +49 7731 939 839 1

www.supermagnete.dk
support@supermagnete.dk

1. Caratteristiche tecniche

Supermagnete al neodimio - Disco magnetico Ø 5 mm, altezza 1 mm, tiene ca. 320 g

ID articolo	S-05-01-N
EAN	7640155437127
Materiale	NdFeB
Forma	Disco
Diametro	5 mm
Altezza	1 mm
Tolleranza	+/- 0,1 mm
Direzione di magnetizzazione	assiale (parallela all'altezza)
Rivestimento	Nichelato (Ni-Cu-Ni)
Modo di produzione	sinterizzato
Magnetizzazione	N45
Forza di attrazione	ca. 320 g (ca. 3,14 N)
Sforzo tangenziale	ca. 64 g (ca. 0,632 N)
Temperatura max. di esercizio	80°C (evtl. inferiore) *
Colore	Argento
Peso	0,1492 g
Temperatura di Curie	310 °C
Rimanenza Br	13200-13700 G, 1.32-1.37 T
Forza coercitiva bHc	10.8-12.5 kOe, 860-995 kA/m
Forza coercitiva iHc	≥12 kOe, ≥955 kA/m
Prodotto di energia (BxH)max	43-45 MGOe, 342-358 kJ/m ³



* A causa delle sue dimensioni è possibile che questo magnete presenti una minore resistenza al calore. La preghiamo di consultare la nostra FAQ: <https://www.supermagnete.dk/ita/faq/Quanto-si-possono-scaldare-i-magneti#pu424>

Figure 38 magnets technical data

The following two images represent the full plate with masses added and a detail to show the position of the mass on the T carving.

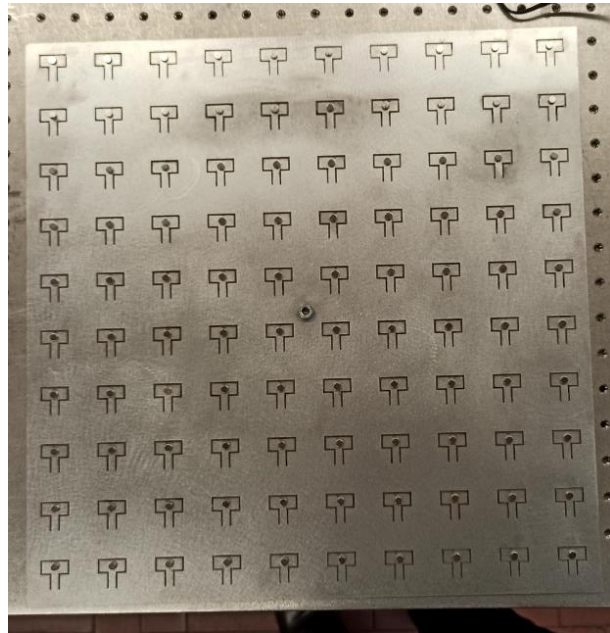


Figure 39a Tplate with added masses

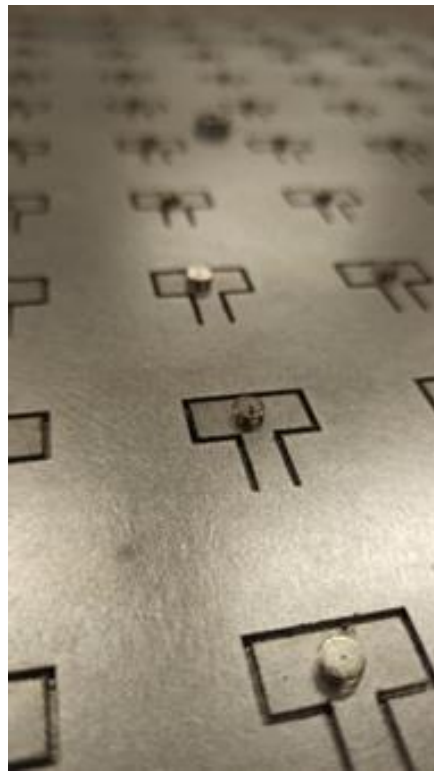


Figure 39b Tplate with added masse

5.2 Chladni results

Below a summary table presenting the sampling frequencies for each test along with the type of excitation applied to the plate during each test.

Test	Sampling frequency [Hz]	Excitation type
Plate original test 1	16000	White noise
Plate original test 2	32000	White noise
Plate with T-shaped carvings test1	16000	White noise
Plate with T-shaped carvings test2	32000	White noise
Plate with T-shaped carvings test6 *	16000	White noise
Plate with T-shaped carvings test7 *	16000	White noise
Plate with T-shaped carvings test8 *	16000	Sweep
Plate with T-shaped carvings and added mass test3 *	16000	White noise
Plate with T-shaped carvings and added mass test4 *	16000	White noise
Plate with T-shaped carvings and added mass test5 *	16000	Sweep

Table 8 test configuration recap

The acquisitions marked with an asterisk (*) underwent an additional process during data analysis because, during acquisition, the force and acceleration signals were recorded in an inverted manner. To correct this issue, the acquired values were multiplied by the reciprocal of the scaling factor by which they were initially multiplied during acquisition. Subsequently, after restoring the data to their original values, they were multiplied by their respective scaling factors to obtain the acceleration and force values in the desired format. Finally, since acceleration and force were recorded on swapped channels, it was necessary to apply this inversion during analysis as well to ensure consistency in data representation.

On the next pages are reported all the obtained results. In each graph is possible to appreciate the comparison of each test versus the result obtained testing the regular square plate putting in evidence differences in the behavior between the two plates.

Comparison between metal plate take as reference and test1 Tplate.

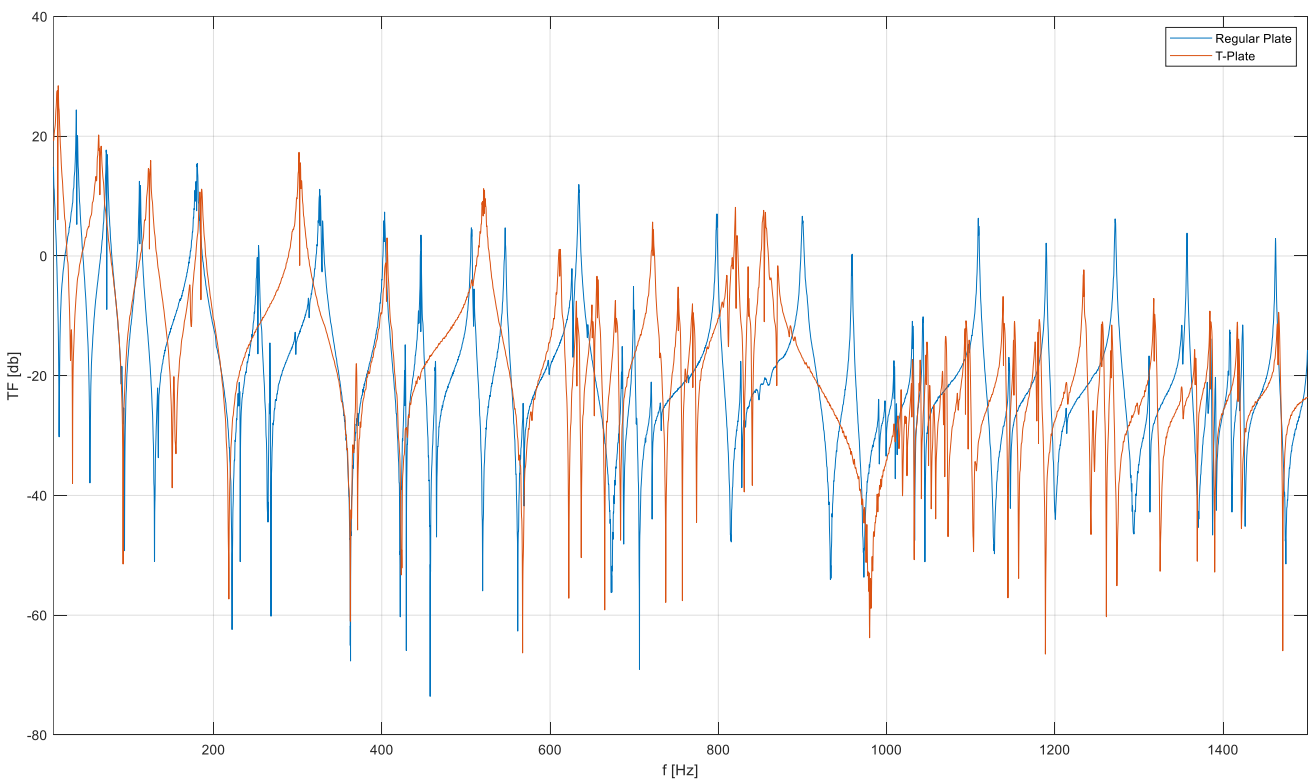


Figure 40 comparison regular plate test1 Tplate

Comparison between metal plate take as reference and test2 Tplate.

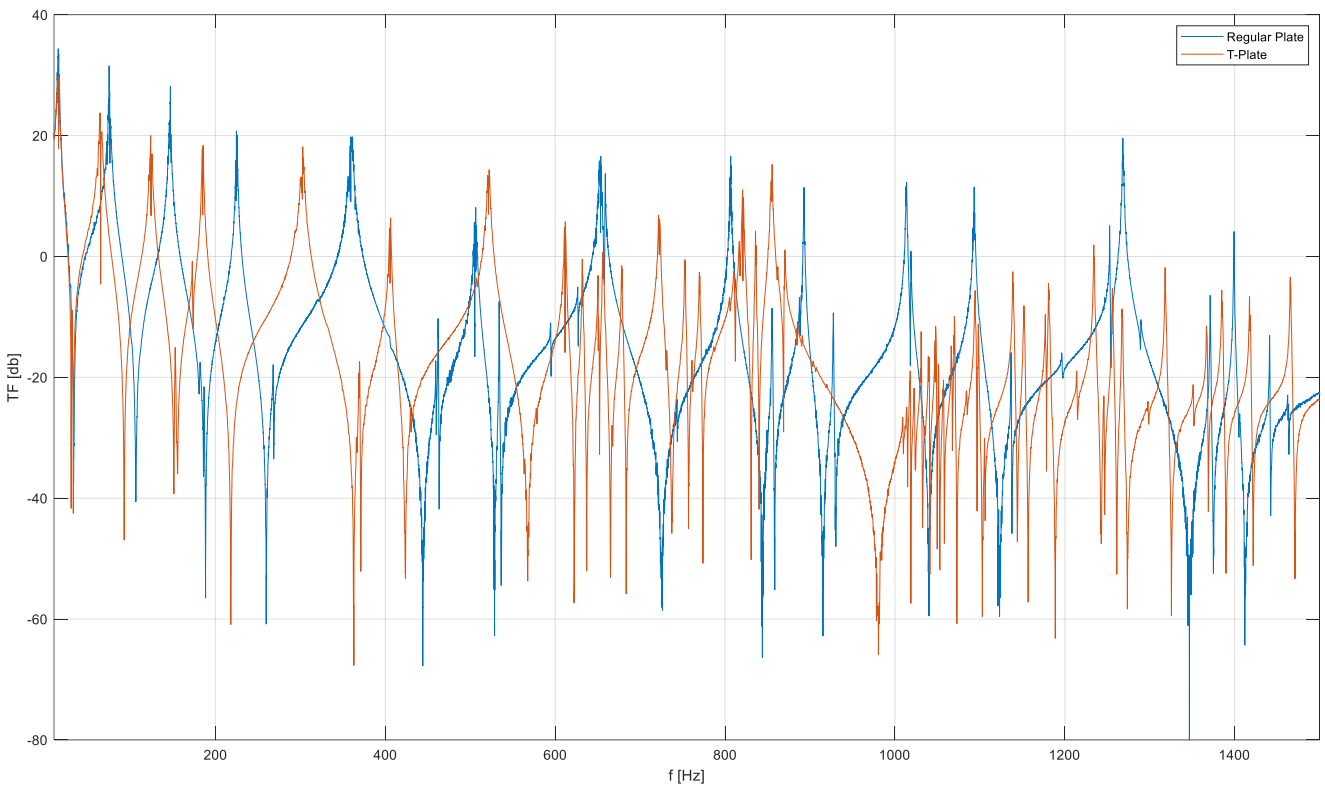


Figure 41 comparison regular plate test2 Tplate

Comparison between metal plate take as reference and test6 Tplate.

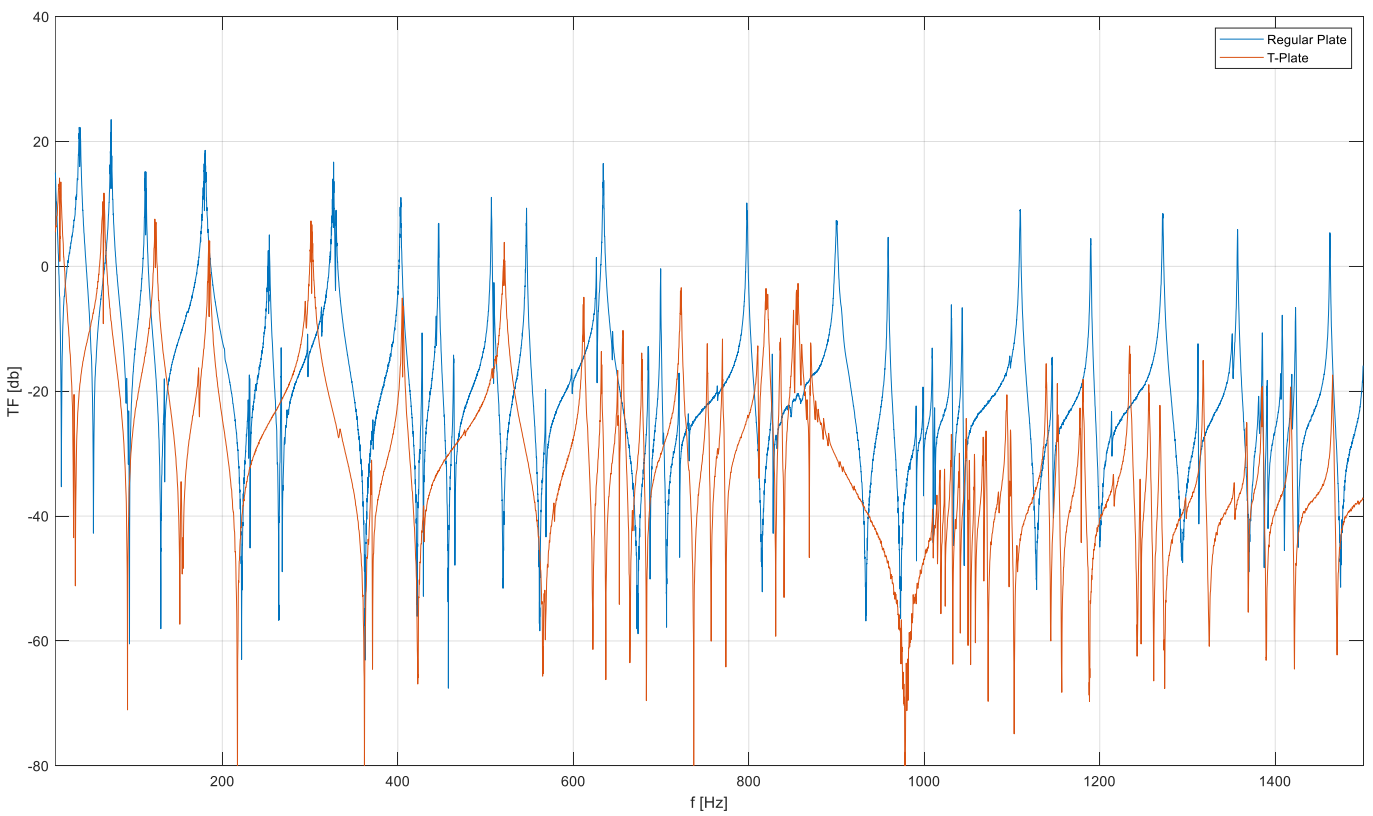


Figure 42 comparison regular plate test6 Tplate

Comparison between metal plate take as reference and test7 Tplate.

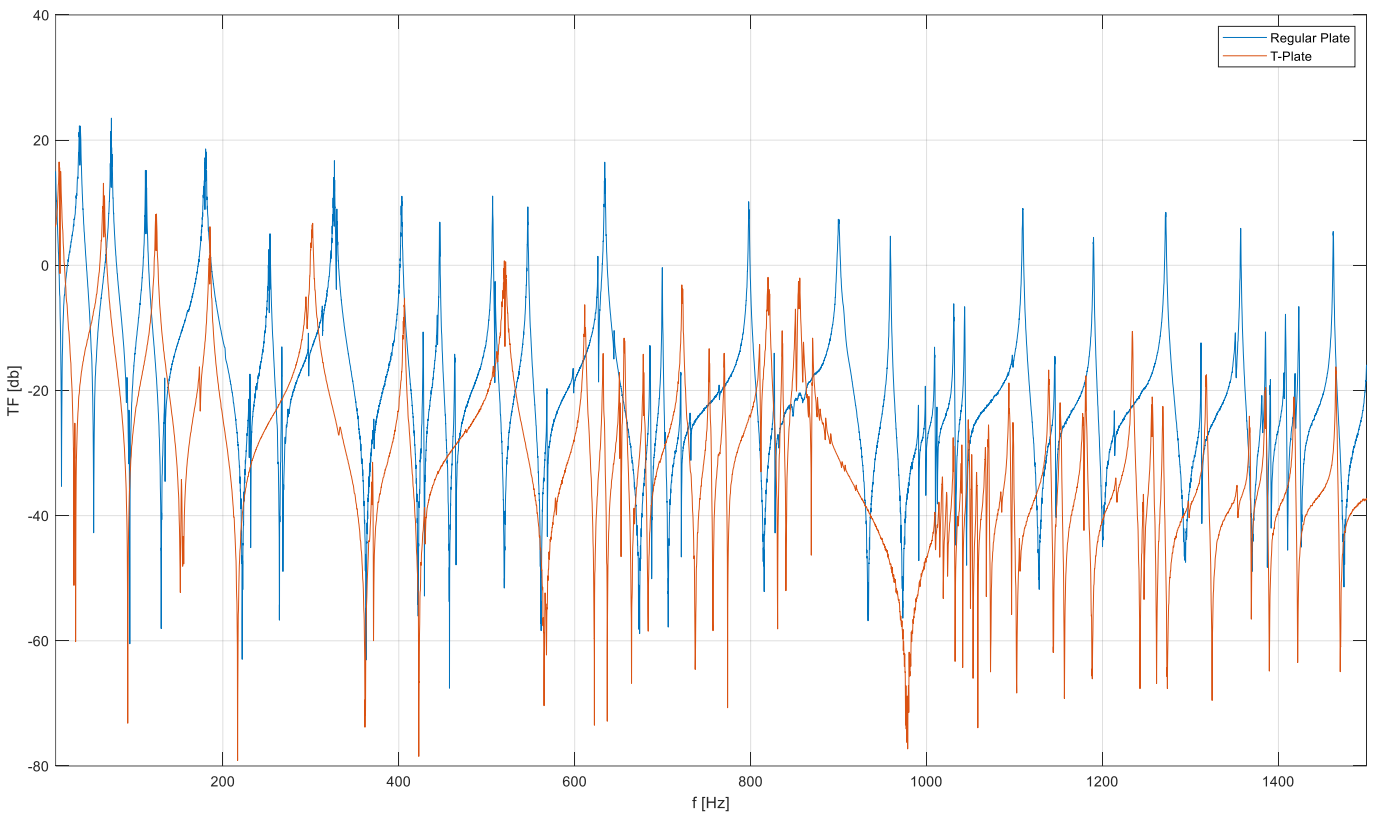


Figure 43 comparison regular plate test7 Tplate

Comparison between metal plate take as reference and test8 Tplate.

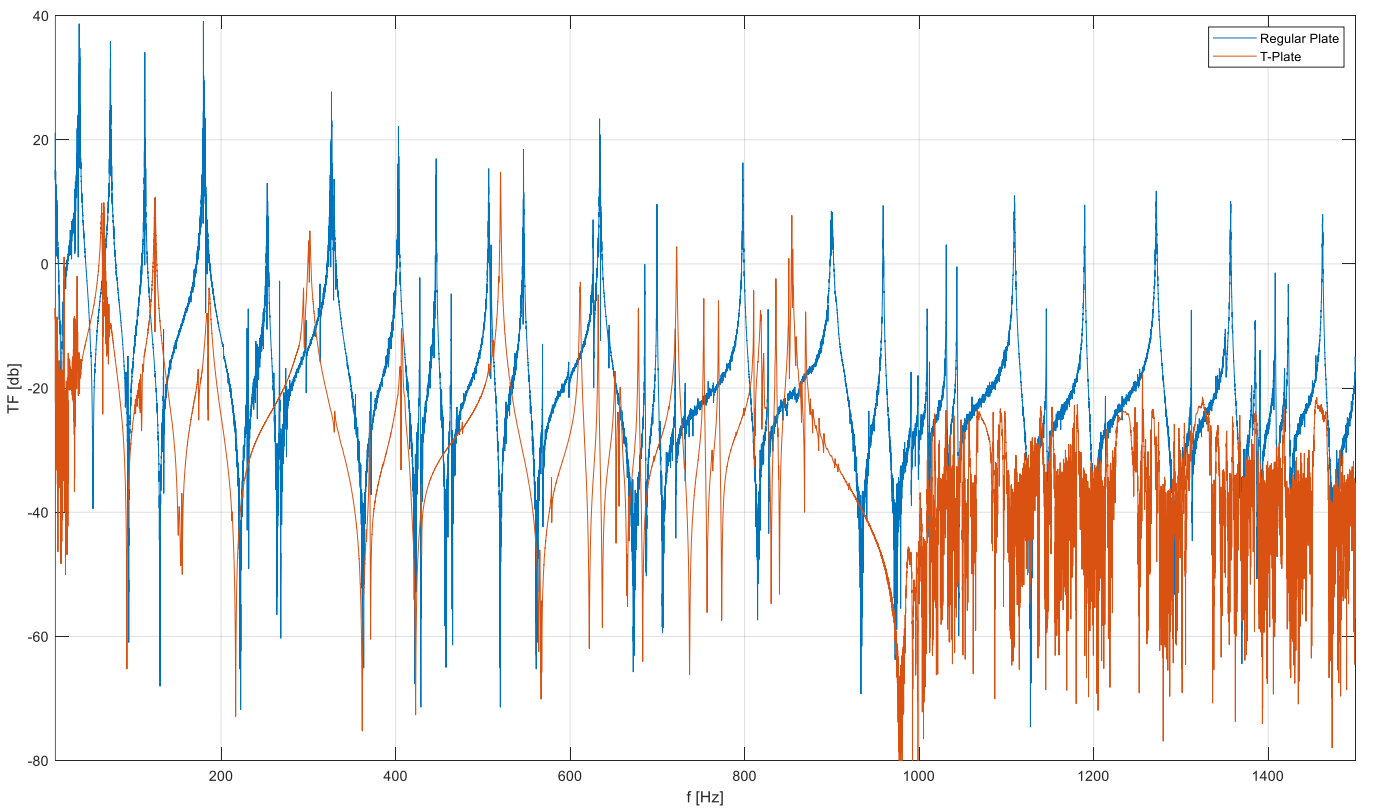


Figure 44 comparison regular plate test8 Tplate

Comparison between metal plate take as reference and test3 TMplate with added mass.

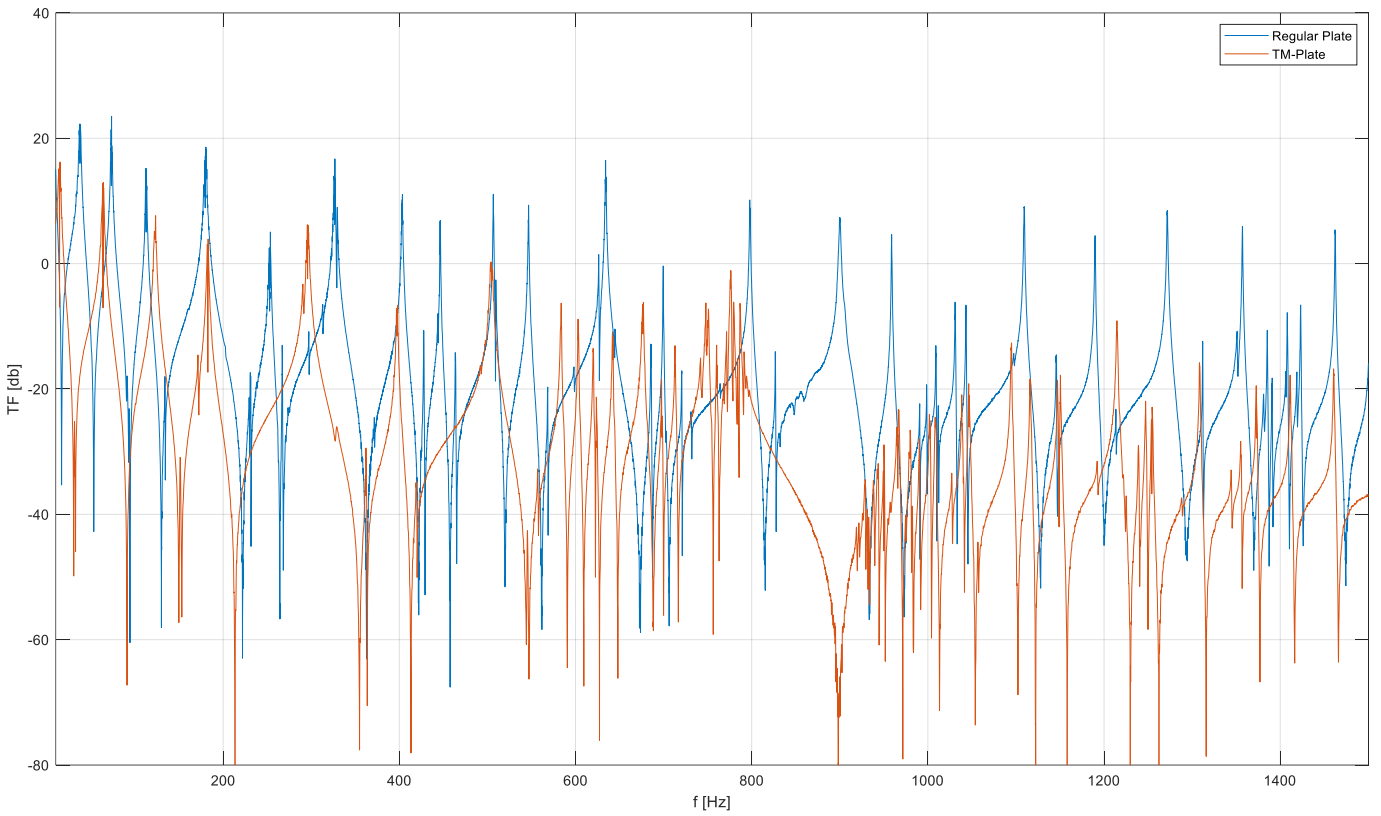


Figure 45 comparison regular plate test3 TMplate

Comparison between metal plate take as reference and test4 TMplate with added mass.

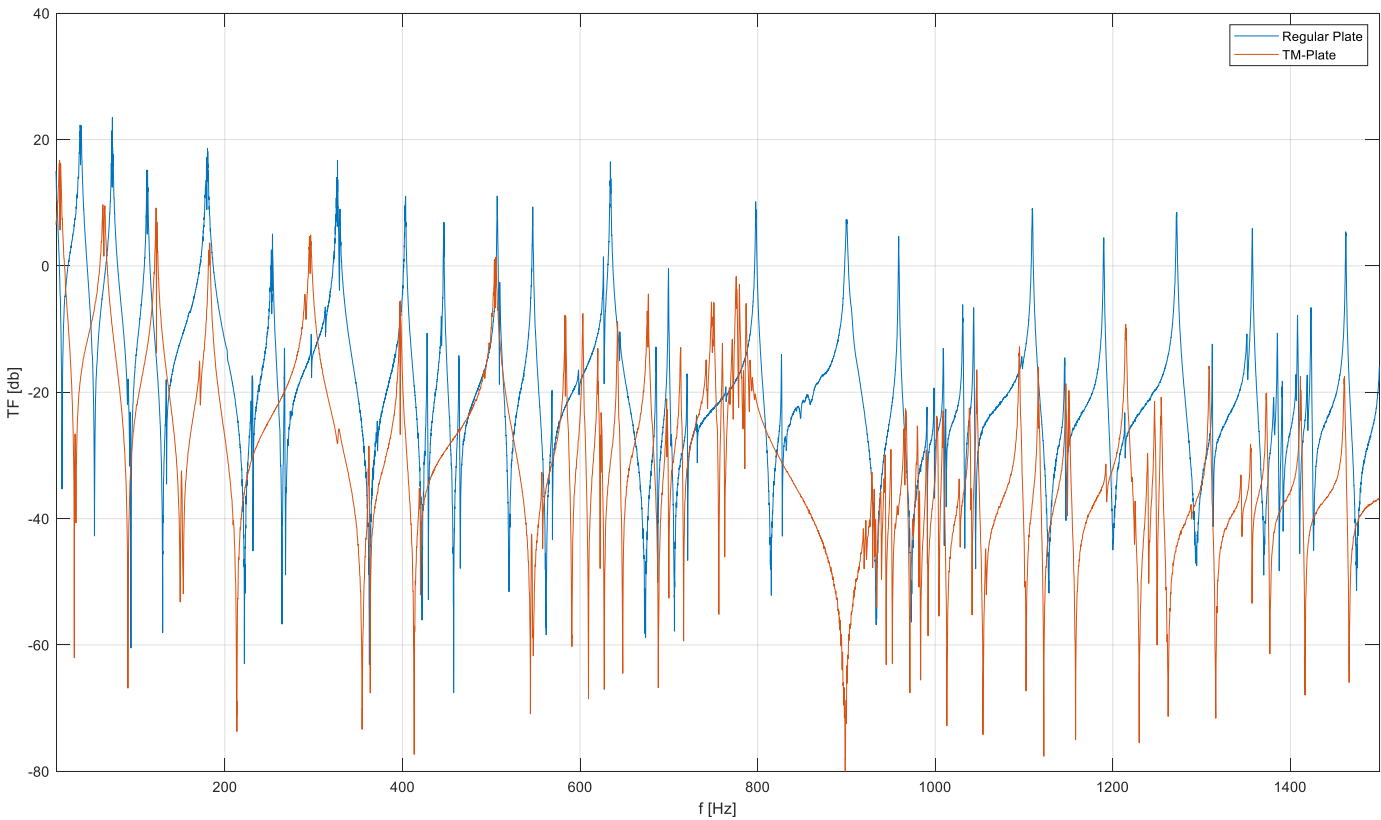


Figure 46 comparison regular plate test4 TMplate

Comparison between metal plate take as reference and test5 TMplate with added mass.

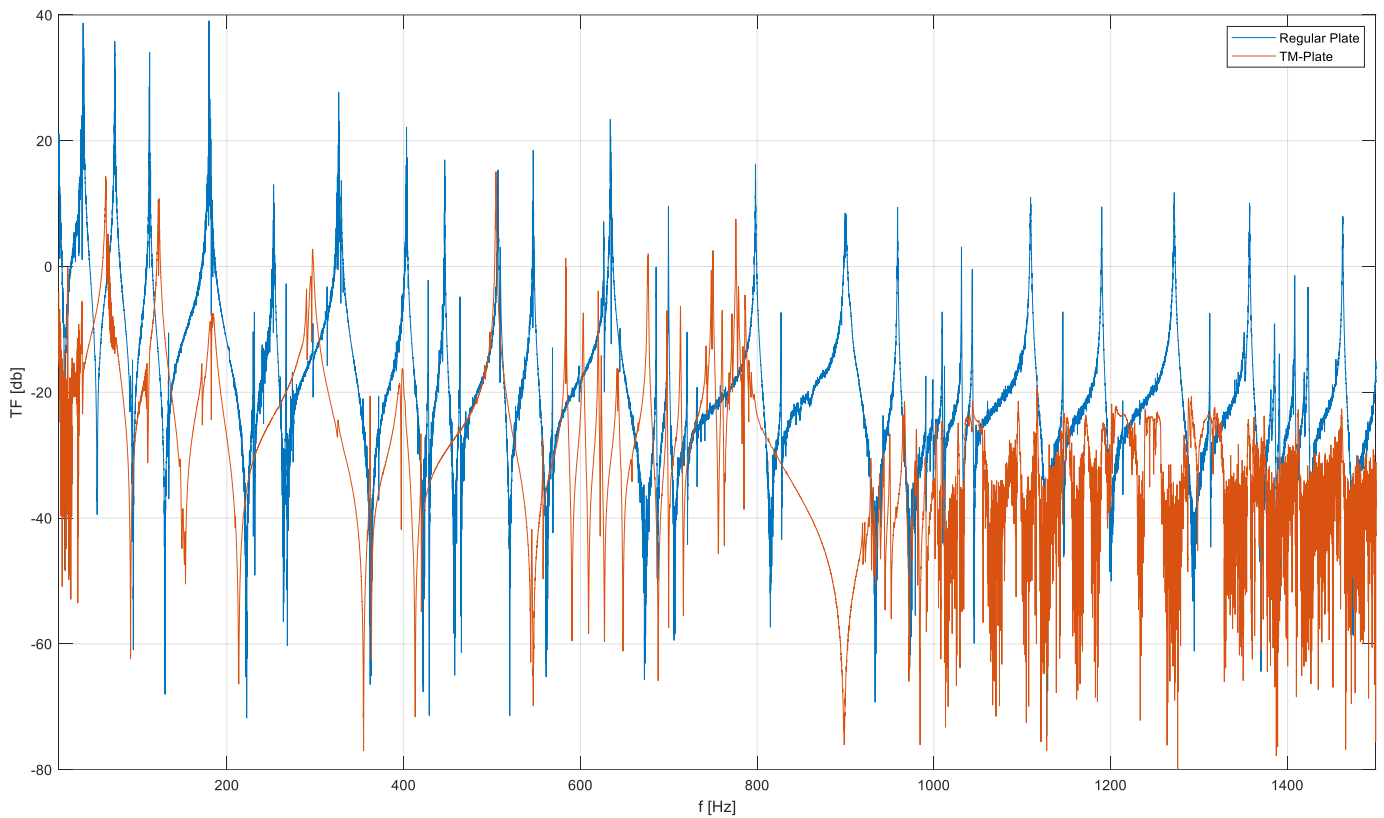


Figure 47 comparison regular plate test5 TMplate

As is possible to notice in all graphs reported above the presence of a bandgap is highlighted in the frequency range 800-900 Hz since the curve representing the metamaterial plate has a reduction in its transfer function around 20 dB and also no spikes are present in this part of the curve compared to the blue line that is the regular plate transfer function taken as reference.

To complete the analysis carried out on these three types of plates, a graph is now presented that overlays the results from each configuration, with the following definitions:

- **Regular plate** refers to the flat plate configuration.
- **T plate** refers to the plate with resonators in the shape of the letter "T".
- **TM plate** refers to the configuration in which masses have been added at the center of each resonator.

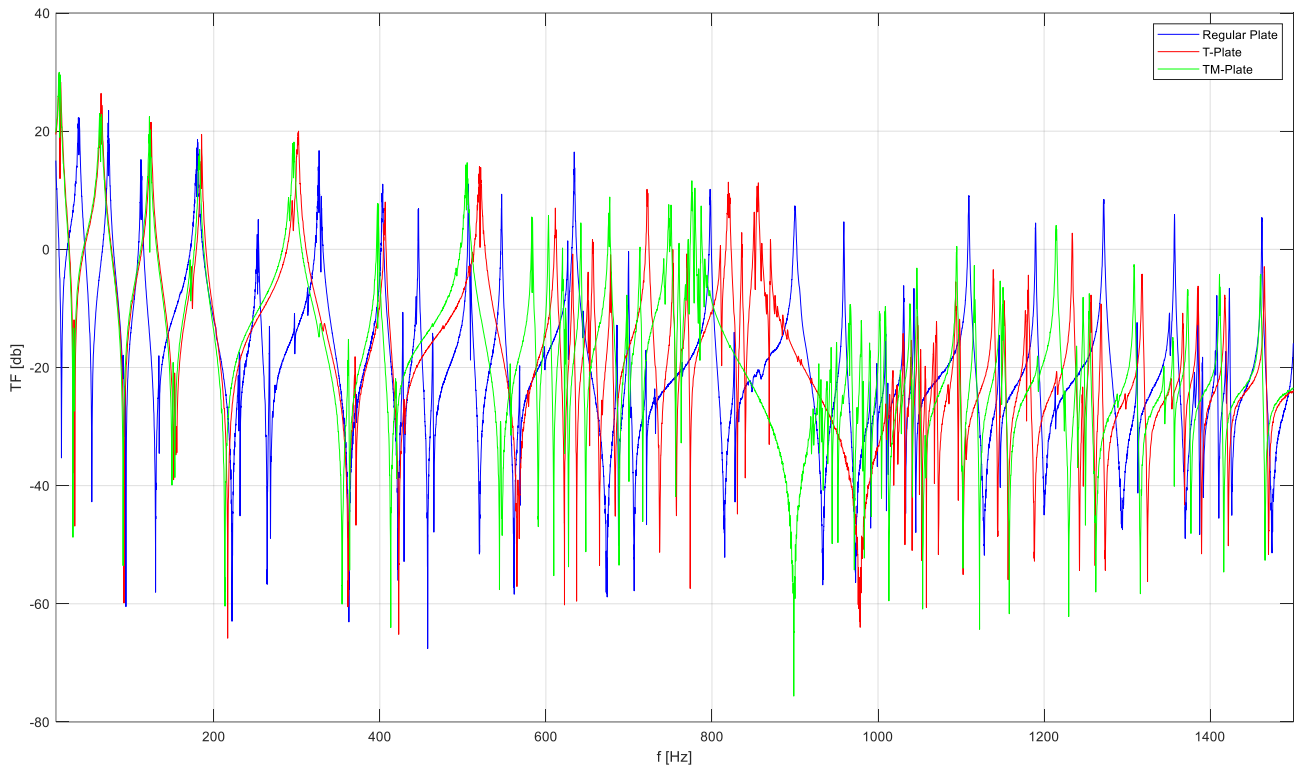


Figure 48 three plate configurations comparison

As can be seen from the graph, the presence of a bandgap is noticeable in both the configuration with only resonators and the one where masses were added. However, it is important to note that in the case of the plate with added masses, the frequencies at which the bandgap appears are shifted to lower values compared to the configuration without masses. Specifically, the bandgap shifts from the range of 870-970 Hz in the plate with only resonators to a bandgap between 800-900 Hz in the configuration with masses added to the resonators. The size of the bandgap remains around 100 Hz, but it decreases slightly by about 100 Hz, which could be due to the system stiffening as a result of the added masses. This event makes it possible to position the bandgap at frequencies that are more suitable for the specific application where the metamaterial is intended to be used, offering wide-ranging possibilities for use and versatility.

As example of the visual output of the test are now reported some of the modal shapes highlighted by the sand during the test execution.

<p>Mode shape at 75 Hz</p>	
<p>Mode shape at 145 Hz</p>	
<p>Mode shape at 224 Hz</p>	
<p>Mode shape at 364 Hz</p>	

Table 9 output modes representation of Chladni experiment

5.3 Laser probe experiment setup

Now is reported another experimental analysis carried out on the 400x400 mm metamaterial plate with T-shaped carvings. Of course the same test is carried out on a regular square metal plate with same dimension without carvings, taken a reference for comparison. In this test 4 spot on the plate are laser measured in order to monitor, during the sweep excitation, the displacement to force transfer function, defined as receptance. To do that the necessary setup is:

- PCB Piezotronics Model K2007E01 Mini Smart Shaker featuring a 9 kHz frequency range and maximum acceleration of 6.4 g pk with a 0.5 kg payload;
- PCB Piezotronics Model 288D01 ICP® impedance head with a 1-5000 Hz frequency range for both force and acceleration measurements;
- Keyence LK-G high speed, high accuracy CCD laser displacement probe and conditioner, featuring a 4 mm/V sensitivity in a ± 10 V (adjustable) range
- Oros OR-38 Data Acquisition system, capable of 8 to 32 synchronous channels acquisitions at 24 bits in a ± 40 V adjustable range.

The input signal is a linear sweep from 10 to 1510 Hz in 150s (10Hz/s) and also the regular plate is tested under the same exciting signal in order to compare results obtained for the Tshaped plate. To constrain the plate to the shaker a M4 threaded nut was attached at the center of the plate. Since is only available one laser to measure displacement, the test procedure and the acquisition is repeated individually for each spot. Smoothing techniques are implemented in order to reduce intensity fluctuations and modulate the spectral profile of the laser beam²². This process ensures uniform energy distribution, minimize interference effects, and improves laser system's performance. Then data are merged together to give total result. The measured points are highlighted in the following image.

5.4 Laser probe results

The merged results obtained from the experiment described in Section 5.3 are presented here, with the outcomes from each measured location displayed together in the same image for both the regular plate and the T-shaped plate. Additionally, to give a better understanding of the differences between the normal plate and the Tshaped plate a graph with all the curves is included showing the receptance measured at each spot for both plates side by side. Also a brief report summarizing the behavior of the measured signal - laser displacement - acceleration - force - at each location in response to the sine sweep input signal. For simplicity is reported for just one spot.

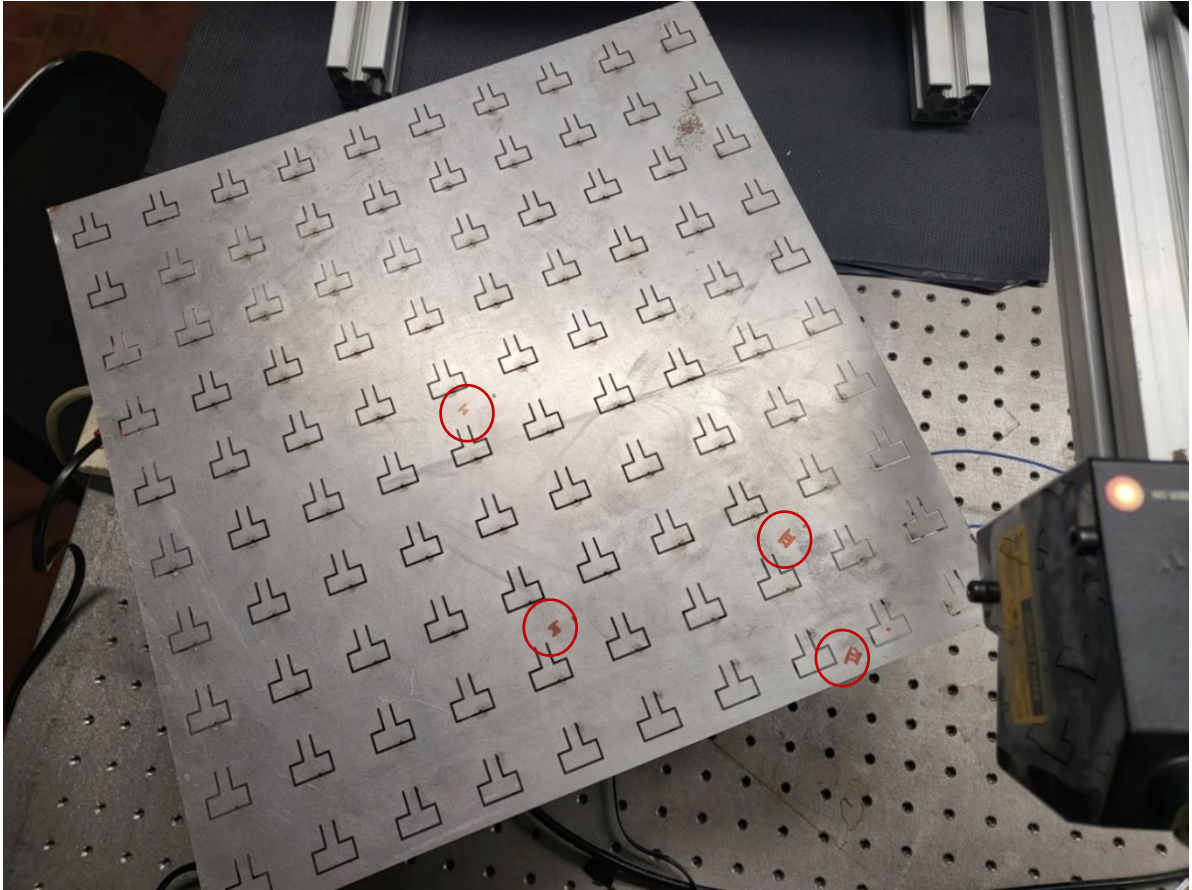


Figure 49 Tshaped plate with laser measured spots

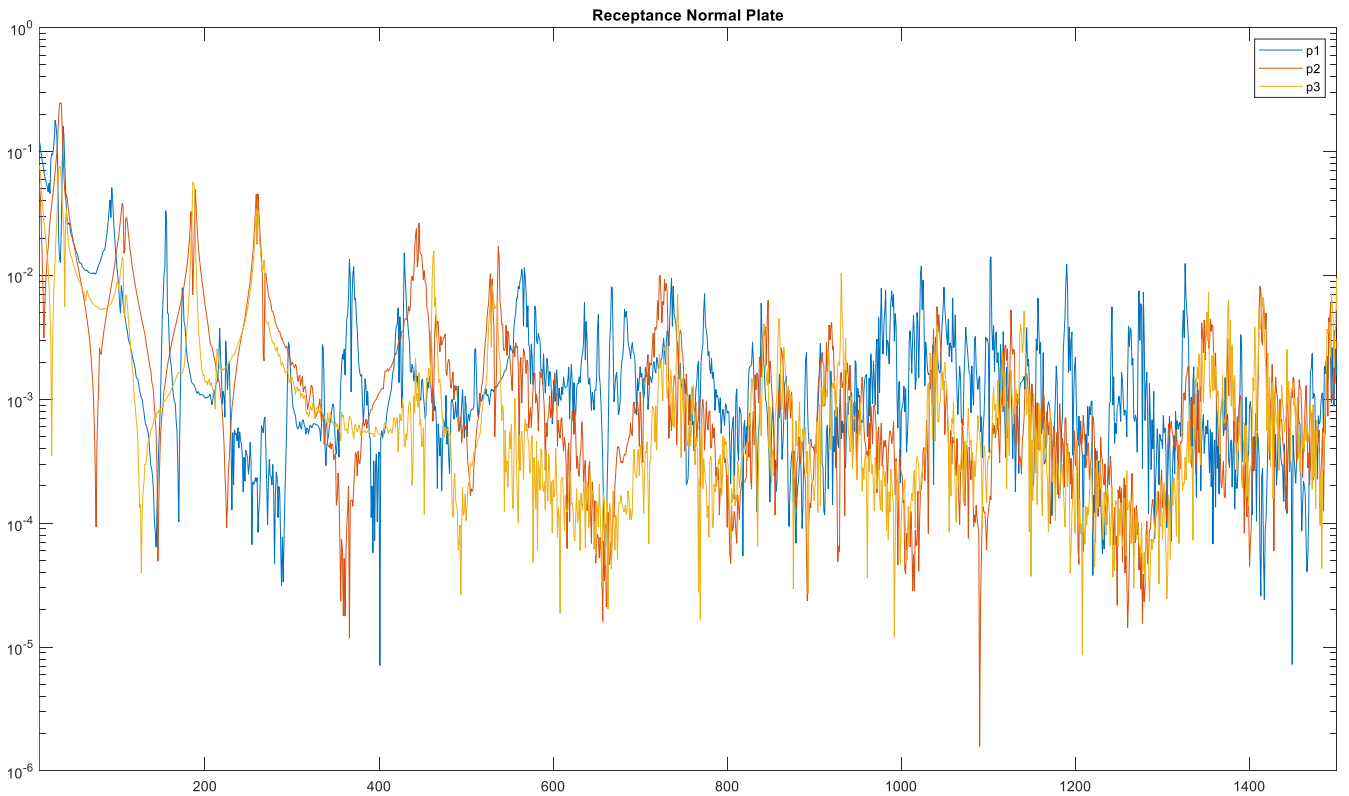


Figure 50 Regular plate receptances

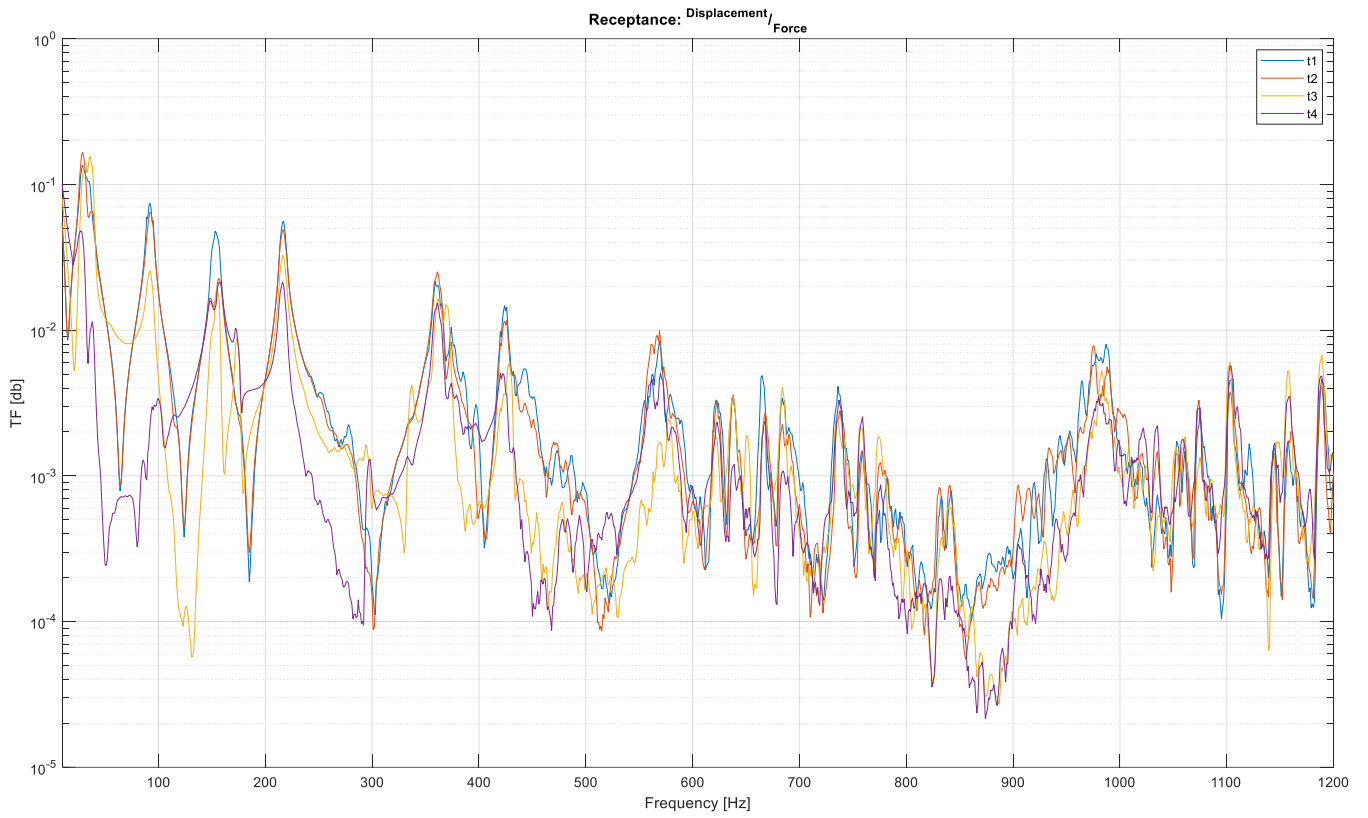


Figure 51 Tshape plate receptances

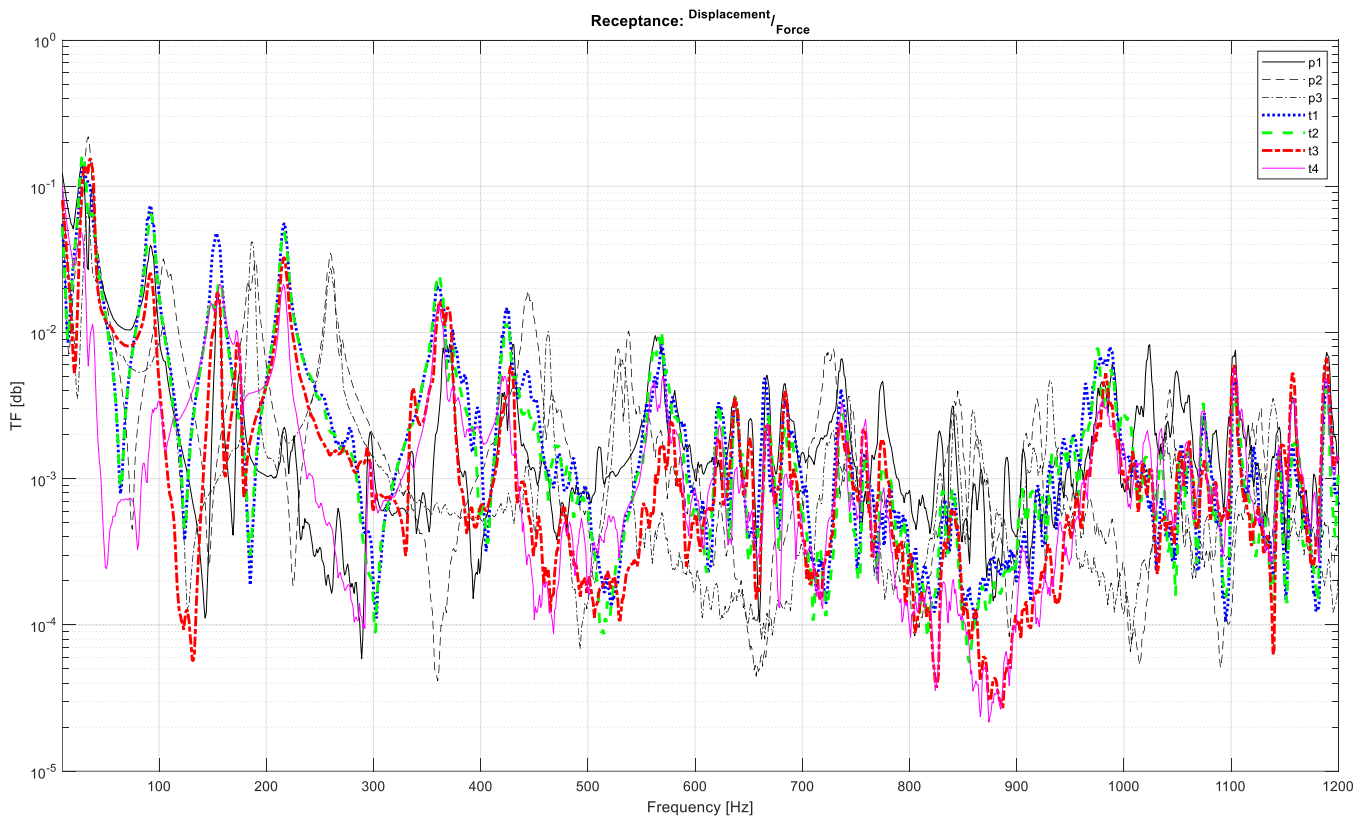


Figure 52 receptances comparison

Looking at the graph above, where all results are displaced, is possible to appreciate in the 870-900 Hz range a stopband that is not visible in the lines related to the regular metal plate. This highlight the presence of a bandgap in this frequency range.

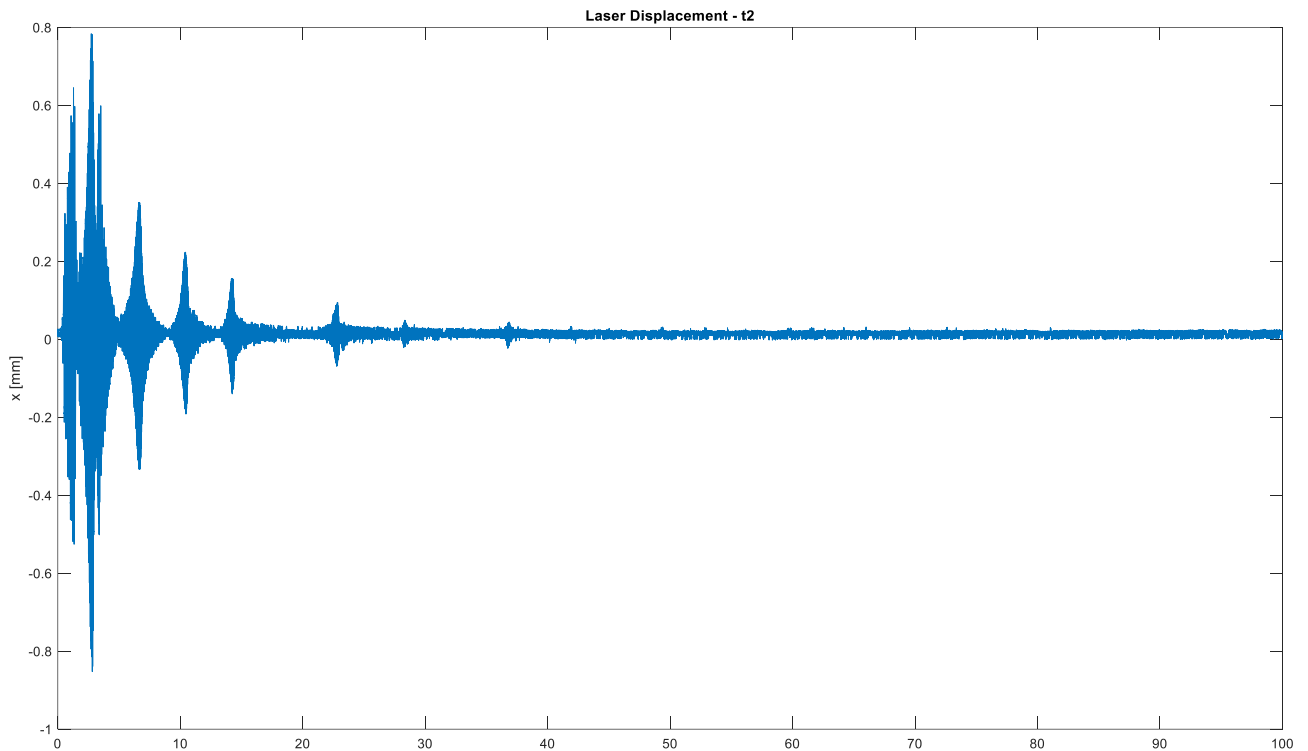


Figure 53 measured displacement at spot 2

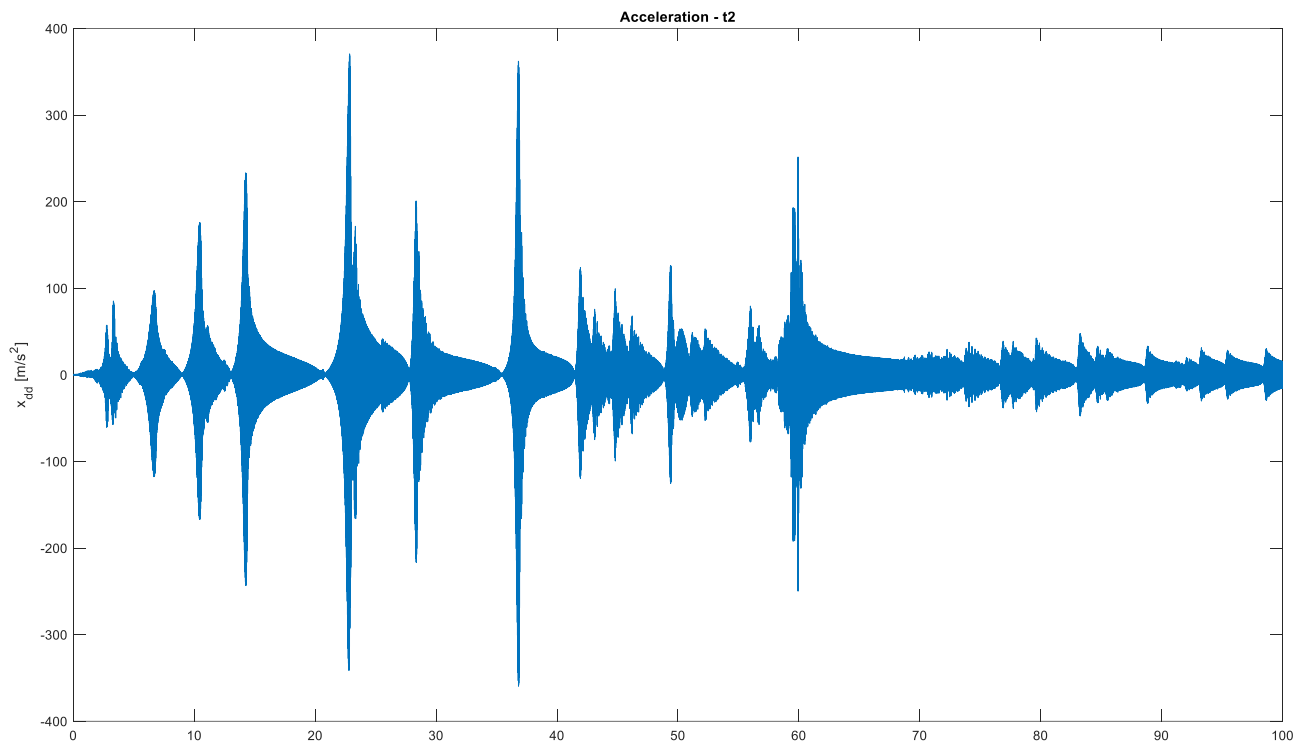


Figure 54 measured acceleration at spot 2

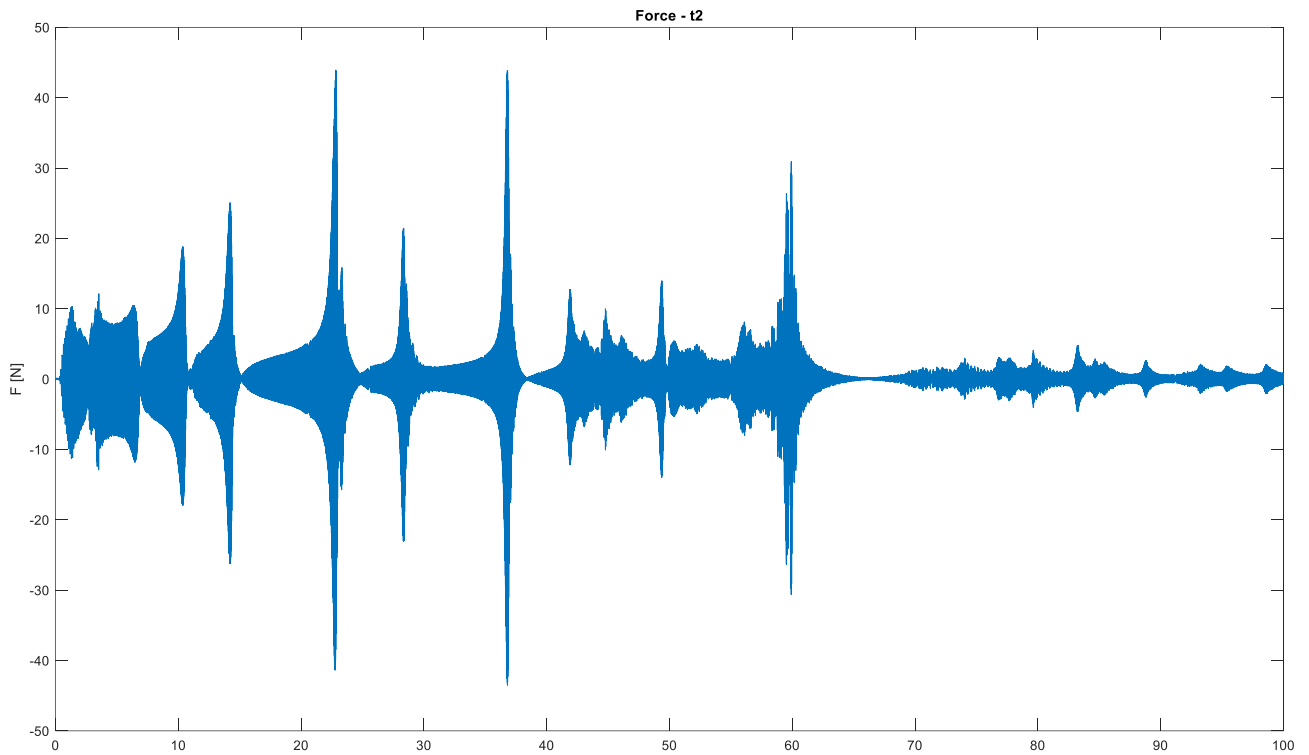


Figure 55 measured force at spot 2

As is possible to appreciate thanks to these three graphs, the behavior of all three measured parameters follows the shape of the sweep input signal.

Chapter 6

Conclusions

In this work is possible to point out a panoramic view of metamaterials characteristics and how are nowadays implemented on actual technology. With the additional information regarding automotive NVH field and all the problems that can be solved thanks to NVH studies, on chapter 1, can be provided a description of how metamaterials can help on each brank of an NVH vehicle analysis improving mechanical behavior but also customer experience. Is important to remember that vehicle homologation needs to respect sound emissions parameters but also parameters for what concern comfort and metamaterials are a good compromise to help reaching homologation goals without loss of vehicle driving experience. The study carried out on metamaterial cubic cell provides an explanation and puts in evidence the parameters that strongly affect the analysis. Parametrization of wave vectors and even most important the Irreducible Brillouin zone are the operations and the parameters that need to be very accurate and specific for each structure. In fact each structure has each own characteristic Brillouin zone that's a parameter that can only be computer with specific method, so if not precisely provided is not possible to replicate results in an effective way. Despite that, COMSOL provide the opportunity to create very accurate model both for geometry description but also for the materials assignation in fact thanks to the eigenfrequency analysis carried out in this study is highlighted the fact that for what concern the structure replication it is pretty the same. As reported in paragraph 2.2 the difference between reference eigenfrequencies and ones obtained in COMSOL is in the order and even under of 1%. Further analysis carried out in this study puts in evidence that the metamaterial under analysis, with some adapted Brillouin zones implemented (in 3 directions X,Y,Z) can provide a smaller bandgap than the one presented in the paper. Simulations carried out on other simplified structures puts in evidence a partial correlation with papers results taken as reference but also in this case the most important consideration and conclusion is that the lack of the specific Irreducible Brillouin zone does not guarantee the perfect correlation results, but also to obtain and puts in evidence the real metamaterial properties and potentiality. Thanks to the experiments reported in this work, it was possible to highlight a practical example of the effectiveness of metamaterials. Both metamaterial configurations demonstrated satisfactory results, showcasing a bandgap and a reduction in transmissibility. These results were further validated by the dual testing performed on the metamaterial samples, providing additional confirmation of the presented findings.

The two versions of the tested metamaterial also offered a clear demonstration of how different outcomes can be achieved through the engineering of the metamaterial. This highlights the potential for further versatility and effectiveness, tailored to the specific requirements of the intended application.

Ringraziamenti

Giunto al termine di questo lungo percorso accademico e di questo lavoro di tesi desidero dedicare alcuni pensieri verso le persone che mi hanno accompagnato in questi anni e con le quali ho condiviso tutte le fasi di questa avventura. Un ringraziamento lo rivolgo al Prof. Garibaldi e al Prof. Daga per avermi proposto questo argomento di tesi e supportato nello sviluppo del lavoro con consigli ma anche comprendendo la mia situazione di studente lavoratore che ha influito su metodi e ritmi di comunicazione durante questo periodo. Ringrazio i vecchi colleghi dell'ente NVH Stellantis, specialmente Marco e Rino, che mi hanno supportato e incoraggiato durante l'ultimo anno del percorso di studi e ringrazio i nuovi colleghi del gruppo Sperimentazione Ferrari, per avermi accolto e per aver compreso fin dall'inizio la mia situazione di studente alle prese con il rush finale per concludere la tesi. Ringrazio i compagni del liceo, tra tutti Alessio, Andrea ed Ernesto, con i quali ho continuato a vivere dei bei momenti di spensieratezza oltre che condiviso tutte le perplessità, i dubbi e le fasi non incontrate in questi anni. Ringrazio anche i nuovi amici, incontrati in seguito al mio rientro a Campobasso, con loro ho condiviso passioni come il nuoto, viaggi, e la Formula 1 che hanno alleggerito il peso dello studio, ma sono stati anche catalizzatori di energie in quanto studenti di facoltà diverse alle prese con lo stesso tipo di sfide che si presentavano ogni giorno davanti ai nostri progetti di vita. Ringrazio Luigi, amico e collega, per aver condiviso tanti momenti di studio, tante esperienze nella vita di tutti i giorni da fuorisede e tante considerazioni una volta entrati nel mondo del lavoro. Un enorme grazie va ai miei fratelli: Francesco fonte di ispirazione e ammirazione per la sua dedizione allo studio e sistematica precisione nell'affrontare la vita accademica e Federico per il suo modo scanzonato e spensierato di vivere ogni giorno aggiungendo un pizzico di allegria senza mai perdere di vista il proprio obiettivo. Un sincero grazie lo rivolgo ai miei genitori che hanno accolto e supportato il mio percorso, che hanno creduto in me e che non hanno passato giorno senza mai spronarmi e ricordarmi di credere in quello che stavo facendo. Hanno condiviso con me tutti gli alti e i bassi di questo percorso, dal giorno del mio test di ingresso al Politecnico fino ad oggi. A loro che dedico questo traguardo ed è a loro che devo essere grato per tutti gli insegnamenti ricevuti che hanno contribuito a rendermi la persona che sono oggi. Infine un ringraziamento lo dedico al mio sogno, quello che mi ha spinto a lasciare casa e che mi ha permesso di resistere e tenere duro nonostante le innumerevoli difficoltà fino a giungere alla fine di questo viaggio.

References

- ¹“ What is Automotive NVH?”, ANSYS BLOG, APRIL 13, 2023, <https://www.ansys.com/it-it/blog/what-is-automotive-nvh>.
- ² L. Garibaldi and A. Daga, Lesson 01 / A – Introduction and basis of NVH in vehicles, 2021, Politecnico di Torino.
- ³ Cummer, S. A., & Schurig, D. (2007). "One path to acoustic cloaking". *New Journal of Physics*, 9(3), 45.
- ⁴ Smith, D. R., & Pendry, J. B. (2004). "Metamaterials and Negative Refractive Index". *Science*, 305(5685), 788-792.
- ⁵ Lakes, R. (1987). "Foam structures with a negative Poisson's ratio." *Science*, 235(4792), 1038-1040. DOI: 10.1126/science.235.4792.1038
- ⁶ Bertoldi, K., Vitelli, V., Christensen, J., & Van Hecke, M. (2017). "Flexible mechanical metamaterials." *Nature Reviews Materials*, 2(11), 17066. DOI: 10.1038/natrevmats.2017.66
- ⁷ Lakes, R. (1987). "Foam structures with a negative Poisson's ratio." *Science*, 235(4792), 1038-1040. DOI: 10.1126/science.235.4792.1038
- ⁸ Hussein, M. I., Leamy, M. J., & Ruzzene, M. (2014). "Dynamics of phononic materials and structures: Historical origins, recent progress, and future outlook." *Applied Mechanics Reviews*, 66(4), 040802. DOI: 10.1115/1.4026911
- ⁹ Deymier, P. A. (Ed.). (2013). *Acoustic Metamaterials and Phononic Crystals*. Springer. ISBN: 978-3-642-31232-8
- ¹⁰ Liu, Z., Zhang, X., Mao, Y., Zhu, Y. Y., Yang, Z., Chan, C. T., & Sheng, P. (2000). "Locally resonant sonic materials." *Science*, 289(5485), 1734-1736. DOI: 10.1126/science.289.5485.1734
- ¹¹ Li, J., & Chan, C. T. (2004). "Double-negative acoustic metamaterial." *Physical Review E*, 70(5), 055602. DOI: 10.1103/PhysRevE.70.055602
- ¹² Ma, G., & Sheng, P. (2016). "Acoustic metamaterials: From local resonances to broad horizons." *Science Advances*, 2(2), e1501595. DOI: 10.1126/sciadv.1501595
- ¹³ Bertoldi, K., Vitelli, V., Christensen, J., & Van Hecke, M. (2017). "Flexible mechanical metamaterials." *Nature Reviews Materials*, 2(11), 17066. DOI: 10.1038/natrevmats.2017.66
- ¹⁴ Li, J., & Chan, C. T. (2004). "Double-negative acoustic metamaterial." *Physical Review E*, 70(5), 055602. DOI: 10.1103/PhysRevE.70.055602
- ¹⁵ Waiel Elmadih, Dimitrios Chronopoulos e Jian Zhu. «Metamaterials for simultaneous acoustic and elastic bandgaps». In: *Scientific Reports* 11 (2021). doi: 10.1038/s41598-021-94053-3. [url:https://doi.org/10.1038/s41598-021-94053-3](https://doi.org/10.1038/s41598-021-94053-3).
- ¹⁶ Miceli, Analisi sui metamateriali, Tesi laurea di primo livello, Politecnico di Torino, A.A. 2022/2023, Garibaldi, Daga.
- ¹⁷ C. Hakoda, J. Rose, P. Shokouhi and C. Lissenden, "Using Floquet periodicity to easily calculate dispersion curves and wave structures of homogeneous waveguides," *AIP Conf. Proc.*, 20 April 2018 1949 (1): 020016. <https://doi.org/10.1063/1.5031513>.

¹⁸ Elmadih, W., Chronopoulos, D., Syam, W.P. et al. Three-dimensional resonating metamaterials for low-frequency vibration attenuation. *Sci Rep* 9, 11503 (2019). <https://doi.org/10.1038/s41598-019-47644-0>

¹⁹ Maldovan, M. Phonon wave interference and thermal bandgap materials. *Nat. Mater.* 14, 667 (2015)

²⁰ Qureshi, A., Li, B. & Tan, K. T. Numerical investigation of band gaps in 3D printed cantilever-in-mass metamaterials. *Sci. Rep.* 6, 28314 (2016).

²¹ Chen, Y., Qian, F., Zuo, L., Scarpa, F. & Wang, L. Broadband and multiband vibration mitigation in lattice metamaterials with sinusoidally-shaped ligaments. *Extreme Mech. Lett.* 17, 24–32 (2017).

²² A.P. Daga , L. Viale , D. Agabiti , A. Fasana , L. Garibaldi, Dynamic analysis of metamaterials for industrial applications: numerical predictions and experimental results, Politecnico di Torino,2024